

Computer simulation of chopper neurons: intrinsic oscillations and temporal processing in the auditory system

Vom Fachbereich Biologie
der Technischen Universität Darmstadt
zur Erlangung des Grades
eines Doktors der Naturwissenschaften
(Dr. rer. nat.)

genehmigte
DISSERTATION

von

Dipl.-Phys. cand.med. Andreas Bahmer
aus Aschaffenburg

Darmstadt 2007
D 17

Referent: Prof. Dr. G. Langner
Korreferent: Prof. Dr. R. Galuske
Tag der Einreichung: 28.2.2007
Tag der mündlichen Prüfung: 20.4.2007

Contents

1	Motivation and Introduction	1
1.1	Neural oscillations	1
1.2	Intention and structure of the thesis	4
2	General Introduction	5
2.1	Oscillations in the auditory system	5
2.1.1	The auditory system	5
2.1.2	Cochlear nucleus (CN)	7
2.1.3	Neurons in the CN	8
2.1.4	Oscillators in the CN: Chopper Neurons	15
2.1.5	Chopper Neurons in the Periodicity Model according to Langner (1981)	16
2.2	Neuron models for the simulation of oscillations	19
2.2.1	Leaky integrate-and-fire (LIF) neuron model	20
2.2.2	LIF network of the Periodicity Model	21
2.2.3	Hodgkin-Huxley (HH) model	23
2.2.4	HH model from Rothman and Manis (2003c)	25
2.2.5	Compartment neuron model	29
2.3	Simulation environments	31
3	Oscillating neurons in the cochlear nucleus: I. Experimental basis of a simulation paradigm	33
3.1	Abstract	33
3.2	Introduction	33
3.3	Neuroanatomy and physiology of chopper neurons in the cochlear nucleus	35

3.4	Methods	36
3.5	Review of experiments on pitch perception and on the physiology of temporal coding	37
3.5.1	Evidence for preferred intervals of intrinsic oscillations	37
3.5.2	Dynamic features of auditory nerve, onset-, and chopper neurons	40
3.6	Discussion	40
3.6.1	Rationale for a synaptic delay of 0.4 ms as a basis for an auditory time constant	40
3.6.2	Rationale for the integration of an input from onset neuron to chopper neurons	46
3.7	Conclusions	47
3.7.1	Physiological and psychoacoustical data	47
3.7.2	Simulation paradigm	47
4	Oscillating neurons in the cochlear nucleus: II. Simulation results	48
4.1	Abstract	48
4.2	Introduction	48
4.3	Neuronal modelling	49
4.3.1	Methods	49
4.3.2	Simulation paradigms: “Circular oscillator” and “Multi-oscillator”	51
4.3.3	Modelling of inner ear, hair cell, and auditory nerve fibers . . .	52
4.3.4	Theory of the implemented neuronal models	52
4.4	Results	58
4.4.1	Simulation of auditory nerve fibers	58
4.4.2	Simulation of onset neurons	58
4.4.3	Circuit of auditory nerve, onset-, and chopper neurons	63
4.4.4	Comparison of the simulation results with properties of real chopper neurons	63
4.5	Discussion	67
4.5.1	Comparison of the model with previous computer models	67
4.5.2	Regularity and periodicity analysis	70
4.6	Conclusions	72

5	Spectral integration in a simulation of onset and chopper neurons in the cochlear nucleus	73
5.1	Abstract	73
5.2	Introduction	74
5.3	Methods	74
5.4	Results	75
5.4.1	Tuning and nonlinear effects of the simulated chopper neurons	75
5.4.2	Periodicity representation of the simulated chopper neurons	76
5.5	Discussion	79
5.5.1	Tuning of the simulated chopper neurons	79
5.5.2	Periodicity representation of the simulated chopper neurons	79
5.5.3	Explanation for a dichotomy of pitch perception?	81
5.6	Conclusions	81
6	Networks of Hodgkin-Huxley-like neuron models for the simulation of oscillating neurons in the cochlear nucleus	82
6.1	Abstract	82
6.2	Introduction	83
6.2.1	Special features of chopper neurons in the VCN	83
6.2.2	VCN neuron models	83
6.2.3	The HH-like “Rothman chopper”	84
6.2.4	Substituting LIF neurons by HH-like neurons in the Multi-oscillator	89
6.3	Methods	90
6.3.1	NEURON and Matlab	90
6.3.2	Neuronal modeling	90
6.3.3	Genetic algorithm in Matlab	92
6.4	Results	93
6.4.1	Patch clamp simulations of a single “Rothman chopper”	93
6.4.2	Patch clamp simulations of a network of two “Rothman choppers”	93
6.4.3	“Acceleration” of the “Rothman chopper” using genetic algorithms (GA)	94
6.4.4	The “fast Rothman chopper” in the Multi-oscillator	97

6.5	Discussion	101
6.5.1	Simulations of single chopper neurons and networks of chopper neurons	101
6.5.2	The optimization of the model using Genetic Algorithms	103
6.5.3	The “fast Rothman chopper” in the Multi-oscillator	105
6.6	Conclusions	105
7	Particular Issues	106
7.1	Input to chopper neurons from onset units: Octopus or D-stellate cells?	106
7.2	Functional role of inhibition of D-stellate cells	107
7.3	Is the nerve input necessary for the Multi-oscillator?	107
7.4	Comparison of particular simulation results with experimental results	108
8	General Discussion and Outlook	111
8.1	General Discussion	111
8.1.1	Biological background for the Circular Oscillator and the Multi-oscillator	111
8.1.2	Regularity and periodicity analysis	112
8.1.3	Effects of changing the width of the frequency channel integration	113
8.1.4	Periodicity coding despite saturation of nerve fibers?	114
8.1.5	Experimental basis for the time constants in VCN neurons	115
8.1.6	The “fast Rothman chopper” in the Multi-oscillator	115
8.2	Outlook	116
8.2.1	Implementation of inhibition	116
8.2.2	Large networks containing the Multi-oscillator	116
8.2.3	Pure tone and AM processing	117
8.2.4	Integration of the results in the periodicity model from Langner	117
9	Summary	118
	Zusammenfassung in deutscher Sprache	120
10	Appendix	122

10.1 Leaky integrate-and-fire neuron and synapses as Matlab function-file . .	122
10.1.1 Synapse	122
10.1.2 Soma	123
10.2 Hodgkin Huxley Equations of the model of Rothman and Manis (2003c)	124
10.3 Programs for NEURON and Matlab	126
10.4 Graphical User Interface of NEURON simulations in Chapter 6	129
10.5 Genetic Algorithm for the optimization of the membrane model of Rothman and Manis (2003c)	134
10.5.1 Initial population	134
10.5.2 Creating the Next Generation	134
10.5.3 Stopping Conditions for the Algorithm	136
10.6 Iteration of Genetic Algorithm for the optimization of the membrane model of Rothman and Manis (2003c)	139
 Bibliography	 140
 Acknowledgements	 148
 Curriculum Vitae	 150
 List of publications	 152

Chapter 1

Motivation and Introduction

“... part of a theory may well be *prae facto* instead of *post factum* and hence invite experimental verification ...” (van Hemmen, 2006, Editorial of “Biological Cybernetics”).

Computational or theoretical neuroscience is a spreading field that is complementary to traditional techniques in neuroscience. In this field, mathematically explicit theory helps to understand the mode of operation of systems. Mathematics plays an important role in the quantitative description of processes in nature as being a clear language to communicate quantitative information.

Theories without a neurobiological substrate are not relevant. However, a theory need not be based on experimental facts alone but can also reveal mathematical principles. These principles again can lead to a coherent explanation of experiments. Neurobiology in the 21st century should tightly connect theoretical and experimental neuroscience.

1.1 Neural oscillations

In the last decades scientists found that oscillations are one important feature in brain processing. Understanding of the synchronization of neuron population activity by oscillations gives insight in neuronal communication.

By definition, oscillations are temporal periodic changes in the state of a system. In nonlinear systems like the brain, oscillations define a stable state. Some of these stable states are speculated to be the equivalent for short term memories and play a role in decision making (Basar-Eroglu et al., 1992). Some authors have described a theory of memory that is equivalent to the optical recording technique that is called holography (Longuet-Higgins, 1968; Gabor, 1968a,b; Westlake, 1970). In their theories memory processes are based on the coherent interplay of many neurons, similar to holography where the coherence of many light waves forms a pattern that is stored.

The history of the description of oscillations in the brain started in the twenties, when neural oscillations were described by means of the Electroencephalography (EEG), which was discovered in 1924 by Hans Berger at the University of Jena. These oscillations were classified according to their frequency as β -, α -, θ -, δ -, and γ -waves. Different states of consciousness are accompanied by different pronounced appearance of the waves (Basar, 1980). But EEG signals show only the summed electrical activity of the brain, as they are measured at the surface of the head. This averaged activity might mask the mechanism of generating oscillations by small populations. Invasive recordings like single unit recordings (extracellular and intracellular) and local field potentials with electrodes directly contacting the brain offer a higher resolution of electrical activity. In these invasive recordings oscillations are also found.

Oscillations occur in different sensory systems, like the visual, olfactory, motor, and auditory system.

In the midbrain, the first functional description of neural oscillations in electrophysiological recordings in the auditory system was by Langner (1978), which led to a model of auditory temporal processing and neural oscillators (Langner, 1981).

Later, sensory segmentation with coupled neural oscillators were described by van der Malsburg (von der Malsburg and Schneider, 1986; van der Malsburg, 1992). He linked the binding problem with neural oscillators. In this case binding means that oscillations of different neural ensembles representing different features of an auditory object like the timbre or the pitch, synchronize (“Cocktail-Party” effect).

Subsequently, in 1990 neural oscillations became a hot topic in the visual system. Studies of Gray and Singer (Gray and Singer, 1989; Gray, 1994), and others (Eckhorn et al., 1988) associated oscillations in the visual system with the binding problem.

For the olfactory system, Gilles Laurent and his colleagues showed in a series of papers that oscillations exist in mammals and insects. Different odors led to different subsets of neurons firing on different sets of oscillatory cycles (Wehr and Laurent, 1996). Disruption of the oscillatory synchronization leads to impairment of behavioral discrimination of chemically similar odorants in bees (Stopfer et al., 1997).

In the motor system coherent 25- to 35- Hz oscillations have been reported by Murthy and Fetz (1992). The oscillations occurred often in the sensorimotor cortex when the monkeys retrieved food using somatosensory feedback. The phase of the oscillations changed continuously from the surface to the deeper layers of the cortex, reversing their polarity completely at depths exceeding 800 μm . Oscillations (15-20 Hz) were also observed in motor cortex of monkeys during periods of movement preparation (Sanes and Donoghue, 1993). In these experiments, the monkeys performed a visually guided, instructed task and the oscillations occurred preferentially before the visual cue to initiate movement. The study demonstrates that oscillations in the motor cortex are not related to the details of movement execution but they play an important role in the movement preparation.

Also in the somatosensory and in premotor cortex oscillating neurons have been reported (Lebedev and Nelson, 1995; Lebedev and Wise, 2004) The oscillations (20-40 Hz) occur often during periods of attentive immobility and typically disappear during

movements.

According to a review of Buhusi and Meck (2005) neural oscillations may have different functional roles in different brain areas and may be also involved in the mechanism of interval timing.

In medicine, large scale neuronal synchronization was found to be a reason for epileptical seizures, which are apparently based on the mutual excitation between neurons (Traub and Wong, 1982). Epileptic seizures can be triggered by various factors. Video screens, including television, video games, and computer displays, are the most common environmental triggers of photosensitive epileptic seizures. Interestingly, in patients with history of photosensitive epileptic seizures outbreaks occurred when certain flashing or patterned images have been broadcast (Fylan et al., 1999; Zifkin and Trenite, 2000).

It has always been a dream to interface the brain with a computer in order to record signals of the brain by a computer and control brain functions with signals from outside. In a study of Pesaran et al. (2002) neural oscillations were suggested as a control signal because in monkeys oscillations changed while preparation of movements (see also Andersen et al., 2004).

In the auditory system computer-brain interfaces have already become reality in the form of cochlea and brainstem implants. Cochlea implants stimulate the auditory nerve in the cochlea with electrical impulses, brainstem implants are located in the cochlear nucleus. The implants are still the aim of research and understanding the role of the oscillations in the cochlear nucleus might be important to improve the performance of these medical aids.

Altogether, oscillations are apparent in a variety of brain functions and are worth to be analyzed for their function. In this work, the neuronal basis of oscillations in the auditory system is analyzed in experimental data and by means of computer simulations. Oscillations are found in different auditory nuclei like the cochlear nucleus and the inferior colliculus and are attributed to a class of neurons in the cochlear nucleus, the so-called “chopper neurons” (see e.g. Blackburn and Sachs, 1989). Chopper neurons are outstanding because of their response pattern. They generate oscillations with a distinct frequency relatively independent of changes of important stimulus parameters (Pfeiffer, 1966; Blackburn and Sachs, 1989; Winter et al., 2001; Wiegrebe and Winter, 2001). It was hypothesized that they play an important role in pitch perception (Langner, 1981; Hewitt et al., 1992; Wiegrebe and Winter, 2001).

1.2 Intention and structure of the thesis

The aim of this work is the investigation of neuronal oscillations and connections in the auditory brainstem. To achieve this goal neuronal networks of “chopper neurons” are simulated. Although previous chopper neurons models can reproduce important aspects of physiological properties, they can not reproduce the special features of real chopper neurons.

In this thesis a new chopper model is simulated and compared to physiological data.

Following this chapter the thesis starts in **Chapter 2** with a general introduction of oscillations in the auditory system, a description of the oscillator in the periodicity model according to Langner (1981), and with an introduction in neuronal models.

Chapter 3 describes the experimental basis for the simulation paradigm of chopper neurons.

Chapter 4 discusses the simulation results of the new chopper topology.

Chapter 5 presents relevant features of the network, which can contribute to pitch perception.

Chapter 6 demonstrates a detailed analysis of a HH-like chopper neuron model and tests for its usability in the proposed network.

Chapter 7 discusses particular issues that are not discussed in the previous chapters but were objective of discussions with other scientists.

Chapter 8 discusses all results of the investigated topics and gives an outlook on potential investigations of the neuronal network.

Chapter 9 concludes the thesis by summarizing all results.

Within the context of this work, several important results were achieved in the field of modeling the auditory brainstem. These led to a number of relevant and acknowledged publications in recognized journals and presentations at national and international conferences (see Chapter “List of publications”).

The financial support for this thesis was provided by a scholarship of the “Hessische Graduiertenförderung”.

Chapter 2

General Introduction

2.1 Oscillations in the auditory system

In the auditory system oscillations in neural responses are found at different stages of auditory processing: in the midbrain oscillations occur in electrophysiological recordings (Langner, 1981, 1983; Langner and Schreiner, 1988) and in the brainstem a class of neurons, namely chopper neurons, show oscillating response patterns (Pfeiffer, 1966). Oscillations in the midbrain are assumed to result from the response of the chopper neurons (Langner, 1992) and they may also play a role in pitch perception (Langner, 1981).

In the following, some anatomical and physiological background is presented, which is important to understand the generation of auditory oscillations.

2.1.1 The auditory system

In the auditory system, many features of the cochlea-signal have to be extracted by several nuclei before they can be transferred into the cortex. For example, location of sound sources or periodicity of sound waves have to be calculated with high temporal precision. The auditory nerve transmits signals from the cochlea to the cochlear nucleus (Fig. 2.1), which is the first processing center in the auditory system. The processed information is then forwarded to the ipsi- and contralateral olives, the nuclei of the contralateral lemniscus lateralis (LL), and the contralateral colliculus inferior (IC) (Fig. 2.1). The colliculus inferior receives input from different nuclei (ipsi- and contralateral), the lemniscus lateralis projects to the IC (ipsilateral), and the olives to the IC and LL (ipsilateral). The colliculus inferior projects via the corpus geniculatum mediale to the cortex (Fig. 2.1).

The following sections focus on the properties of the cochlear nucleus, which is the anatomical structure that contains the oscillating chopper neurons.

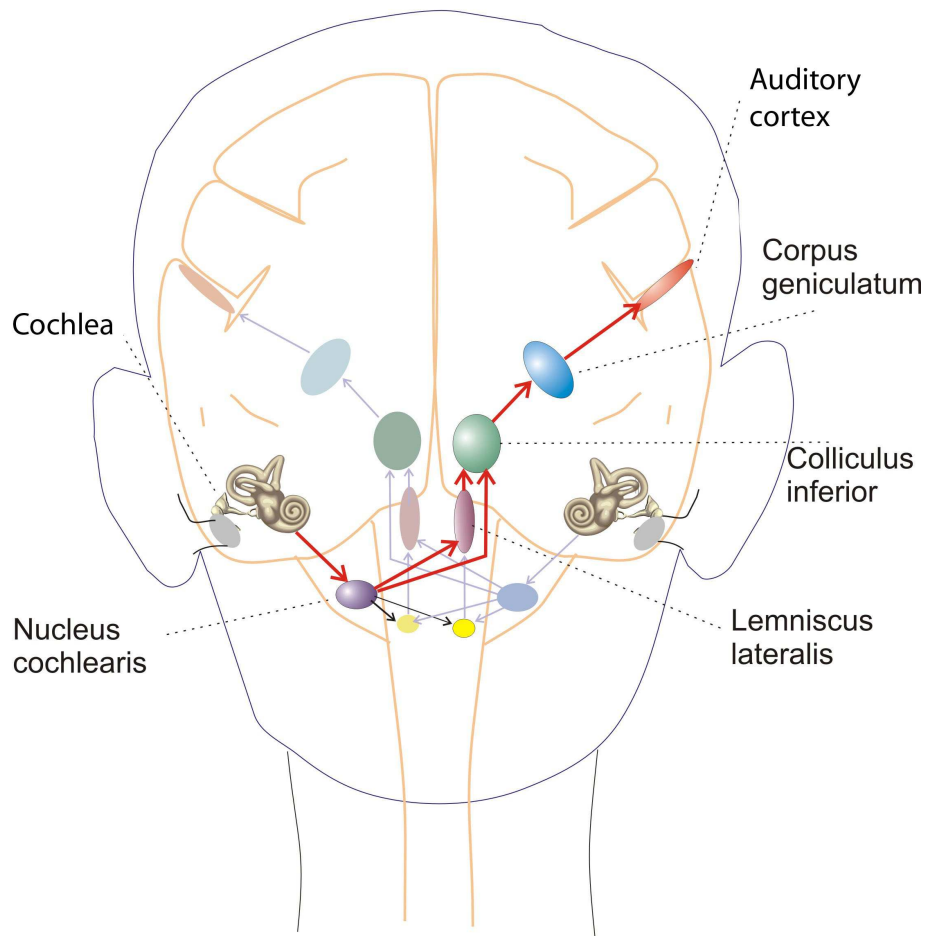


Figure 2.1: Scheme of the central auditory system. In this scheme the most important brain structures for auditory processing and the ascending connections from the cochlea to the cortex are depicted. The cochlear nucleus is the first processing center following the cochlea.

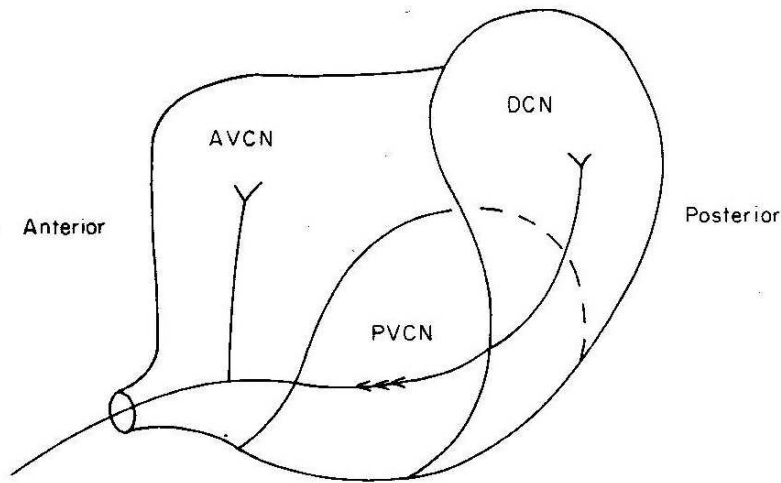


Figure 2.2: Scheme of a sagittal section of the cat cochlear nucleus. The nucleus shows three subdivisions, which are innervated by a branching auditory nerve fiber. AVCN, anteroventral cochlear nucleus; PVCN, posteroventral cochlear nucleus; DCN, dorsal cochlear nucleus (from Evans, 1975).

2.1.2 Cochlear nucleus (CN)

Anatomy

The cochlear nucleus is the exclusive target of the axon terminals of the spiral ganglion and is therefore the first nucleus of the central auditory pathways and contains the secondary auditory neurons. The auditory nerve enters the cochlear nucleus from ventral (Ryugo and Parks, 2003). The cochlear nucleus receives ascending information from the AN fibers (Fig. 2.2). The anteroventral part of the CN (AVCN) receives ascending inputs predominantly from the ascending (anterior) branch of AN fibers. Caudal to the nerve entrance and bifurcation zone is the posteroventral part of the CN (PVCN). The PVCN receives its ascending inputs principally from the posterior collaterals of AN fibers. The dorsal cochlear nucleus (DCN) forms the most caudal and dorsal extent of the CN. The DCN is characterized by a distinct layering pattern, closely resembling the cortical appearance of the cerebellum, whereas the VCN is not layered (Ryugo and Parks, 2003).

Auditory nerve input

The auditory nerve consists of bundles of thick and thin fibers. These fibers can be traced back along the auditory nerve into the cochlea where the thick fibers are found to arise from type I spiral ganglion neurons and the thin fibers arise from type II spi-

ral ganglion neurons. These fibers can also be traced back centrally into the cochlear nucleus. The thick fibers are myelinated, whereas the thin fibers are unmyelinated. The thick fibers give rise to one or several large endings called “endbulbs of Held”, which are among the largest synaptic endings in the brain. The functional importance of endbulbs of Held is that they correspond to secure synaptic transmission; when an action potential reaches such an axon terminal, the probability to generate an action potential in the postsynaptic cell is very high. Both thick and thin fibers give rise to short collaterals with many en passant swellings and terminal boutons. These small endings are roundish and represent approximately 95% of the total endings. Most of these boutons are distributed within the VCN.

The fibers, whether myelinated or unmyelinated, show a cochleotopic projection pattern. Their distribution is systematically related to their origin. Both, type I and II fibers send a common branch into the anteroventral cochlear nucleus (AVCN), and a second branch through the posteroventral cochlear nucleus (PVCN) and into the dorsal cochlear nucleus (DCN).

In mammals, individual type I auditory nerve fibers may be defined by three fundamental properties: 1. frequency selectivity, 2. response threshold, and 3. spontaneous discharge rate. Frequency selectivity refers to the fibers tendency to be most sensitive to a single frequency, which is called the characteristic frequency (CF), i.e. the frequency which leads to a neural response for the lowest threshold in dB SPL. The CF reflects the longitudinal location of fiber termination along the organ of Corti.

Ganglion cells innervating hair cell in the apical region of the cochlea distribute their axon and terminals in a ventral zone of the nucleus, whereas ganglion cells innervating progressively more basal hair cells project to progressively more dorsal zones of the nucleus. The nerve fibers bifurcate into an ascending branch and a descending branch. The ascending branch has a relatively straight trajectory into the AVCN and terminates as a large, axosomatic ending. The descending branch has a straight trajectory through the PVCN before entering the DCN. Fibers of similar CFs form a 3-dimensional sheet through the nucleus, and these sheets represent isofrequency laminae of the nucleus (Fig. 2.3). These projections underlie the tonotopic organization of the resident neurons of the cochlear nucleus. Both divisions of the cochlear nucleus are tonotopically organized.

2.1.3 Neurons in the CN

Cell types

The distribution of CN cells types provides a basis for dividing the CN into distinct subdivisions (see Fig. 2.4 in Osen, 1969). The anterior part of the AVCN contains large neurons called spherical cells. Immediately posterior to the spherical cell area globular neurons are apparent that can be distinguished from spherical cells by the excentric position of their nucleus in the soma. The location of globular neurons corresponds to

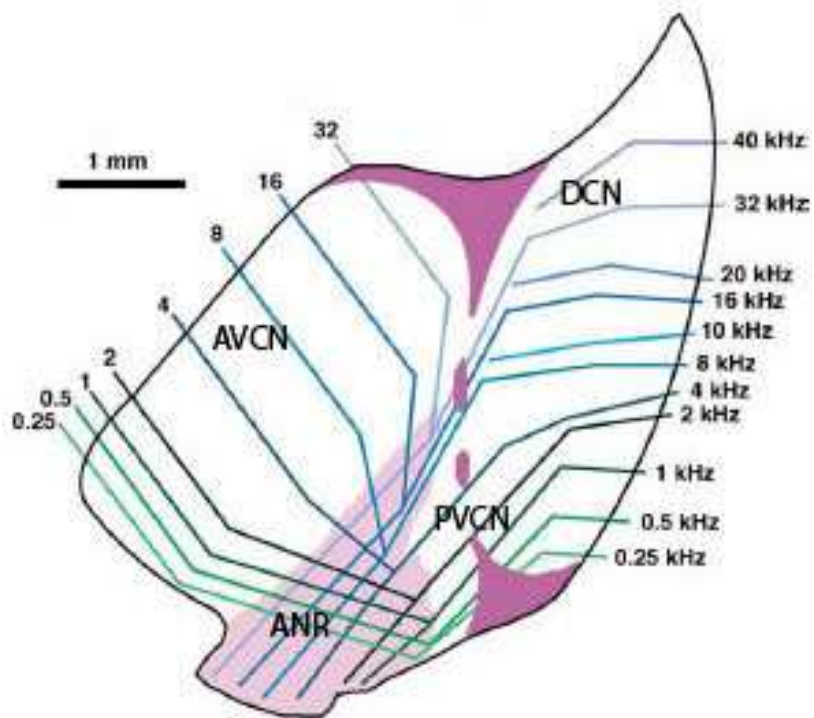


Figure 2.3: Tonotopic organization of cochlear nucleus cells. ANR, auditory nerve root; AVCN, anteroventral cochlear nucleus; DCN, dorsal cochlear nucleus; PVCN, posteroventral cochlear nucleus (modified from Ryugo and Parks, 2003).

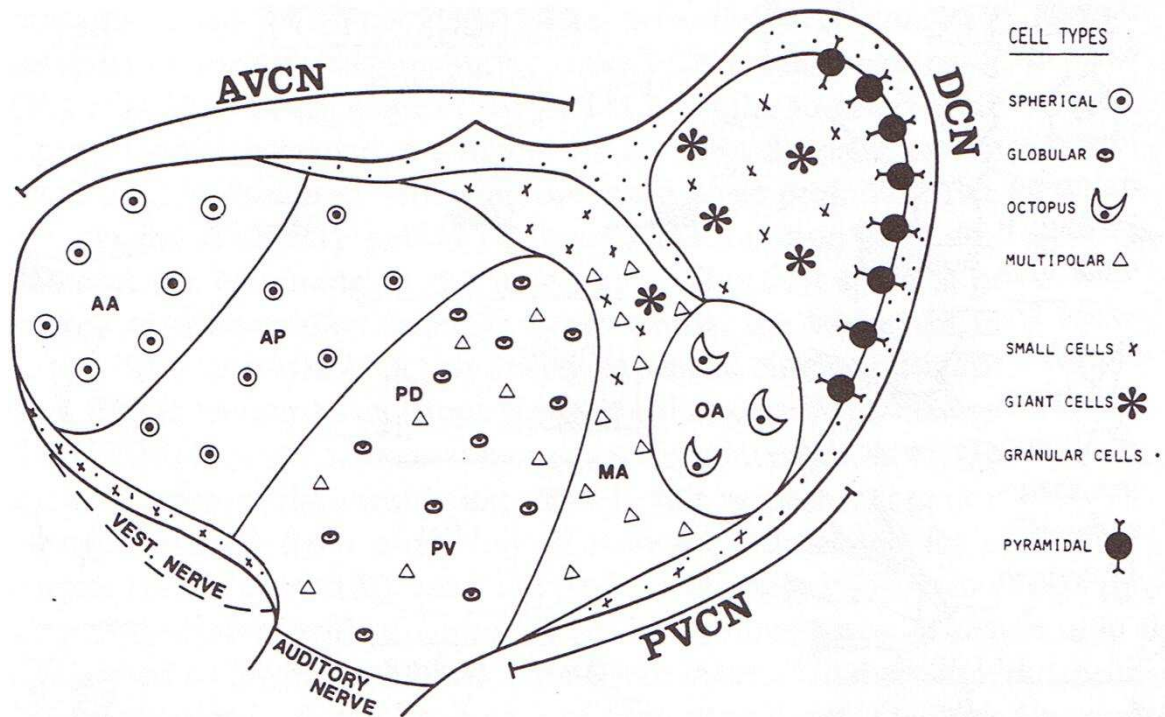


Figure 2.4: Scheme of the cochlear nucleus indicating its subdivisions (lateral view, cat) AA = anterior part of the anterior division of AVCN; AP: posterior part of the anterior division of AVCN; AVCN: anteroventral cochlear nucleus; DCN: dorsal cochlear nucleus; MA: multipolar cell area; OA: octopus cell area; PD: dorsal part of the posterior division of AVCN; PV: ventral part of the posterior division of AVCN; PVCN: posteroventral cochlear nucleus (modified from Osen, 1969).

the zone of entrance and bifurcation of AN fibers referred to as the nerve root region. The spherical and globular neurons have a similar appearance both belonging to the class of bushy neurons because of the characteristic aspect of their dendritic trees (Fig. 2.5). Caudal to the nerve root region is the posteroventral part of the CN (PVCN), which contains two main classes of neurons. First, the multipolar (Fig. 2.4), or stellate neurons are located preferentially in the rostral part of the PVCN. The multipolar or stellate neurons are not restricted to the PVCN since some are also present in the AVCN. Second, the octopus neurons occupy a well-defined location in the caudal part of the PVCN (Fig. 2.4). The dorsal cochlear nucleus (DCN) also contains several types of neurons. A layer parallel to the external border of DCN is formed by large cells called fusiform, or pyramidal neurons (Fig. 2.4). The DCN is also rich in two other types of neurons, both of smaller size than the other types: small and granular neurons (Fig. 2.4). The two latter types of neurons are also present in the PVCN, as well as in a smaller proportion in the AVCN. The large variety of cell types in the CN is correlated with a wide variety of response types (Bourk, 1976).

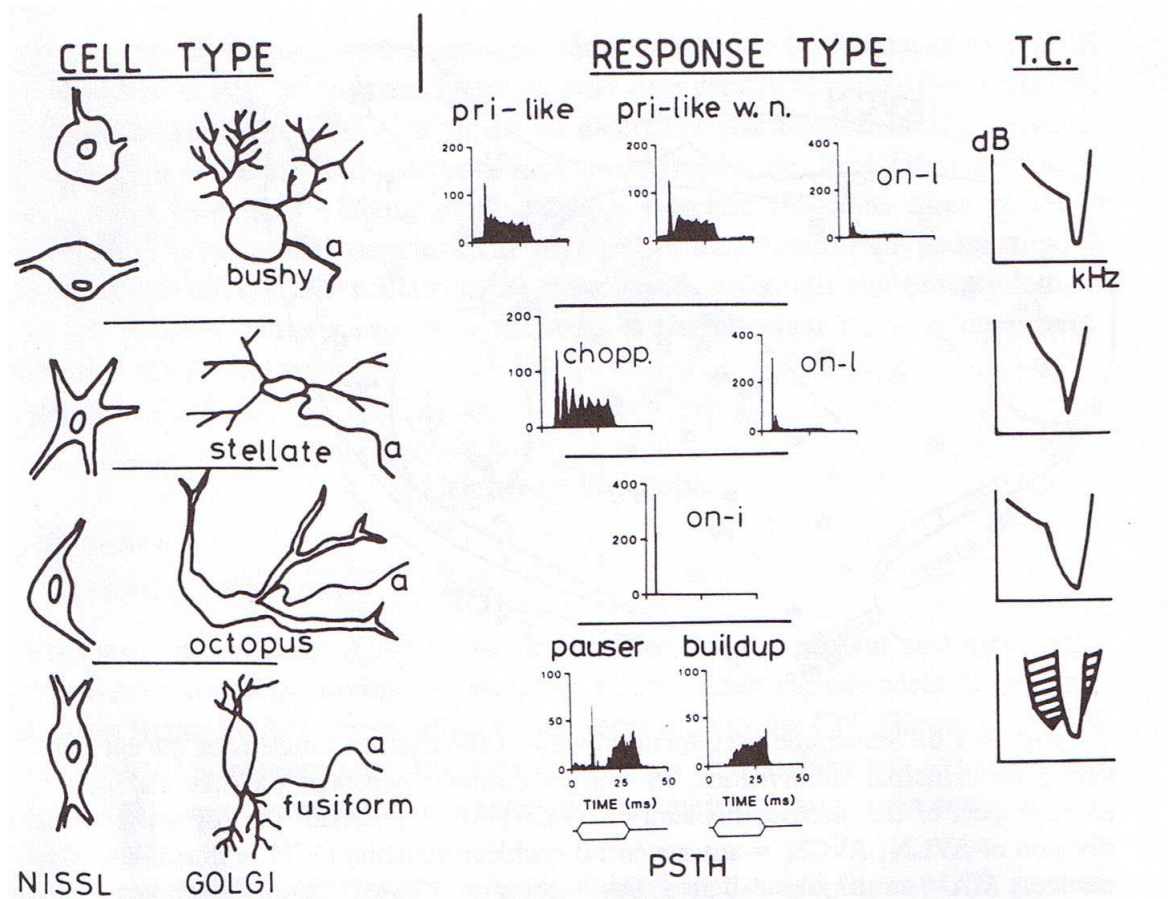


Figure 2.5: Cell types and corresponding response types (by PSTH and tuning curves) in the cochlear nucleus. Dashed portions of the T.C. indicate zones of inhibition, the white inner portion represents the excitatory area. a: axon; on-i: discharge only to stimulus onset; on-l: onset response and weak discharge during rest of tone-burst; pri-like: primary-like; pri-like w.n.: primary-like-with-notch; chopp.: chopper (from Ehret and Romand, 1997).

Response types

Various response types have been reported for CN single units on the basis of peri-stimulus time histograms (PSTH) derived from responses to tone bursts (Pfeiffer, 1966; Winter et al., 1990, e.g.). In the VCN of the cat, some type of neurons show a response (as seen in PSTHs) similar to that of auditory nerve fibers. Such VCN units are called primary-like (Fig. 2.5).

A second type of neurons have a response to tone bursts that is called primary-like with notch (Fig. 2.5). The envelope of the PSTH is similar to primary-like responses, except for the presence of a notch (i.e. a short decrease or even absence of discharge) immediately following the sharp onset peak of activity, which is precisely time locked to the stimulus onset.

A third category of neurons, the chopper neurons (Fig. 2.5), exhibits a PSTH having an envelope similar to that of primary-like responses, but with multiple peaks separated by regular time intervals that are not related to the frequency of the stimulating tone (Pfeiffer, 1966). In this respect, chopper responses are clearly different from phase-locked responses illustrated for AN fibers since the peaks in chopper PSTHs are not synchronized with the stimulus waveform.

A fourth type of neurons (Fig. 2.5) show a response, which is defined by an increase in discharge rate primarily or exclusively at the beginning of each tone burst. On-type I responses (on-i in Fig. 2.5) are characterized by discharges restricted exclusively to stimulus onset, whereas on-type responses (on-l in Fig. 2.5) show a weak excitation during the rest of the tone-burst duration in addition to the main response at onset, but clearly less than in primary-like or primary-like-with-notch responses.

In addition, a different classification scheme for CN units is based on the presence of inhibitory components recorded mainly in the DCN. These response types consist of (see Fig. 2.5):

1. A suppression of activity during the tone burst.
2. A suppression following a first initial peak of activity and preceding a rate activity during the second half of the tone burst (pauser).
3. An initial suppression followed by a progressive increase in discharge rate until the end of the tone burst (buildup).

The complexity of responses is greater in the DCN than in the VCN, and a different classification scheme has been proposed for the DCN, taking into account the importance of the inhibitory components. Response types in the DCN are significantly different in anesthetized animals as compared to non-anesthetized preparations.

In contrast, response types in the AVCN and PVCN are not or very little affected by the level of anesthesia (e.g. see Winter et al., 1990). The large variability of response types in the CN reflects the transformation of signals from AN fibers to the various types of CN neurons. The modification is believed to depend both on the spatial arrangement of synaptic endings from both cochlear and non-cochlear inputs on the CN cells and on the convergence of excitatory and inhibitory inputs on a given neuron. Therefore, the generation of responses depends on the timing of various convergent synaptic inputs.

In addition, recent data (Manis and Marx, 1991) derived from intracellular recordings in *in vitro* preparations of the guinea pig CN indicate that intrinsic properties of the membrane of VCN and DCN cells (variation in ion channels) may also contribute to the observed response to acoustic stimuli.

Correlation between response types and cell types

The different types of response patterns observed in the CN are related to specific areas (Bourk, 1976). Primary-like responses are observed principally in the most anterior region of the AVCN and primary-like-with-notch responses predominantly in the posterior part of the AVCN. Chopper responses are widely distributed in the AVCN and PVCN (also a few in the DCN), but with a relatively high concentration in the posterior half of the AVCN and the anterior part of the PVCN. Transient responses (on-type I) are mainly restricted to the posterior region of the PVCN, whereas pauser and buildup response patterns are typically found in the DCN. These data therefore provide indirect evidence for a correlation between unit type (electrophysiological category) and neuron type (anatomical category). Primary-like, primary-like-with-notch, chopper, and on-type I are thought to be associated with spherical, globular, multipolar, and octopus neurons, respectively (Fig. 2.5). The pauser and buildup responses have been associated with fusiform neurons of the DCN (Fig. 2.5). There are indications that these correlations are not strict because it has been shown in the gerbil that response properties may sometimes be independent of the neuronal structure (Ostapoff et al., 1994).

Tuning properties

In addition to the differences mentioned above, single units in the CN can differ from auditory nerve fibers by the shape of their tuning curves (Fig. 2.5).

First, single units characterized by patterns of response to tone bursts as found in primary-like, primary-like-with-notch, on-type I, and chopper units have a tuning curve comparable to that of nerve fibers (Bourk, 1976).

Pauser and buildup units have more complex tuning curves with a zone of activation surrounded by zones of inhibition (Fig. 2.5).

The discharge rate as a function of tone intensity of chopper, primary-like, and primary-like-with-notch is a monotonic function with a dynamic range comparable to that found in the auditory nerve (30-40 dB).

In contrast, non-monotonic intensity functions have often been observed for pauser and buildup units.

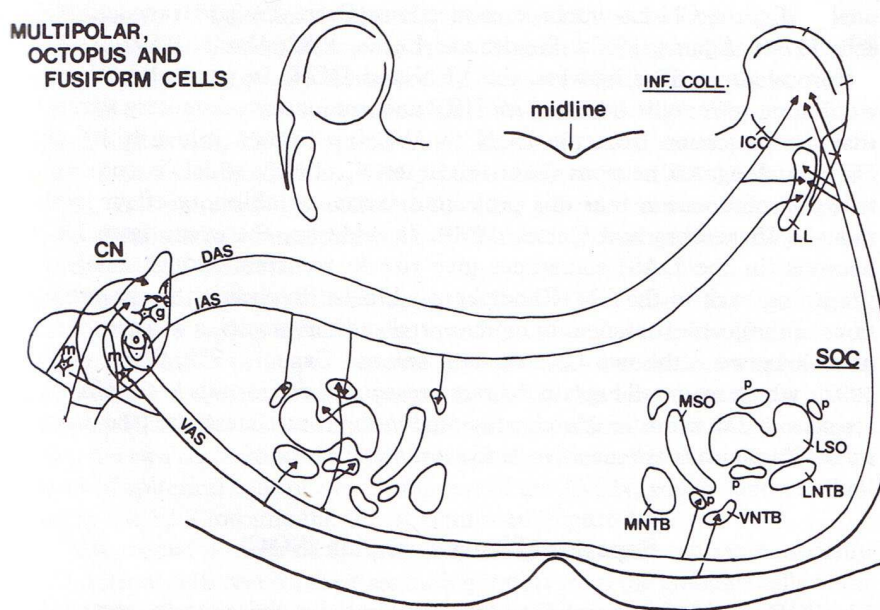


Figure 2.6: Schematic representation of the efferent projections of the cochlear nucleus (CN). The target nuclei of the axons emitted by the multipolar (m), octopus (o), giant (g) and fusiform (f) CN neurons are shown.

INF. COLL.: inferior colliculus, SOC: superior olivary complex, DAS: dorsal acoustic stria (stria of Monakow), IAS: intermediate acoustic stria (stria of Held), VAS: ventral acoustic stria (trapezoid body), ICC: central nucleus of the inferior colliculus, LL: lemniscus lateralis, MNTB: medial nucleus of the trapezoid body, VNTB: ventral nucleus of the trapezoid body, LNTB: lateral nucleus of the trapezoid body, LSO: lateral superior olivary nucleus, MSO: medial superior olivary nucleus (from Ehret and Romand, 1997).

Efferent projections

The role of the CN is to receive the information from the AN fibers, to process this information, and to distribute the modified signals to higher auditory nuclei.

To understand how the auditory system operates, it is therefore essential to know the projection patterns of their axons from the different types of CN neurons.

CN neurons show a high degree of collateralization of the axons which makes it very difficult to determine these patterns. Figure 2.6 shows the projection of the multipolar or stellate, octopus, and fusiform cells schematically.

The CN has three main output pathways:

The first, the ventral acoustic stria (VAS), contains axons originating mainly from the neurons of the AVCN, namely bushy cells, and PVCN, namely stellate and some octopus cells. The axons of the stellate and octopus cells project via the VAS through the

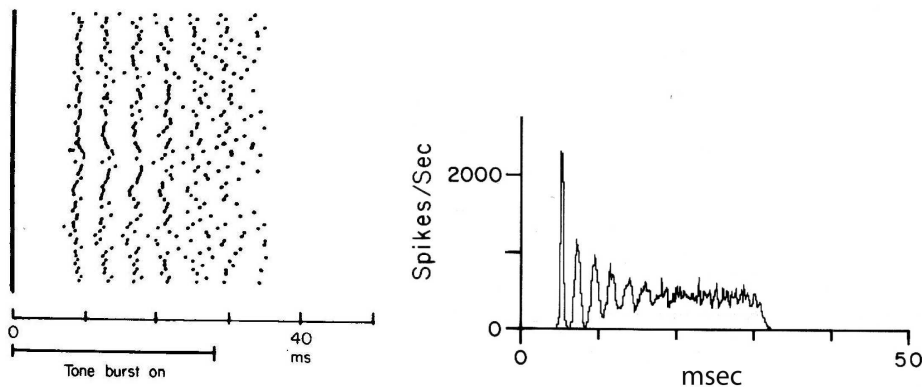


Figure 2.7: *Left*: Point plot of a chopper response (Pfeiffer, 1966). Each dot stands for a spike of the cell, each row is a recording at the same stimulus condition. Ab-scissa represents time after presentation of each tone burst (Stimulation frequency at characteristic frequency of 7 kHz.). *Right*: Peri-stimulus-time-histogram (PSTH) of a chopper neuron (Blackburn and Sachs, 1989). Although the peaks of the PSTH vanish, the interspike intervals stay constant. The small variations of the intervals accumulate and therefore peaks in the PSTH disappear.

lateral lemniscus (LL) and to the inferior colliculus (IC).

The second output pathway, the intermediate acoustic stria (IAS), or stria of Held, includes axons originating primarily from the octopus cells of the PVCN, terminating in the so-called periolivary nuclei (p) and higher in the ventral nucleus of the LL and the IC.

These two latter structures also receive ascending inputs via the third CN output pathway, the dorsal acoustic stria (DAS), or stria of Monakow, containing axons from DCN neurons, which do not project to the SOC.

Finally, the CN has intrinsic connections (Osen, 1969; Adams, 1983) such as projections between the VCN and DCN.

2.1.4 Oscillators in the CN: Chopper Neurons

The chopper responses are among the most widespread throughout the CN. They are found in all divisions, although with a higher percentage in the PVCN and a cell layer of the DCN (Godfrey et al., 1975). Chopper responses are generally well defined for stimulus levels of at least 20 dB above threshold and show multi-peaked temporal pattern in which the interpeak intervals are not related to stimulus frequency (Pfeiffer, 1966) (Fig. 2.7).

Several categories of chopper responses have been defined on the basis of PSTH characteristics (Bourk, 1976; Rhode and Smith, 1986), such as responses with long inter-

vals between peaks, mainly found in the DCN, responses with shorter intervals, and responses with a chopper part only at the beginning of stimulation. The chopper responses are related mainly to stellate cells. However, a too strict relationship seems to be an oversimplification in view of several types of stellate cells in the CN (Oertel, 1983) and because response patterns may be quite independent of cell structure (Ostapoff et al., 1994). Different stellate cells, membrane properties, and synaptic organization might be the reason for the differences of chopper responses in the CN. The interspike intervals of chopper responses have a small standard deviation. Most chopper responses have a very low coefficient of variation (CV), which is defined as the ratio of the standard deviation to the mean of the interspike intervals, of less than 0.5 (Young et al., 1988; Blackburn and Sachs, 1989; Banks and Sachs, 1991). No large differences have been found between chopper tuning curves and tuning curves of nerve fibers. The rate-intensity function of most chopper units are monotonic as in AN fibers, only 14% are non-monotonic (Rhode and Smith, 1986).

2.1.5 Chopper Neurons in the Periodicity Model according to Langner (1981)

Langner (1981) proposed a periodicity analyzing model that consists of networks of neurons and connections that are located in the cochlear nucleus and the inferior colliculus. The periodicity model is a bio-inspired neural network. The included neurons of the cochlear nucleus are depicted in Fig. 2.8.

The model contains a “trigger neuron”, an “oscillator”, an “integrator complex”, and a “coincidence” neuron. The properties of the trigger neurons are similar to that of onset cells in the NC, the required oscillator neurons are similar to chopper cells (marked by a circle in Fig. 2.8), the output of the integrator complex is evident in cells in the DCN and ascending inhibitory connections project from cells of the ventral nucleus of the lateral lemniscus (VNLL) to the IC (not shown in Fig. 2.8). In this thesis physiological relevant oscillatory responses of the stellate cells, which are part of the periodicity model, are modeled.

The neural network is a correlation network of neurons. For better understanding a scheme of the model and its function is shown in (Fig. 2.9), where all the parts described above can be found. Exemplary neuronal potentials describing the function of the classes of neurons are shown in the right part of the figure.

The function of the network is based upon the correlation of delayed and undelayed neuronal responses of the depicted neurons to envelopes of AM signals. These responses converge at neurons acting as coincidence detectors. Each modulation period of an AM signal activates the trigger neuron, which again activates a rapid oscillation (oscillator potential with a predefined frequency). Parallel to that process, the integrator neuron responds to the same cycle but with a longer delay (integration period of the integrator). The coincidence neuron will be activated, despite the different delay times of the two

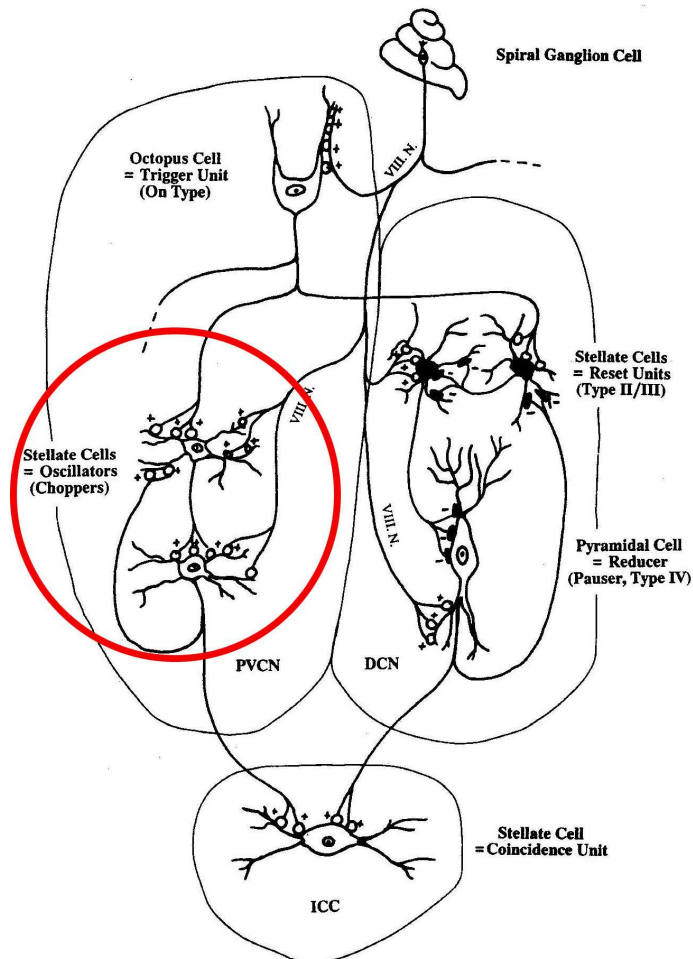


Figure 2.8: A periodicity analyzing network model including oscillating stellate neurons (marked by a circle), octopus cells which synchronize to envelope modulations. Pauser neurons in the DCN integrate over its nerve input and other neurons of the cochlear nucleus. The stellate cells are arranged in a circular network. The oscillating neurons of the PVCN and the pauser neurons of the DCN are supposed to project in the central nucleus of the inferior colliculus onto the same neuron (from Langner, 1988). The mode of operation of this network model is described in the following figure and in the text.

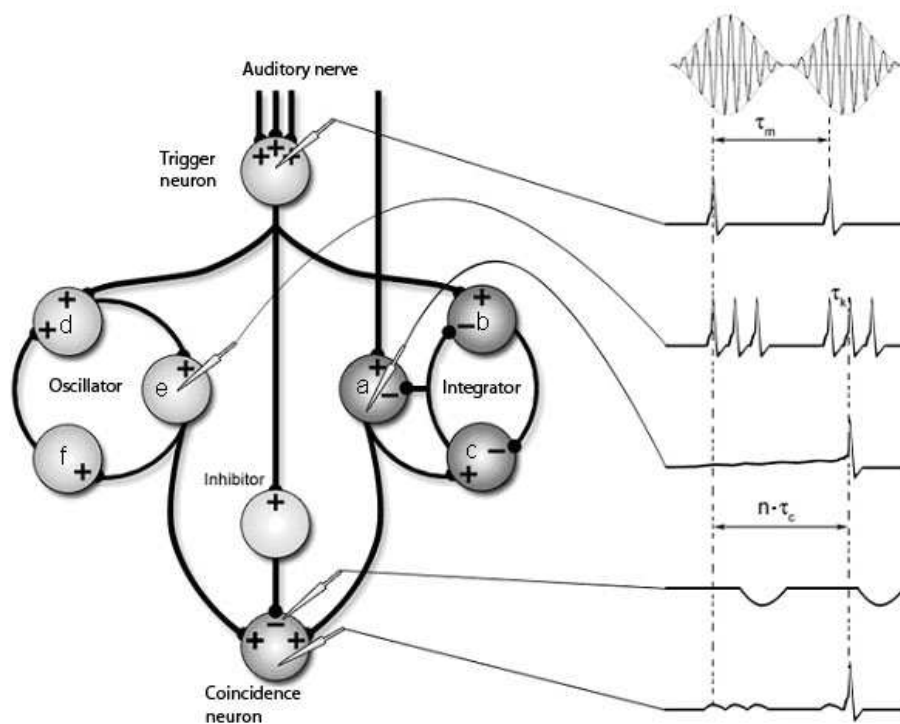


Figure 2.9: The periodicity analyzing neural model and some exemplary neuronal potentials. The model is driven with a stimulus generating equal oscillation and integration delay periods and therefore a coincidence for the specific module.

previous units, provided that the integration period equals the period of the AM signal. A coincidence neuron will respond more often, when its inputs are synchronized, i.e. when the spikes of the oscillator and of the integrator converge at the same time. Thus, modulation periods (periodicities), $m \times \tau_m$, with $m = 1, 2, \dots$, which activate the oscillations and drive the coincidence unit can be computed from the following linear equation:

$$m \times \tau_m = n \times \tau_c - k \times \tau_k \quad (2.1)$$

where k, m, n are small integers. $n \times \tau_c$ is the integration period, which consists of n carrier periods and which is the time the integrated input signal needs to reach a certain threshold. $1/\tau_c$ is the carrier frequency of the AM signal, $1/\tau_k$ the frequency of the oscillations. Eq. 2.1 will be referred to as coincidence equation. The parameter m takes into account the fact that coincidence neurons respond also to harmonics ($m > 1$) of the modulation frequency of the AM signal, which implicates ambiguity of IC neurons with respect to harmonically related signals. A solution to this problem is proposed by an input from the inhibitor. Because of the cochlear frequency analysis, a neuron responds strongest at its characteristic frequency (CF). In addition to its CF, a coincidence neuron is tuned to a certain periodicity, i.e. a certain modulation frequency of an AM signal, also called the best modulation frequency (BMF). Therefore, different trigger, oscillator, integrator, and coincidence units are needed to cover the range of periodicity of AM signals.

The functional details of a computer model simulating such a periodicity analysis network, along with the description of its components is given in Section 2.2.2, in Borst et al. (2004), and Voutsas et al. (2005).

2.2 Neuron models for the simulation of oscillations

In computational neuroscience different models are used to simulate neurons and neuronal networks. The models differ in their level of abstraction. For simulating large networks mostly simple neuron models like the leaky integrate-and-fire neuron are used because they can be calculated in a reasonable time. They simply generate a pulse if excitation is sufficient. In contrast, in simulating single neurons or micro-circuits Hodgkin-Huxley-like models are often used. They are related more closely to biological processes e.g. the ion flux of channels is calculated. The underlying formulas were developed by Hodgkin and Huxley (1952). Another aspect in modeling is the spatial dimension of cells. The detailed description in time can therefore be expanded by a detailed description in space. So called compartment models simulate not only the soma, but the dendritic tree and the axon in any spatial resolution. But again calculation time rises with higher resolution. The different aspects of models and modeling is depicted in Fig. 2.10.

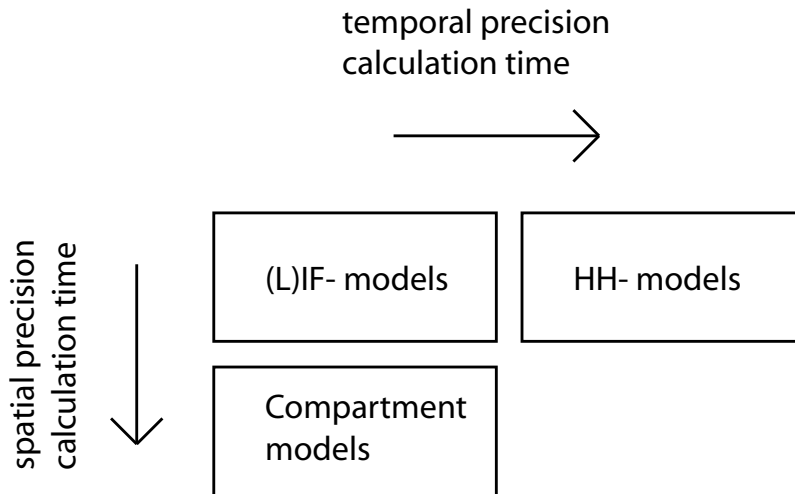


Figure 2.10: Advantages and disadvantages of different neuron models. The higher the spatial or temporal resolution of a model, the higher the calculation time.

The highest level of abstraction are rate models (rate model for chopper neurons see Bleeck, 2007). They only simulate the pulse rate of a neuron and not single pulses. They are used for example in simulating muscle control, which essentially depends on the pulse rate. Temporal aspects of signal processing are nearly neglected, which makes these models nearly useless for correlation processes and for our simulation purposes.

2.2.1 Leaky integrate-and-fire (LIF) neuron model

In this section, the most common description of the LIF model is presented. The basic circuit of the model consists of a parallel circuit of a capacity C with a resistor R , which is driven by a current $I(t)$ (see Fig. 2.11). This circuit is a leaky integrator, which fulfills the equation

$$I(t) = \frac{u(t)}{R} + C \frac{du}{dt} \quad (2.2)$$

$u(t)$ is the current at the capacity. With $\tau = RC$ as the time constant of the integrator, the equation can be written as:

$$\tau \frac{du}{dt} = -u(t) + RI(t). \quad (2.3)$$

Thus, $u(t)$ can be interpreted as the membrane voltage and τ as the membrane time constant of the cell. If the voltage reaches a threshold Θ , a spike will be elicited and the membrane voltage is set to a fixed value. After the spike, a fixed refractory period

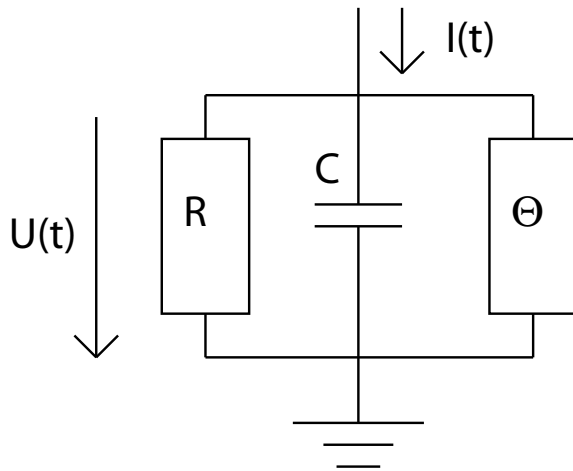


Figure 2.11: Circuit diagram of a leaky integrate-and-fire neuron

follows. Some aspects of the behaviour of the LIF model can be approximated to the HH model by choosing adequate parameters Θ , R , and C .

2.2.2 LIF network of the Periodicity Model

The periodicity analyzing network proposed by Langner (1981) is implemented with LIF neuron models (Borst et al., 2004; Voutsas et al., 2005). The soma and the synapses of each neuron are modeled with the help of leaky integrate-and-fire processes. Each module of the periodicity model is a so-called “block” in Simulink (see Fig. 2.12). Simulink is a graphical user interface for the simulation environment Matlab that gives a fast overview of the topology of the network and the network can be easily build and modified by the user. The LIF neuron models with synapses that are used in this work are closely related to the implementation in Simulink (see Fig. 2.13) because parts of this work are planned to be inserted in the Simulink model. In this model the resting potential of the soma is set to zero, the synapses integrate their input in a leaky manner and release a transmitter amount that is looked up in a table. The transfer functions of the synapses have a sigmoidal shape (for details see Voutsas et al., 2005). Simulations of the periodicity model in Simulink showed that it is possible to replicate part of responses found in the IC (Voutsas et al., 2005; Langner and Schreiner, 1988). Technically, the periodicity model is able to compute the ratio of modulation and carrier frequency of harmonic sound signals (Fig. 2.14). In the latest update of the model (Voutsas et al., 2005) an inhibition module has been integrated that is physiologically related to the output of the lateral lemniscus. This inhibition suppresses higher harmonics (see Fig. 2.14, right) as found in Ochse (2004). The periodicity model may be used in audio signal processing applications, such as sound source separation, periodicity analysis and a solution to the cocktail party problem.

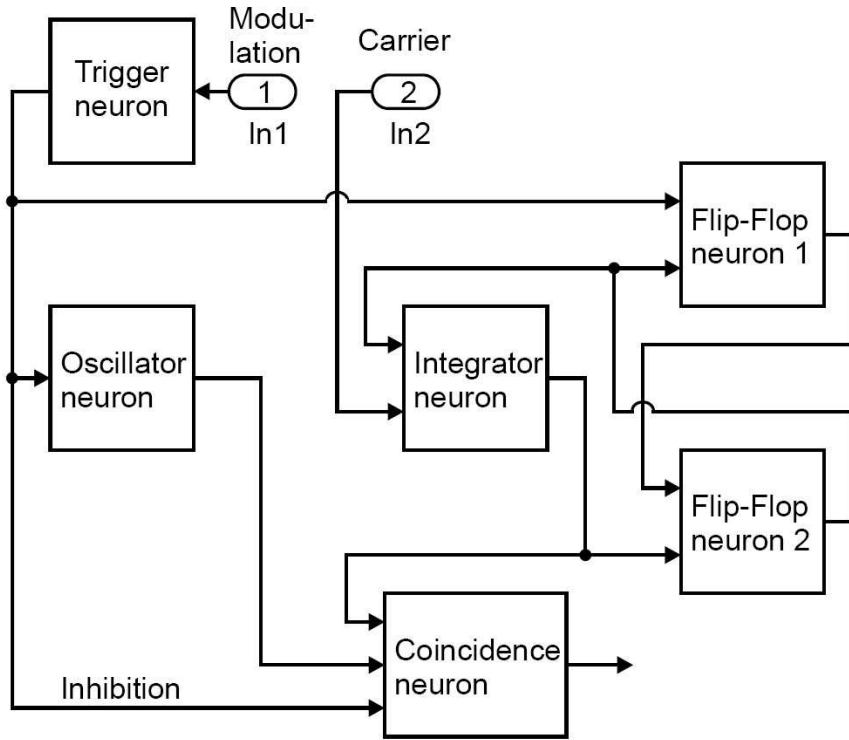


Figure 2.12: Block diagram of the periodicity model implemented in Matlab Simulink (from Voutsas et al., 2005).

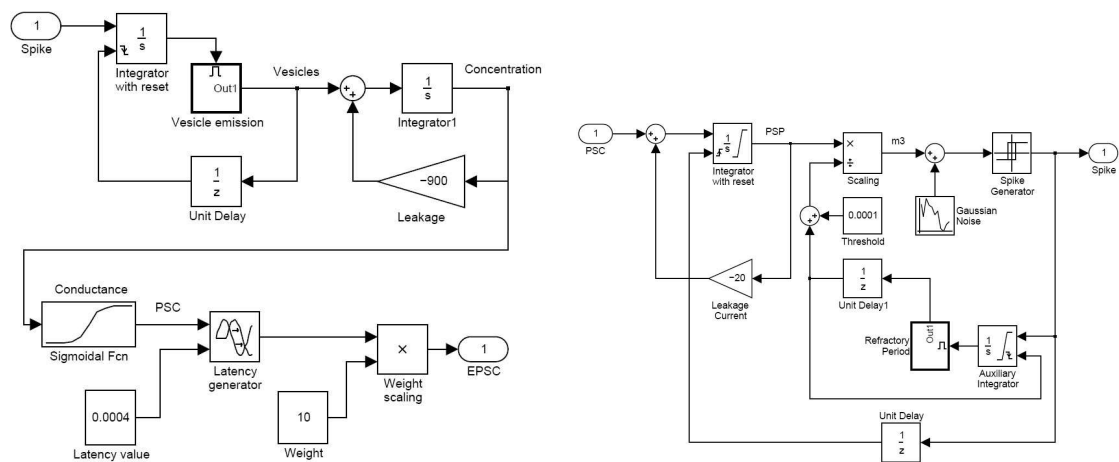


Figure 2.13: Block diagram of the used leaky integrate-and-fire synapse (*left*) and LIF soma (*right*) in Simulink. The functional principle of this synapse and soma is used in this work as LIF neuron models. Leakage currents and weights are variable (from Voutsas et al., 2005).

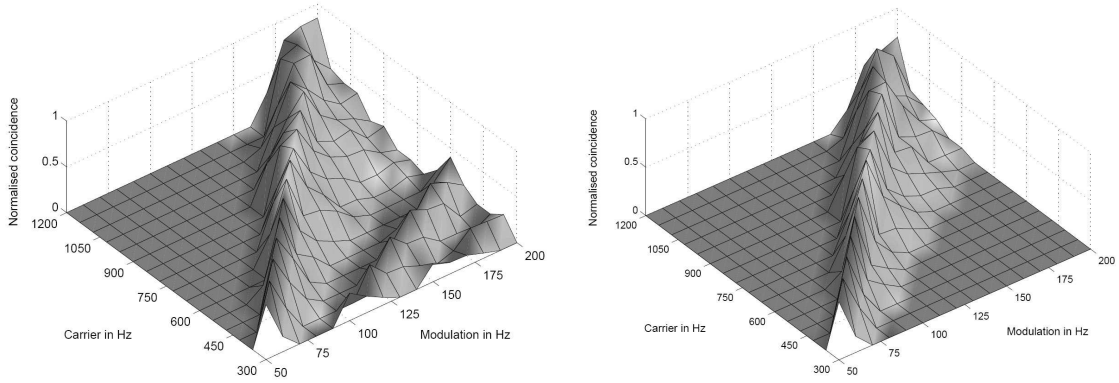


Figure 2.14: Simulation results of the periodicity model without (left) and with (right) an inhibitory connection. The response results from 16 periodicity models tuned to characteristic frequencies (CF) and best modulation frequencies (BMF) with the ratio 6:1 (CF/BMF). Stimuli are 256 combinations of 16 carrier and 16 modulation frequencies. The carrier frequency axes corresponds to the CF of one periodicity model (from Voutsas et al., 2005).

2.2.3 Hodgkin-Huxley (HH) model

Experiments of A. L. Hodgkins and A. F. Huxley in the early 1950s with the giant axon of the squid are the origin of most neuron models, which are described by the dynamic behaviour of channel kinetics. The work of these english physiologists led to a Nobel prize award. They developed a model fitting their experimental results, which can be described by several equations.

One part of their work was the description of the capacitive behaviour of the cell membrane by

$$C \frac{du}{dt} = -\sum_k I_k + I(t), \quad (2.4)$$

with $I(t)$ as an external current and $\sum_k I_k$ the sum of all ion currents through the cell membrane. The HH model describes three different channel or currents: a sodium (Na), a potassium (K) and a leakage current (L).

Thus, if Ohms law is applied ($I = g V$; g is the conductance) the sum of the currents is as follows:

$$\sum_k I_k = g_{Na}(u - V_{Na}) + g_K(u - V_K) + g_L(u - V_L) \quad (2.5)$$

The parameter g_i are the conductances of the corresponding channels and V_i are the Nernst equilibrium potential of the corresponding ions. u is the membrane voltage. Depolarization produces a transient increase in g_{Na} , and a slower and sustained increase in g_K . Immediately after a step depolarization g_{Na} is much greater than g_K , but after

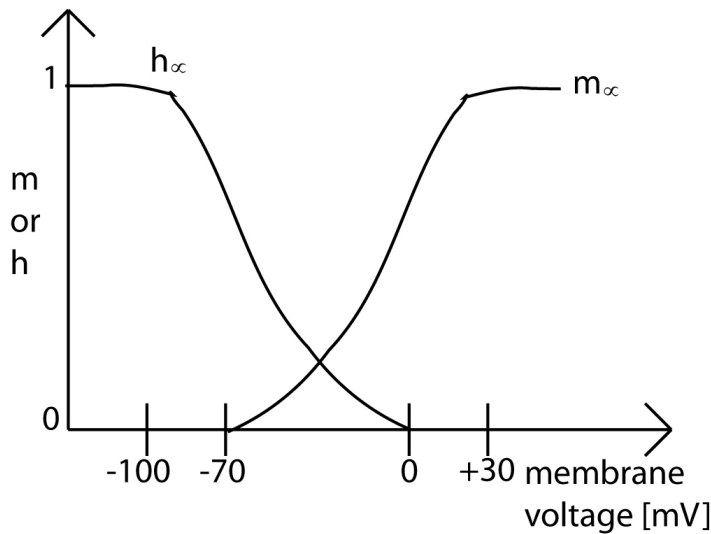


Figure 2.15: Voltage dependence of the activation variable m and inactivation variable h of the sodium channel of the Hodgkin Huxley model. The values are reached at each voltage after a long time. m and h are both voltage and time dependent.

the cell has been depolarized for a time, g_K becomes greater than g_{Na} . Hodgkin and Huxley introduced the variables m , h , and n to express the time and voltage dependence of the conductances:

$$g_K = n^4 G_K \quad (2.6)$$

$$g_{Na} = m^3 h G_{Na} \quad (2.7)$$

G_K and G_{Na} are the maximum conductances of the corresponding channel. In the following, only the mechanism for the sodium channel is described because it is the most difficult, but analogue to the potassium channel. The time progression of G_{Na} shows in the beginning a fast increase and then a slow decrease, which is the reason for choosing two variables m and h . The fast activation part is described by m , the slower inactivation part by h . Sodium passes the membrane through channel proteins in the membrane, and these can open and close. The variables m and h each change between 0 and 1 as functions of time and voltage. The power of the variables stand for the number of the “gates” in each activation and inactivation part. The functional role of these gates are described later. The product $m^3 h$ represents the fraction of the total sodium conductance at any given time. The graphs in Fig. 2.15 show the values reached by m and h when the membrane is held at various potentials for long times.

The variables m and h are also time dependent. To illustrate this, the modeled cell is kept at 0 mV for a long time, then voltage is stepped quickly to -70 mV. The variables

m and h change to new steady state values with a time progression depicted in Fig. 2.16. An important fact is that m changes quickly while h changes more slowly.

The concept of arbitrary variables might be confusing, but Hodgkin and Huxley suggested a simple physical model which may or may not represent reality. The sodium channel behaves as if it has two sets of gates. One set, the activation gates, opens fast when the cell is depolarized above a threshold voltage. The other gates, the inactivation gates, close slowly when the cell is depolarized.

For a single channel, the variable m described by Hodgkin and Huxley is the probability that 1 m gate will be in the open position. The variable m cubed is the probability that all three m gates will be open. When m is near 1, as it is when voltage is near 0 mV, there is a very high probability that all 3 m gates are open. When m equals 0, as it is when voltage is at the resting potential, there is a high probability that the three m gates are all shut. For a single channel, the variable h is the probability that the single h gate will be in the open position. When h equals 1 (near the resting potential), the h gate is likely to be open. When h equals 0, as it does in the steady state at depolarized voltages, the h gate is likely to be closed. The product m^3h is the probability that all of the gates are open, so that the channel can conduct sodium across the membrane. The detailed formulas for the variables are highly complex and nonlinear (see appendix). In Fig. 2.18 the different possible states of these gates at different times after a suprathreshold current injection are depicted.

2.2.4 HH model from Rothman and Manis (2003c)

Rothman and Manis developed a detailed HH-like model of VCN neurons which is described in three papers (Rothman and Manis, 2003a,b,c). In the first paper (Rothman and Manis, 2003a) their experimental results are described, the second paper (Rothman and Manis, 2003b) explains the fitting of the results with mathematical models, and in the third paper (Rothman and Manis, 2003c) a HH-like model is presented to simulate the electrical behaviour of VCN neurons and to give insight in the functional role of the channels for the physiological response properties of VCN neurons. They found that there are some currents that all VCN neurons have in common, others differ and can distinguish response pattern. In particular, they have shown that VCN neurons possess one or more distinct potassium currents, namely a rapidly inactivating current, a rapidly activating, slowly inactivating low-threshold current, and a non-inactivating high-threshold current. The potassium currents play a major role for spike shape, spike rate, spike adaptation, and regularity of discharge (Rothman and Manis, 2003a). The low-threshold, slowly non-inactivating potassium current is suggested to be the key for changing the response pattern from chopper-like to onset-like (Rothman and Manis, 2003c). Cells containing this current enter a high conductance state following an initial discharge (Rothman and Manis, 2003a) and do not fire any more. The low-threshold current has a low activation voltage (-70 mV). The high-threshold current is apparent

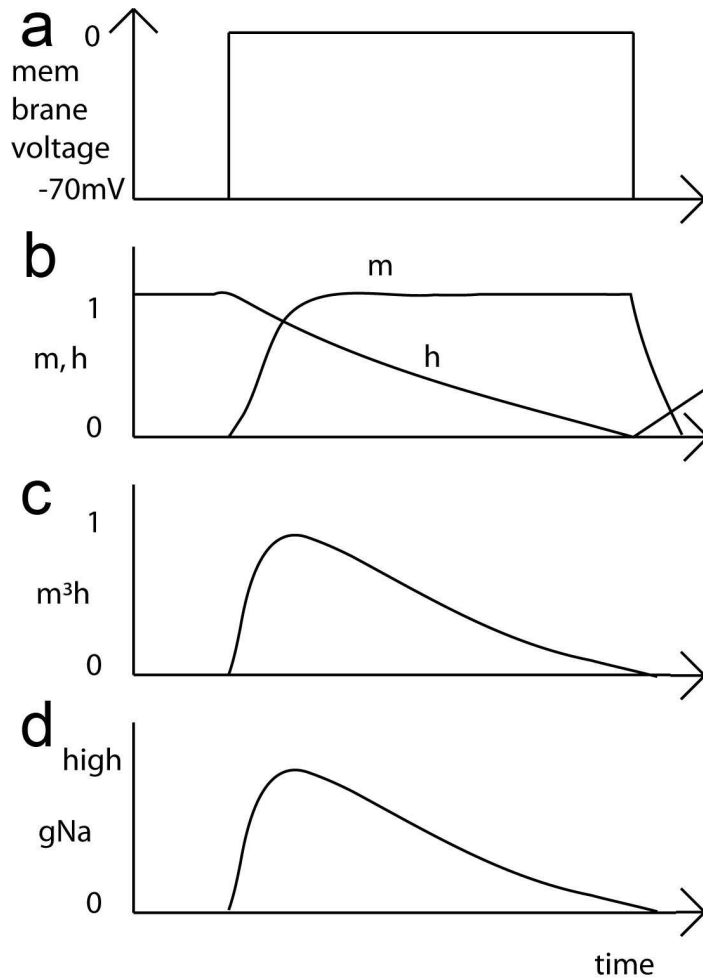
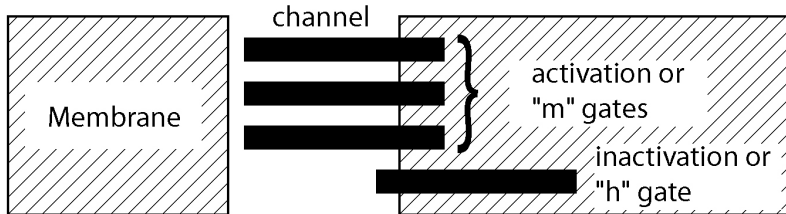


Figure 2.16: Time progression of the activation variable m and inactivation variable h of the sodium channel of the Hodgkin Huxley model after a voltage step (a). m and h are both voltage and time dependent. The time progression of m and h (b), of m^3h (c), which is the term in the HH model, and of the corresponding sodium conductance (d) is depicted.

Resting (polarized) membrane



Depolarized for long time

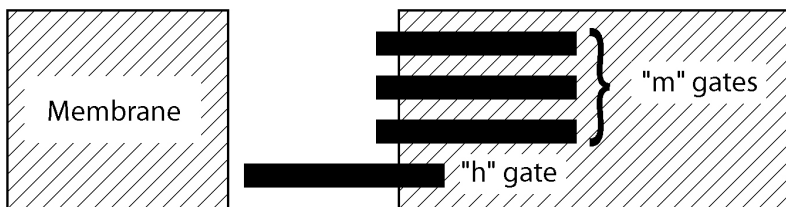


Figure 2.17: Explanation for the arbitrary variables m and h of the sodium channel. M is a set of three fast activation gates, and h is one inactivation gate. If the membrane is at the resting potential, the activation gates are closed and the inactivation gate is open, whereas if the membrane is depolarized for a long time the activation gates are open and the inactivation gate has closed.

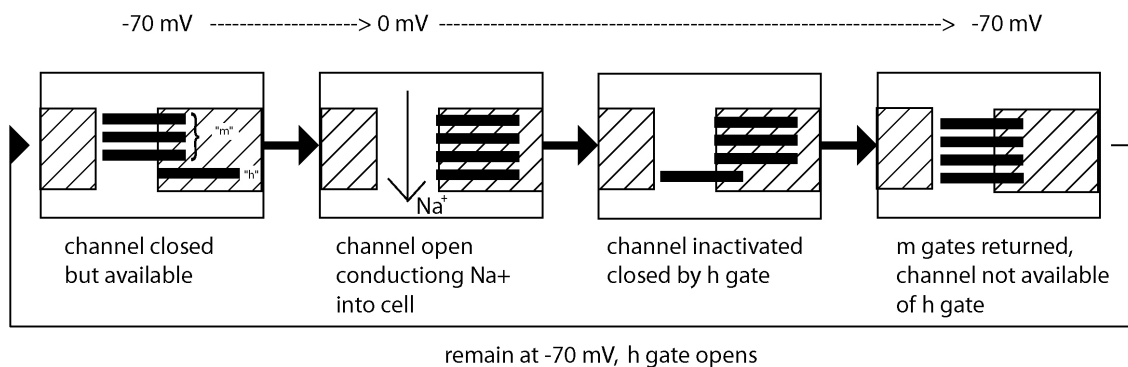


Figure 2.18: Scheme of the dynamic behaviour of the activation and inactivation variables m and h of the sodium channel in the HH model after a depolarization. Each step in the cycle from -70 mV to 0 and back is described in the figure.

in all VCN neurons (including stellate (choppers) and octopus cells (onset), see Bal and Oertel (2001)). The characteristics of this current are similar to the channel KCNC1, which is known to be expressed throughout the VCN and allows to fire at high rates by a rapid repolarization of their action potentials (Grigg et al., 2000).

The VCN model is described by the following equation:

$$C_m \frac{dV}{dt} = I_A + I_{LT} + I_{HT} + I_{Na} + I_h + I_{lk} + I_E - I_{ext} \quad (2.8)$$

with

C_m : membrane capacitance

I_A : fast inactivating K^+ current

I_{LT} : fast-activating slow-inactivating low-threshold K^+ current

I_{HT} : high-threshold K^+ current

I_{Na} : fast-inactivating Na^+ current

I_h : hyperpolarization-activated cation current

I_{lk} : leakage current

I_E : excitatory synaptic current

I_{ext} : external electrode current source

The detailed equations are shown in the appendix. In the following details of the low-threshold K^+ current are demonstrated because the presence of this current determines mainly the difference between a chopper and onset response pattern. The current is determined by the activation variable w and the inactivation variable z ,

$$I_{LT} = \bar{g}_{LT} \cdot w^4 z \cdot (V - V_K). \quad (2.9)$$

As described in Section 2.2.3, w^4 can be interpreted as four activation gates and z as one inactivation gate. The change of each variable is described by the differential equation

$$\frac{dx}{dt} = (x_\infty - x)/\tau_x \quad (2.10)$$

with x either w or z . The variables w and z are both voltage and time dependent by

$$w_\infty = [1 + \exp(-(V + 48)/6)]^{-1/4} \quad (2.11)$$

$$z_\infty = (1 - \zeta) \cdot [1 + \exp((V + 71)/10)]^{-1} \quad (\zeta = 0.5) \quad (2.12)$$

$$(2.13)$$

and

$$\tau_w \propto [6 \cdot \exp((V + 60)/6) + 16 \cdot \exp(-(V + 60)/45)]^{-1} + 1.5 \quad (2.14)$$

$$\tau_z \propto [\exp((V + 60)/20) + \exp(-(V + 60)/8)]^{-1} + 50. \quad (2.15)$$

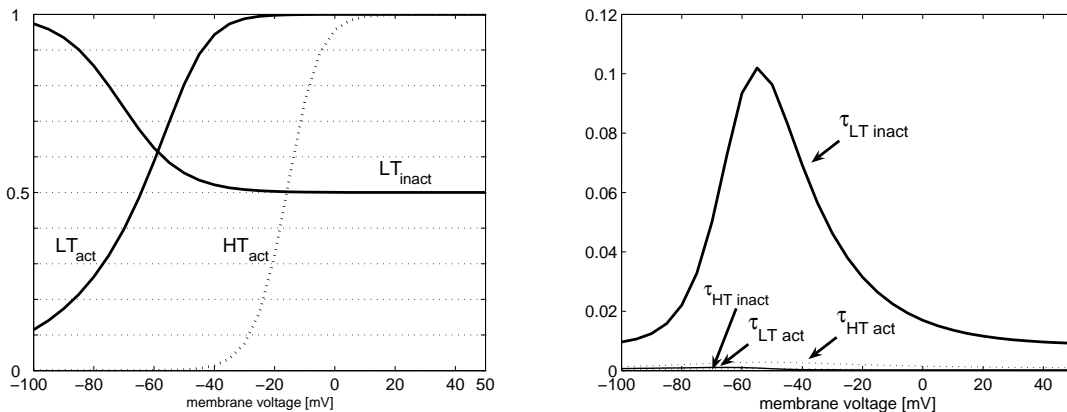


Figure 2.19: Activation and inactivation variables and time constants of the low threshold (LT) and the high threshold (HT) current. *Left:* The activation variable of the low threshold current is shifted to lower voltages in comparison to the one of the high threshold current. The inactivation variable of the low threshold current does not reach zero, that means the channel is never completely closed. *Right:* The time constant of the inactivation variable of the low threshold current is much higher than the other time constants of LT and HT currents.

The latter equations show that the time dependence is again voltage dependent. The corresponding curves for voltage dependence dependence are depicted in Fig. 2.19 (left) in comparison to high threshold current, and for the time dependences in Fig. 2.19 (right).

The voltage dependence shows that z_{∞} (the inactivation variable) does not reach zero if the voltage rises, which means that z gate does not close completely. This is in contrast to the inactivation variable in Fig. 2.15. The inactivating variable and the low threshold together with the slow time constant τ_z of the low threshold current (Fig. 2.19) is the major reason for typical onset behaviour of the cells with this current.

2.2.5 Compartment neuron model

In addition to the detailed description of the ion currents by the Hodgkin and Huxley model, compartment models introduce the spatial structure of the neurons in the model. The neuron is no longer a point-like unit, but the neuron and its dendrites and axons are described by equivalent electrical circuits (Fig. 2.20).

The dendritic tree or any other part of the neuron can be modeled in an optionally detailed way, but available calculation time limits the depth of simulated details. Compartment models are mostly used for simulation of single cells and small networks.

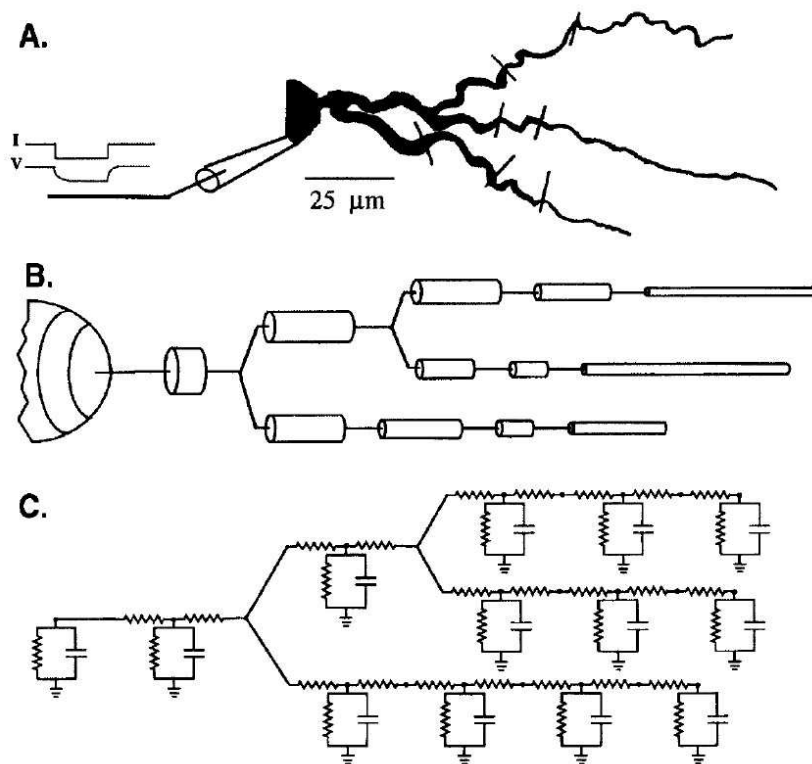


Figure 2.20: Procedure of building a compartment model. Neuroanatomical and neurophysiological data (A) are the basis for a cable model, which is divided in short sections (B). These sections are described by electrical circuits (C) (from Bower and Beeman, 1994)

1997). UNIX is the original operating system for NEURON, but it is also possible to run it on WINDOWS because an emulating software is part of the package. NEURON is often used because it is freeware and it features tools that can easily be used and fit experimental data mathematically. Besides, it is well-known and established in the neuroscience community, which means that many models of different cell types already exist. A great amount of models is stored in a world wide web database, called “ModelDB” (Migliore et al., 2003; Hines et al., 2004). The model of Rothman and Manis (2003c), which is also stored in the “ModelDB”, was simulated in this work in NEURON and Matlab.

Chapter 3

Oscillating neurons in the cochlear nucleus: I. Experimental basis of a simulation paradigm

3.1 Abstract

Anatomical and physiological auditory data and pitch measurements are presented including some additional analysis. The data provide the basis for a new computer model of sustained chopper neurons in the ventral cochlear nucleus. New and old evidence indicating a preference for multiples of 0.4 ms in oscillations of chopper neurons in the cochlear nucleus of different species such as man, cat, and Guinea fowl, is summarized. The hypothesis here is that the time constant of 0.4 ms is due to the minimum synaptic delay of chopper neuron connections. Anatomical findings show that chopper neurons are indeed connected and can excite each other; thus a model of a circular network of neurons that are connected via synapses with a delay of 0.4 ms is plausible. Results concerning frequency tuning and dynamical properties of periodicity encoding from chopper neurons are reviewed. Furthermore, it is concluded that chopper neurons receive input both from auditory nerve fibers and onset neurons.

3.2 Introduction

Oscillations are ubiquitous in biological organisms. In neuroscience, describing and understanding oscillations is crucial because they are a pervasive feature of signal processing in neuronal networks, and neuronal population oscillations are to be found throughout all kinds of neurobiological systems. Examples are pattern generating circuits in human and animal physiology (Glass, 2001). Furthermore, oscillations are supposed to play a role in consciousness and perception (Singer, 1998). Last but not least, high-

frequency (0.2-1 kHz) oscillations, so-called “intrinsic oscillations,” can be found in chopper neurons in the cochlear nucleus (CN), which seem to play a role in the processing of fast temporal signals.

Chopper neurons have an oscillating response pattern and multi-peaked PSTHs with relatively constant interspike intervals unrelated to the stimulus frequency and with the mean interspike interval and the standard deviation stable over the response time (Pfeiffer, 1966; Blackburn and Sachs, 1989; Winter et al., 2001; Wiegrebe and Winter, 2001) (see Section 3.3 for details). Among neurons in the auditory system, chopper neurons are outstanding because they show stable interspike intervals even when the amplitude of the incoming signal changes. As a consequence of findings from electrophysiological recordings in the auditory midbrain chopper neurons with a preference for interspike intervals which are multiples of 0.4 ms were included in a model of temporal processing of pitch (Langner, 1981, 1983, 1992; Rees and Langner, 2005). Similarly, a recent modelling study suggests that chopper neurons are involved in the transformation of a temporal pitch code into a place code (Wiegrebe and Meddis, 2004). In this chapter, old and new evidence for a preference for multiples of 0.4 ms in interspike intervals of chopper neurons will be summarized (see Section 3.5.1). In contrast to the model, which is introduced here, previous computer simulations can not explain this preference (e.g. Banks and Sachs, 1991; Hewitt et al., 1992; Wiegrebe and Meddis, 2004). The time constant of 0.4 ms is related here to the minimum synaptic delay of a chemical synapse (see Section 3.6.1) as reported by Li and Guinan (1971), Hackett et al. (1982), and Taschenberger and Gersdorff (2000). Similarly, Ferragamo et al. (1998a) found a synaptic delay of about 0.5 ms in T-stellate cells excited by interneurons. Accordingly, a synaptic delay of 0.4 ms was included in my computer simulation. As described in the following chapter, chopper neurons are set up in a network with excitatory interconnections and receive input both from the auditory nerve fibers and onset neurons. The intention is to test the role of interconnections and synaptic delays in the cochlear nucleus for the response patterns of these neurons.

Therefore this chapter is organized as follows:

Section 3.3 outlines some anatomical and physiological details of the cochlear nucleus, including some findings concerning statistics of chopper properties. Section 3.4 describes the methods used to analyze data from a previously published experiment. In Section 3.5, some experiments are reviewed and new results are presented to justify the idea of the simulation paradigm in the following chapter. Section 3.6 discusses the results of this evaluation and presents the main thesis.

Section 3.7 concludes the chapter with a summary of the main points and the consequences for the computer simulation.

3.3 Neuroanatomy and physiology of chopper neurons in the cochlear nucleus

The cochlear nucleus (CN) is divided into three sub-nuclei: the anterior ventral cochlear nucleus (AVCN), the posterior ventral cochlear nucleus (PVCN), and the dorsal cochlear nucleus (DCN, Osen, 1969). The auditory nerve projects tonotopically into all three of these areas and bifurcates into a ventral and dorsal branch. The ventral ascending branch crosses areas of the AVCN and makes contacts with cells via collateral endings, the dorsal descending branch innervates the PVCN and ends in the DCN (Arnesen and Osen, 1978). The CN contains a variety of cell types, e.g. stellate, octopus, and bushy cells (Osen, 1969). Physiological classification of cells in the CN is based on their different auditory response characteristics (Blackburn and Sachs, 1989). For example, multipolar stellate cells in the PVCN were characterized as chopper or onset (chopper-) neurons, and octopus cells as onset neurons (Ostapoff et al., 1994). T-stellate cells, a subclass of stellate cells named for their axons that run through the trapezoid body, have also been identified as chopper neurons (Oertel et al., 1990). They receive excitatory input from a small number of Type-I auditory nerve fibers and from collaterals of other T-stellate cells (Ferragamo et al., 1998a). Choppers seem to excite other choppers which are tuned to similar frequencies (Ferragamo et al., 1998a). After electrical stimulation of the nerve T-stellate cells respond with a delay between 0.48 ms and 0.92 ms (Ferragamo et al., 1998a). Allowing for a short travel time, these results indicate that the shortest synaptic delay from the AN-synapses is in the range of 0.4 ms which is here suggested as the minimum synaptic delay. Measurements of the fine-structure of the EPSP in T-stellate cells led to the conclusion that these cells receive only about 5 monosynaptic inputs from the auditory nerve. This suggests that their input covers only a small range of the frequency spectrum represented in the auditory nerve (Ferragamo et al., 1998a). These findings are in line with the model introduced here and suggest, as also stated by Ferragamo et al. (1998a), that other models requiring the integration of many inputs might be inappropriate (e.g Banks and Sachs, 1991).

Chopper neurons are characterized by spike trains with comparatively constant interspike intervals that are unrelated to the stimulus frequency and level (Pfeiffer, 1966). According to Blackburn and Sachs (1989), chopper neurons may be divided into the following subtypes: sustained choppers with constant interspike intervals, transient choppers with interspike intervals changing over time, and, onset choppers with prominent onset peaks.

Moreover, the authors suggested a further subdivision of choppers into transiently adapting choppers (a subtype of transient choppers), which show an abrupt increase of their mean interspike intervals followed by a plateau phase, and slowly adapting choppers (a subtype of transient and sustained choppers), which show a linear increase of their mean interspike intervals with time.

Although chopper neurons were found to be more sharply tuned than auditory nerve fibers, they have similar rate functions in response to auditory signals (Frisina et al.,

1990a).

Furthermore, auditory nerve, onset, and chopper neurons demonstrate a hierarchy both in the enhancement of encoding amplitude modulation (AM) and their latencies (Frisina et al., 1990a; Blackburn and Sachs, 1989; Rhode and Smith, 1986). Both auditory nerve fibers and VCN units show strong synchronous responses to low-intensity, low-frequency amplitude modulation, which decrease with increasing AM frequency (Frisina et al., 1990a). The dynamical range of periodicity encoding of VCN units is even larger than that of auditory nerve fibers. Onset units show the strongest synchronous responses of all VCN units, followed by chopper neurons, with the largest enhancement at high intensities (Frisina et al., 1990a). This hierarchy is the same for the encoding of AM frequencies between 20 and 1000 Hz. In the sample reported by Frisina et al. (1990a) both onset and chopper neurons tended to be tuned near 150 Hz. At low intensities chopper as well as onset units show a more low-pass characteristic, which changes into a more band-pass-like characteristic at high frequencies changes. Onset neurons show the largest response gain and are the best encoders for AM in the CN (Frisina et al., 1990a). Latency measurements suggest the following hierarchy: auditory nerve, onset neurons, onset chopper neurons, and other chopper neurons (Rhode and Smith, 1986; Young et al., 1988).

3.4 Methods

In this chapter certain data previously reported by Young et al. (1988) will be evaluated. Relevant details of their methods are therefore presented here. The stimuli used in their experiments were 25-ms tone bursts at the best frequency of the unit and were presented once every 200 ms. The rise/fall times of the trapezoidal envelopes tone bursts were 1.6 ms. The units were classified by their PSTH and by regularity analysis. In the case of chopper neurons, PSTHs showed regularly spaced peaks of discharge with spike intervals that were not related to the stimulus waveform (no phase locking). Regularity analysis was performed by measuring the mean and standard deviation of the interspike intervals. The coefficient of variation, which is a measure for the regularity of interspike intervals, separates regular (sustained) choppers ($CV < 0.35$) from irregular (transient) choppers ($CV > 0.35$).

Since the original data of the mean intervals could not be provided by the authors, results presented in Fig. 7 of their paper were digitised by using a data-thief program. In order to test that a preference for multiples of 0.4 ms exists in the raw data of the digitised interspike intervals of the 163 recorded chopper neurons, two classes of test-intervals were generated. The intervals of the first class were centered at multiples of 0.4 ms with an interval-width of 0.2 ms, and the remaining intervals of the second class were centered at multiples of 0.4 ms + 0.2 ms. The class centered at multiples of 0.4 ms contained 93 recorded interspike intervals of the chopper neurons, the other class 70 intervals.

3.5 Review of experiments on pitch perception and on the physiology of temporal coding

3.5.1 Evidence for preferred intervals of intrinsic oscillations

Evidence for a time constant of 0.4 ms in the inferior colliculus

Evidence for multiples of 0.4 ms of preferred intervals in intrinsic oscillations was first found in the central nucleus of the IC of Guinea fowls (Langner, 1981, 1983) and cats (Langner and Schreiner, 1988). They were described as brief bursts of spikes occurring at onsets of tones or of modulation cycles of amplitude modulated sounds. In the cat these oscillations were present in 30% of the samples and showed preferences for intervals that were multiples of the same base period of 0.4 ms. The intrinsic oscillations were only weakly influenced by changes of stimulus frequency or intensity (Langner and Schreiner, 1988). The distribution of single unit intervals with standard deviation of <10% in their PSTHs is shown in Fig. 3.1. Only the first interval of each oscillation was considered. As can be seen in Fig. 3.1, peaks are prevalent at intervals of 1.2, 1.6, 2.0, and 2.4 ms, which are all multiples of a base period of 0.4 ms. Since the IC receives a major input from chopper neurons of the CN (Adams, 1983), it was hypothesized that the origin of the intrinsic oscillations found in IC is the CN (Langner, 1992). Fig. 3.2 illustrates the responses of 13 units in the auditory midbrain of Guinea fowls to the onset of pure tones at the center frequencies of the units (Langner, 1983). The responses of the units reveal that neither the BF nor the frequency of the stimulus define the periods of the oscillations. The preference of integer multiples of 0.4 ms in the presented units is obvious.

Evidence for a time constant of 0.4 ms in pitch shift experiments

In a certain range the pitch of a SAM equals the pitch of the modulation frequency (f_m), provided the carrier frequency (f_c) is a multiple of it. However, when the carrier is varied, pitch deviates systematically from the pitch of f_m and changes linearly (first effect of pitch shift), corresponding approximately to the pitch of a subharmonic of the carrier (Schouten, 1970). The pitch shift effect was studied in detail by varying f_c of SAM signals in small steps (1%) and matching their pitch to the pitch of pure tones (Langner, 1981). The analysis of the pitch shift in terms of carrier and pitch period instead of the corresponding frequencies gave evidence for an underlying temporal correlation analysis. As an additional effect, steps with pitch values corresponding to periodicities in multiples of 0.4 ms were frequently observed in the resulting pitch curves (Fig. 3.3). A correlation mechanism was proposed as a model for the underlying neuronal pitch estimation in the time domain (Langner, 1981). It includes neuronal mechanisms which seem to offer an explanation not only for the pitch shift effect and

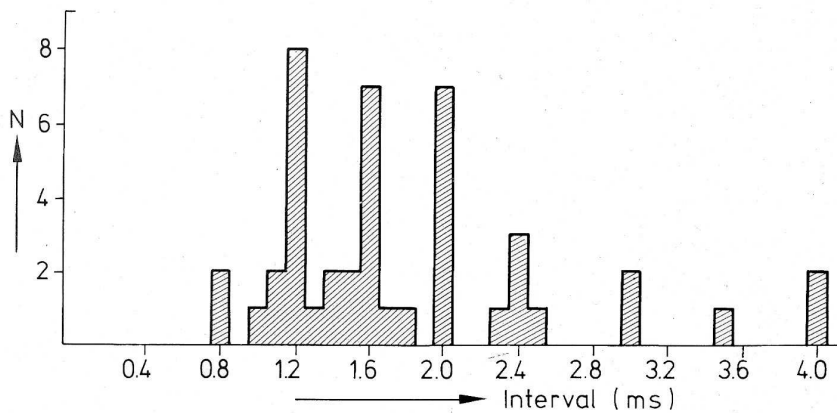


Figure 3.1: Distribution of neurons (IC of the cat) with the first interspike interval depicted on the x-axis. Peaks at multiples of 0.4 ms are clearly visible (data from Langner and Schreiner, 1988).

the steps in the pitch curve, but also for the responses of periodicity tuning of neurons in the midbrain. The model consists of an oscillator, a frequency reducer and a coincidence neuron, which are assumed to have their correlatives in chopper neurons in the VCN, pauser neurons in the DCN, and disc cells in the IC (Langner, 1992). In this model the oscillator plays a role as a time reference in pitch perception. It was postulated that the observed steps in the pitch curve result from a correlation process that includes the oscillation intervals of chopper neurons as a time reference.

Evidence for a time constant of 0.4 ms in the cochlear nucleus

Responses of units in the VCN of decerebrate cats were recorded by Young et al. (1988). A scatter plot of the interspike intervals for all the units is shown in Fig. 3.4 (Young et al., 1988, Fig. 7). The data presented in Fig. 3.4 were analysed for the preference of certain oscillation intervals. The mean intervals of regular and irregular chopper neurons are shown as a histogram (Fig. 3.5). Note that the variance of the modes in Fig. 3.5 seems to increase with the order of the modes.

The null hypothesis, which assumes that interspike intervals of chopper neurons are equally distributed, was tested statistically for the digitised raw data of Fig. 3.4 (see Methods for details). For this purpose two classes were generated. One class contained intervals centered at multiples of 0.4 ms with an interval-width of 0.2 ms, and the other class contained the remaining intervals, which have the same probability (0.5) for a hit. The null hypothesis was rejected for the binomial distribution ($p = 0.05$), indicating

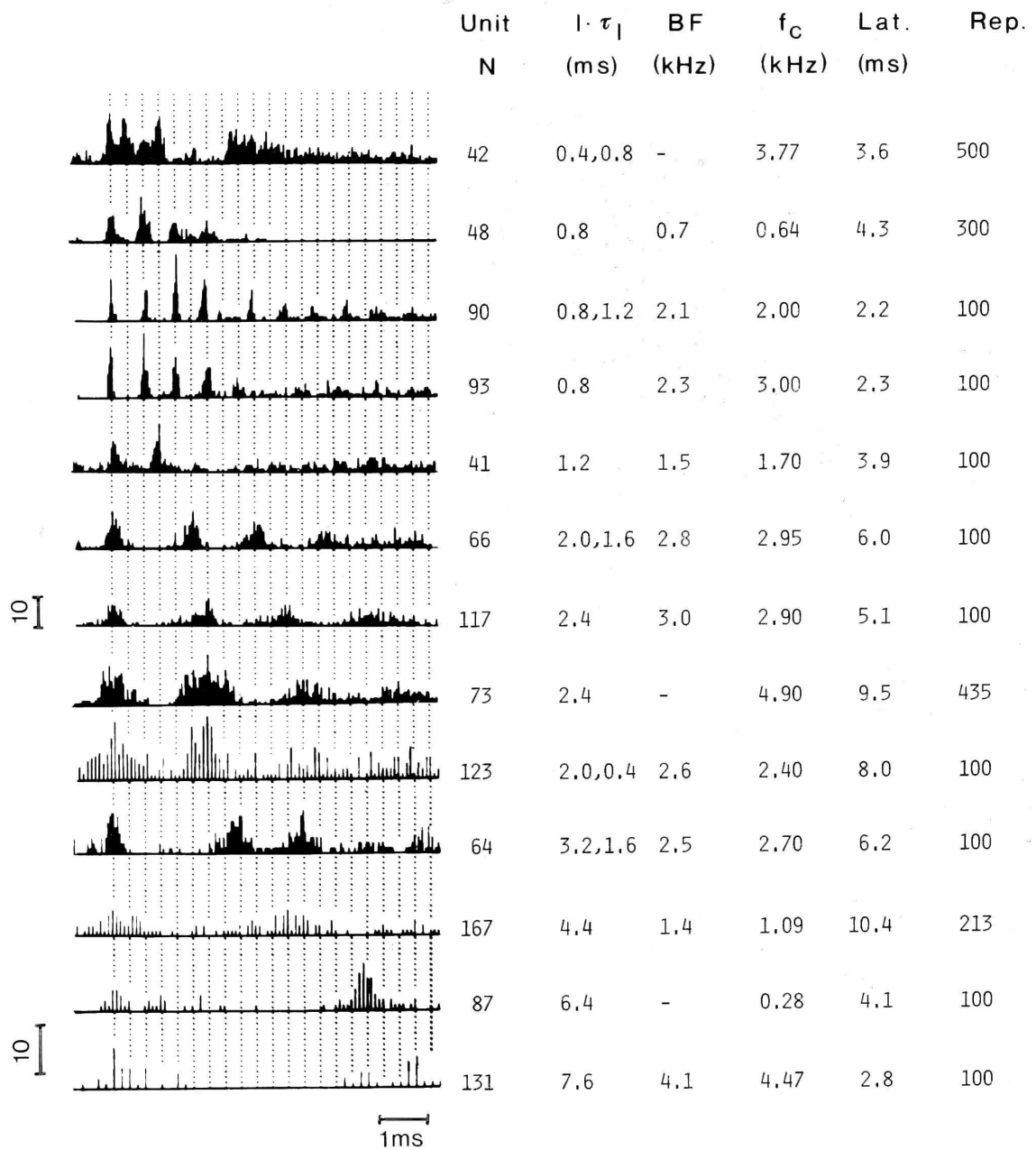


Figure 3.2: Intrinsic oscillations with periods in multiples of 0.4 ms in the midbrain of Guinea fowl (Langner, 1983). The scale for all of the x-axes is given by a bar at the bottom. The scales for the y-axes of the first 7 and the last 6 PSTHs are given by two bars on the left side. Six columns of numbers specify the units and the experiments: 1. unit number, 2. oscillation period, 3. best frequency, 4. stimulus frequency, 5. latency of the first maximum, 6. number of repetitions. The intervals between the dotted lines are 0.4 ms. The first maximum of each PSTH was adjusted to the first line.

that there is a significant preference for intervals centered at multiples of 0.4 ms.

3.5.2 Dynamic features of auditory nerve, onset-, and chopper neurons

Physiological data show that chopper neurons exhibit a dynamic range of periodicity encoding over up to over 90 dB, whereas auditory nerve fibers show only a dynamic range of only 30-40 dB (Frisina et al., 1985). There is a hierarchy of periodicity encoding in auditory nerve fibers, chopper neurons, and onset neurons. The best encoding of periodicity is by onset neurons (Frisina et al., 1990a). The difference in periodicity enhancement between onset neurons, chopper neurons, and auditory nerve fibers is shown in Figs. 3.6 and Fig. 3.7. In contrast to the high dynamic range of periodicity encoding of chopper neurons, their rate function may saturate within a range of 10 dB (Fig. 3.8), which is even smaller than the dynamic range of single auditory nerve fibers (Winter et al., 1990). Palmer et al. (1996) suggested that chopper units may respond as energy detectors, which have filtering characteristics that can be deduced from their pure-tone response areas. This sharp frequency tuning may be basically due to the input of a small number of auditory nerve fibers tuned to a narrow frequency range. However, the assumption that chopper neurons are involved in periodicity coding raises a problem: single fibers can not encode periodicity if the fiber is saturated, because in this situation, the modulation of the amplitude has no effect on the firing rate. Fibers saturate within a dynamical range of about 30-40 dB. Hence, if chopper neurons receive input only from sharply tuned auditory nerve fibers, they could only encode periodicity over a small dynamic range, which is not the case (see above).

3.6 Discussion

3.6.1 Rationale for a synaptic delay of 0.4 ms as a basis for an auditory time constant

As demonstrated above, evidence for a time constant of 0.4 ms emerges in recordings of neurons in the IC (Langner, 1981, 1983; Langner and Schreiner, 1988), in psychoacoustical experiments (Langner, 1981), and in recordings in the CN (Young et al., 1988). Consequently, a neuronal model for a temporal correlation analysis was suggested as a basis for pitch perception. This model included multiples of 0.4 ms as preferred intervals for intrinsic neuronal oscillations (Langner, 1983, 1992). Obviously, an explanation for the observation is required that the same time constant is apparent in different measurements and in various species such as man, Guinea fowl, and cat.

Several explanations for the observed interval preference may be considered:

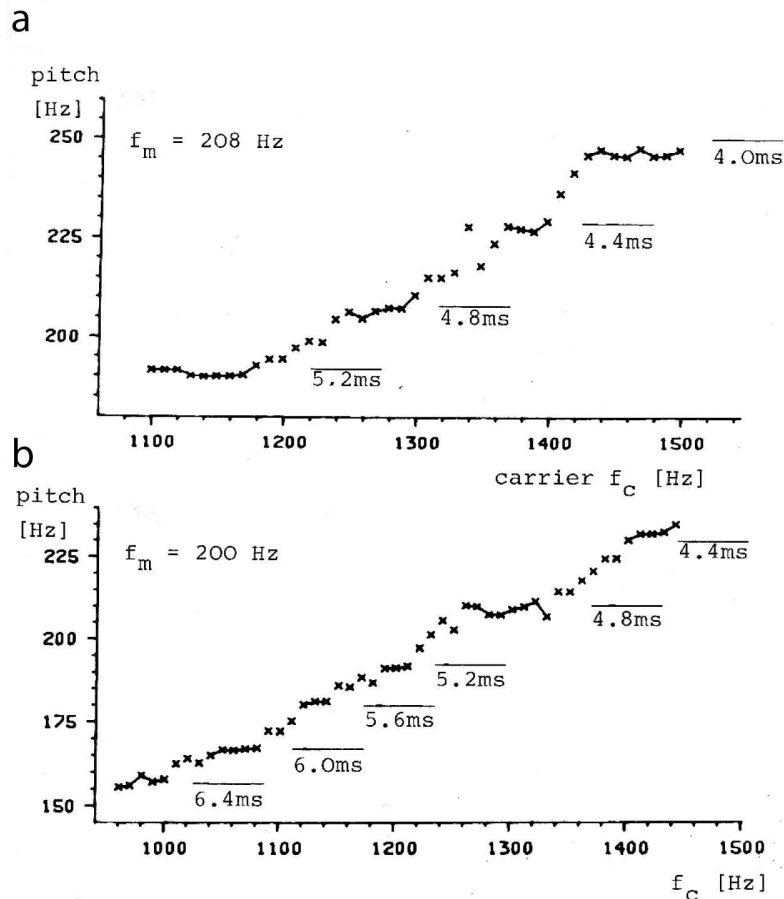


Figure 3.3: Psychophysical pitch measurements of SAM (Langner, 1981). a: Modulation frequency is 208 Hz, carrier frequency varies from 1100 Hz to 1500 Hz. b: Modulation frequency is 200 Hz, carrier frequency varies from 950 Hz to 1500 Hz. Both of the pitch curves show steps at multiples of 0.4 ms. It was proposed that the observed steps in the pitch curve result from the oscillations of chopper neurons which are part of a neuronal correlation analysis for pitch estimation.

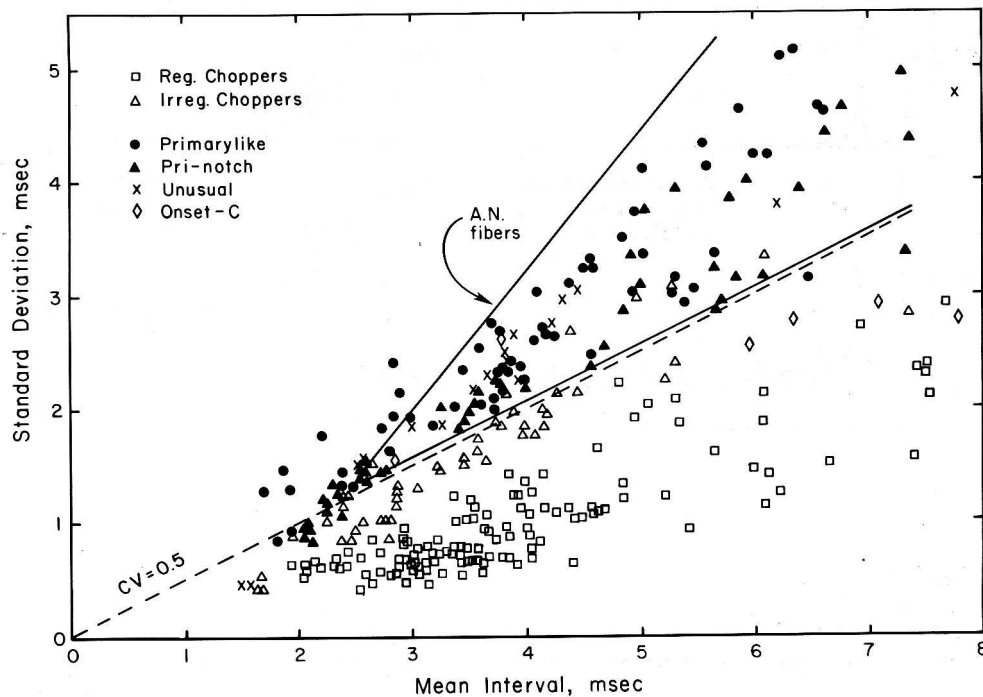


Figure 3.4: Regularity data of VCN neurons from Young et al. (1988). The x-axis shows values of mean interspike intervals, the y-axis shows values of the standard deviation for times between 12 and 20 ms after stimulation. The dashed line marks the CV which equals 0.5. A similar analysis of auditory nerve fibers results in data falling within the solid lines. The data include intervals from regular and irregular chopper neurons, primary-like and primary-like with notch neurons, unusual and onset neurons (for classification see: Blackburn and Sachs, 1989).

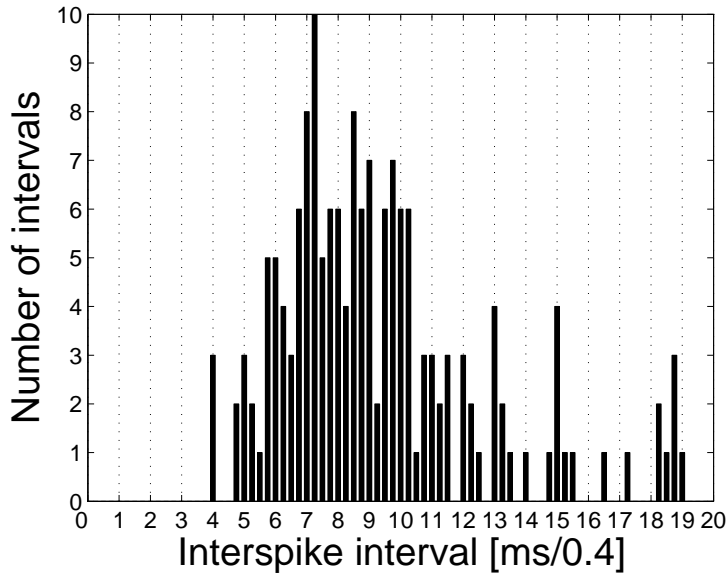


Figure 3.5: Histogram of interspike intervals (data from Fig. 3.4). The binwidth is 0.1 ms, the number along the x-axis indicates the lower edge of the interval.

1. The time constants are due to membrane properties.
Since time constants of membranes can be easily varied, it is difficult to understand why a preference for multiples of 0.4 ms would emerge in quite different species.
2. The time constant is based on axonal or dendritic delays.
Even in the case of slow neuronal velocity of 1 m/s, a time span of 0.4 ms results in a distance of 400 microns. For larger multiples of 0.4 ms, unrealistically long distances in neuronal circuits would be required. Again, it is difficult to understand why and how the same time constant is present in different animals.
3. The basis for the time constant of 0.4 ms is a synaptic delay introduced by a chemical synapse.
Processing times in the auditory system are the shortest in the brain. It may therefore be a reasonable assumption that optimization processes for auditory temporal processing resulted in the same synaptic delay of 0.4 ms in different species (Li and Guinan, 1971; Hackett et al., 1982; Taschenberger and Gersdorff, 2000).
A time constant based on the minimum synaptic delay would be the same in any kind of neuronal system working in the same temperature range.

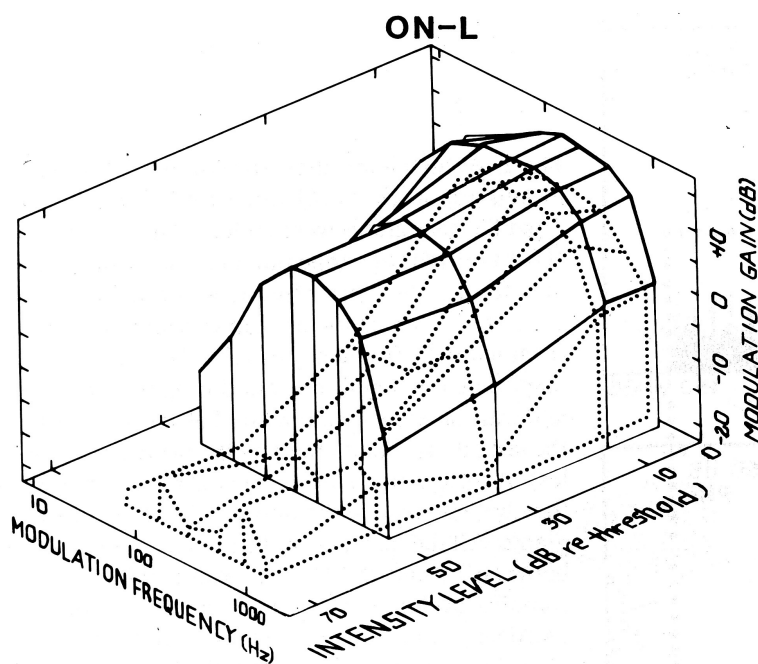


Figure 3.6: Response surfaces for the neuronal encoding of AM in onset neurons and auditory nerve fibers of the gerbil. The response of the onset neuron (solid line) is plotted over a corresponding surface of a typical auditory nerve fiber (dotted line). Onset neurons show a larger gain than chopper neurons and auditory nerve fibers (CF = 12.0 kHz, threshold = 33 dB SPL, stimulus modulation depth = 35%; plot copied from Frisina et al., 1990a).

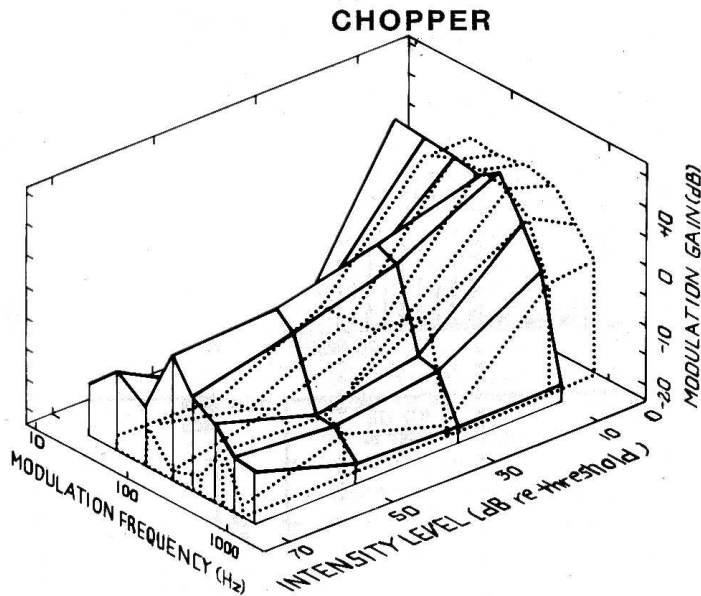


Figure 3.7: Response surfaces for the neuronal encoding of AM in chopper neurons and auditory nerve fibers of the gerbil. The response of the chopper neuron (solid line) is plotted over a corresponding surface of a typical auditory nerve fiber (dotted line). Chopper neurons show a larger gain than nerve fibers (CF = 9.9 kHz, threshold = 9 dB SPL, stimulus modulation depth = 35%; plot copied from Frisina et al., 1990a).

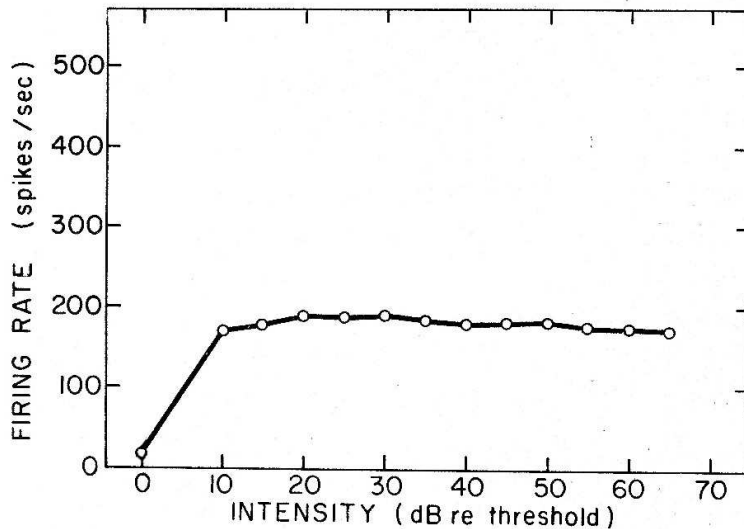


Figure 3.8: Rate-intensity function for a chopper unit in the VCN of an adult gerbil in response to a tone burst at the characteristic frequency (6.3 kHz, threshold 11 dB). The open circles indicate quasi steady-state rates measured during a 20-ms interval starting 25 ms after onset (redrawn from Frisina et al., 1990b).

3.6.2 Rationale for the integration of an input from onset neuron to chopper neurons

The high dynamic range of periodicity encoding as well as the rate function of chopper neurons described above can not be understood unless one assumes that their input comes from nerve fibers that code only a narrow frequency range. Two different mechanisms may provide an explanation of the dynamic features of chopper neurons:

1. Auditory nerve fibers from a broader frequency range around the CF may project to a chopper neuron.

Even if fibers close to the CF saturate, neighbouring fibers not yet saturated would still be able to encode periodicity. However, two facts contradict this theoretical solution:

- Chopper neurons are sharply tuned. If auditory nerve fibers from a wide frequency range would project to a chopper neuron this would not be the case. One might assume that lateral inhibition could sharpen the frequency tuning in spite of a broadband input, but tuning curves of chopper neurons seem to show no or only minimal lateral inhibition (Bourk, 1976; Caspary et al., 1994).
- If nerve fibers with different CFs projected to a chopper neuron, it would also result in a higher dynamic range of the neuron for pure tone responses. This is because with higher SPL off-CF fibers start to respond and to increase the firing rate of the chopper neuron. In contrast to this assumption, chopper neurons show an even smaller dynamic range of their firing rate than single auditory nerve fibers (Frisina et al., 1990b; Winter et al., 1990).

2. Onset neurons may activate chopper neurons.

Onset neurons show the best periodicity encoding in the VCN. Provided that they are able to trigger chopper neuron oscillations, they could enhance their periodicity encoding. The input of onset neurons from a broad frequency range permits periodicity encoding even if single auditory nerve fibers saturate.

Since chopper neurons code periodicity similarly to that of onset neurons and they are located close to these neurons, it seems reasonable to assume that they could receive an input from onset neurons which may be octopus cells. However, an actual connection between octopus cells and chopper neurons has not yet been demonstrated. Note that this model is in line with the assumption that onset-chopper neurons which have similar response properties as octopus cells trigger other chopper neurons.

3.7 Conclusions

3.7.1 Physiological and psychoacoustical data

- Multiples of 0.4 ms were demonstrated in intrinsic oscillations in the auditory system and in pitch shift experiments. The time constant of 0.4 ms is explained by the assumption of a minimum chemical synaptic delay of this size between chopper neurons.
- The large dynamic range of periodicity coding, the small dynamic range of pure tone response, and the sharp frequency tuning of chopper neurons can be explained by simultaneous projections from both the auditory nerve fibers and onset neurons to chopper neurons.

3.7.2 Simulation paradigm

As a consequence of the above conclusions, the topology of the simulation in the following chapter is as follows:

- To ensure the preference for multiples of 0.4 ms, chopper neurons are arranged in a circular network. The minimum number of two chopper neurons in this network corresponds to the proposed minimum refractory period of 0.8 ms.
- Chopper neurons receive input from both auditory nerve fibers and onset neurons.

Chapter 4

Oscillating neurons in the cochlear nucleus: II. Simulation results

4.1 Abstract

A computer model of sustained chopper neurons in the ventral cochlear nucleus is presented and investigated. In the previous chapter, the underlying neurophysiological and neuroanatomical data are demonstrated. To explain the preference of chopper neurons for oscillations with periods which are multiples of a 0.4 ms synaptic delay, a model is suggested of circularly connected chopper neurons. In order to simulate chopper neurons within a physiological dynamic range for periodicity encoding, it is necessary to assume that they receive an input from onset neurons. My computer analysis of the resulting simple neuronal network shows that it can produce stable oscillations. The chopping can be triggered by an amplitude modulated signal (AM). The dynamic range and the synchronous response of the simulated chopper neurons to AM are enhanced significantly by an additional input from onset neurons. Physiological properties of chopper neurons in the cat, such as mean, standard deviation, and coefficient of variation of the interspike interval are matched precisely by my simulations.

4.2 Introduction

In the previous chapter the physiological properties of chopper neurons are described in detail. Their outstanding constant interspike intervals, even if frequency and amplitude of a stimulus are changed, their preference for intervals that are multiples of 0.4 ms, and their dynamic ranges of both spike-rate in responses to pure tones and periodicity encoding are features that have to be attributed to neuronal mechanisms. Computer models based on membrane properties of single neurons (e.g. Banks and Sachs, 1991; Hewitt et al., 1992; Wiegrebe and Meddis, 2004) have suggested possible mechanisms

to explain the constant interspike intervals and to match the regularity analysis of chopper oscillations based on membrane properties of single neurons. However, the dynamic range and the preference for multiples of 0.4 ms in chopper intervals can not be explained by these models. Here the time constant of 0.4 ms is related to the minimum synaptic delay of chemical synapses (see previous chapter for details). Consequently, this synaptic delay is the basis for my simulation paradigm: chopper neurons are arranged in a network with excitatory interconnections. They receive input from both the auditory nerve and an onset neuron to guarantee precise timing, sustained chopping, and the dynamic range of chopper neurons for periodicity encoding and firing rate. This topology is an alternative to existing models and a new way to simulate chopper neurons. It is in line with the periodicity model (Langner, 1992; Rees and Langner, 2005) referred to in the previous chapter.

The chapter is organized as follows:

Section 4.3 describes the implemented neuronal models and the topology of the network.

Section 4.4 presents the results and compares them to physiological data.

Section 4.5 provides a discussion of the results.

Finally, Section 4.6 presents conclusions and highlights different aspects of the model.

4.3 Neuronal modelling

4.3.1 Methods

Implementation

The commercial software “Matlab” (The MathWorks, Inc.) was used as the simulation environment because of its visualisation abilities and also because it is in common usage. The differential equations are numerically realized by the Euler method in “Matlab”. Time steps of 25 μ s were sufficient for the relevant time scales of about 0.1 ms. Signal, onset neuron, and chopper neurons are implemented as script-files, and ANF response is calculated within a mex-file in “Matlab”. Programs were executed on a PC with 2.0 GHz and 512 MB RAM.

Signals

In the model, SAMs with different modulation depths and constant carrier and modulation frequency were used as input signals. They represent the sound pressure of acoustic signals and were presented directly as an input to a hair cell model. In Fig. 4.1 a typical SAM is plotted.

Mathematically, a SAM is described by

$$SAM = \sin(2\pi f_c t) \cdot (1 + m \cdot \cos(2\pi f_m t)) \quad (4.1)$$

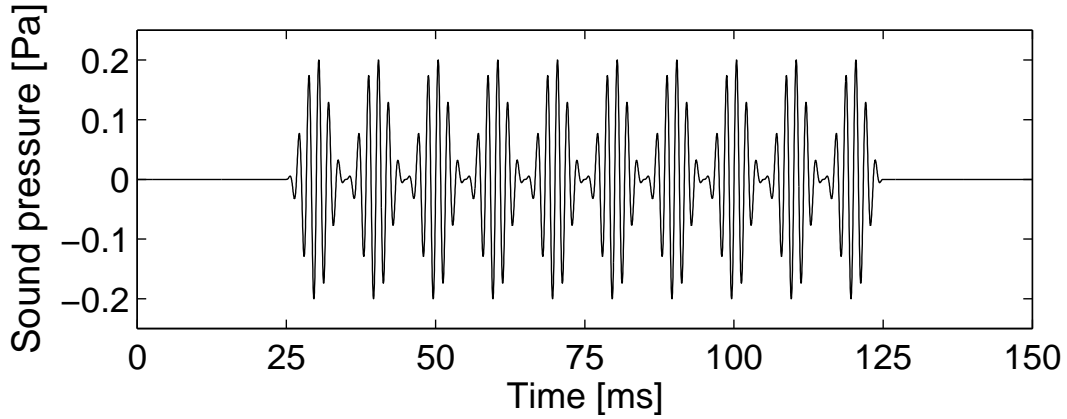


Figure 4.1: SAM as a standard input signal of the simulations. SAM is depicted in the time domain. The ordinate shows the sound pressure of the signal. The carrier frequency is 600 Hz, the modulation frequency 100 Hz. The modulation depth is 100%.

$$\begin{aligned}
 &= \sin(2\pi f_c t) + \\
 &\quad + \frac{1}{2}m \cdot \sin(2\pi(f_c + f_m)t) \\
 &\quad + \frac{1}{2}m \cdot \sin(2\pi(f_c - f_m)t), \tag{4.2}
 \end{aligned}$$

where f_m and f_c are the modulation and the carrier frequency, respectively. The frequency of the sidebands are denoted by $f_c \pm f_m$, the modulation depth by m .

In the following an unmodulated signal is indicated by a modulation depth of 0%. In the simulations 2 standard signals are mainly used:

- “Standard tone”:

frequency 600 Hz

- “Standard SAM”:

carrier frequency 600 Hz,

modulation frequency 100 Hz,
modulation depth 100%.

These stimulation parameters are for signals in electrophysiological experiments (Batra et al., 1989; Heil et al., 1995; Langner and Schreiner, 1988; Mueller-Preuss et al., 1994).

4.3.2 Simulation paradigms: “Circular oscillator” and “Multi-oscillator”

Physiological and anatomical findings presented in the previous chapter led to the following simulation paradigm:

1. Chopper neurons are arranged in a circle, where each neuron can activate its subsequent neighbour.
2. The first of two additional inputs is transmitted via five synapses from auditory nerve fibers.
3. The second additional input comes from an onset neuron and activates only one of the choppers in the circle.
4. As an alternative topology, two or three chopper neurons which are connected as described above operate as a pace-maker and project to other chopper neurons that have a larger refractory period. This reduces the number of chopper neurons that are required to produce interspike intervals greater than 0.8 ms (Fig. 4.3).

The two different simulation topologies are shown in Figs. 4.2 and 4.3, referred to in the following as “circular oscillator” and “multi-oscillator”, respectively. The input signal of the chopper circuit is a transformation of a sound signal that is processed in the cochlea and translated into spikes (detailed description in the subsequent sections). The spikes travel along the auditory nerve which projects to both chopper and onset neurons. Onset neurons are innervated by a broadband input from the auditory nerve that is weighted in a Gaussian shape. In accordance with the estimates of Ferragamo et al. (1998a) chopper neurons receive 5 inputs from the auditory nerve. Chopper neurons are connected to each other in a circular unidirectional way as shown in Fig. 4.2. Input from the nerve depolarizes the membrane of the chopper neurons. This change in membrane voltage enables chopping but does not initiate it. The reason is that the weights of auditory nerve synapses are adjusted in such a way that auditory nerve input alone can not drive the membrane voltage to threshold. Instead, chopping is initialized by a spike from the onset neuron. In Fig. 4.3 two or three fast chopper neurons are again arranged again in a circular network. These neurons act as a pace-maker with a clock-rate of 0.4 ms and project to slower chopper neurons which, due to their larger refractory period, skip shorter intervals while leaving intervals which are

multiples of 0.4 ms. With this topology, the number of neurons required for long ISI and the redundancy of phase information is diminished in comparison to the previous topology.

4.3.3 Modelling of inner ear, hair cell, and auditory nerve fibers

Inner ear

A wave-digital filter model describes the vibrations of the basilar membrane on the basis of the passive inner ear hydrodynamics; it consists of 125 mass-spring resonators that are connected by a coupling-mass (Strube, 1985; Zwicker, 1986). In order to simulate outer hair cell functions, the amplitude of the vibration of the basilar membrane is amplified and the travelling-wave along the basilar membrane is sharpened at low levels. This is performed by second-order resonators that are added at the outputs of the cochlear filter bank. The quality factors of the resonators are altered in every iteration step depending on the displacement of each resonator. Four stages of resonators are cascaded to achieve physiological amplification and reasonable filter shapes.

Inner hair cell model and auditory nerve fibers

The stereociliary bundles of the sensory cells are deflected by fluid motion from the movements of the basilar membrane (Mountain and Cody, 1999). When the hair bundle is deflected, ion channels open and K^+ -ions diffuse into the cell. The diffusion depolarizes the inner hair cell membrane. Due to this depolarization, Ca^{2+} -ions enter the cell through voltage activated Ca-channels. High Ca^{2+} -concentration within the cell leads to a fusion of synaptic vesicles with the cell membrane (Beutner et al., 2001; Moser and Beutner, 2000). The neurotransmitter produces an action potential at the postsynaptic membrane. As there is a depletion of vesicles, spiking probability of the auditory nerve is diminished after a strong stimulus (adaptation). The model also includes a refractory period of about 1 ms (Carney, 1993). Randomness of the nerve action potentials is due to statistical vesicle fusion. One inner hair cell is connected to 20 synapses of the auditory nerve.

4.3.4 Theory of the implemented neuronal models

The implemented neuronal network (Figs. 4.2, 4.3) consists of the following different types of neurons.

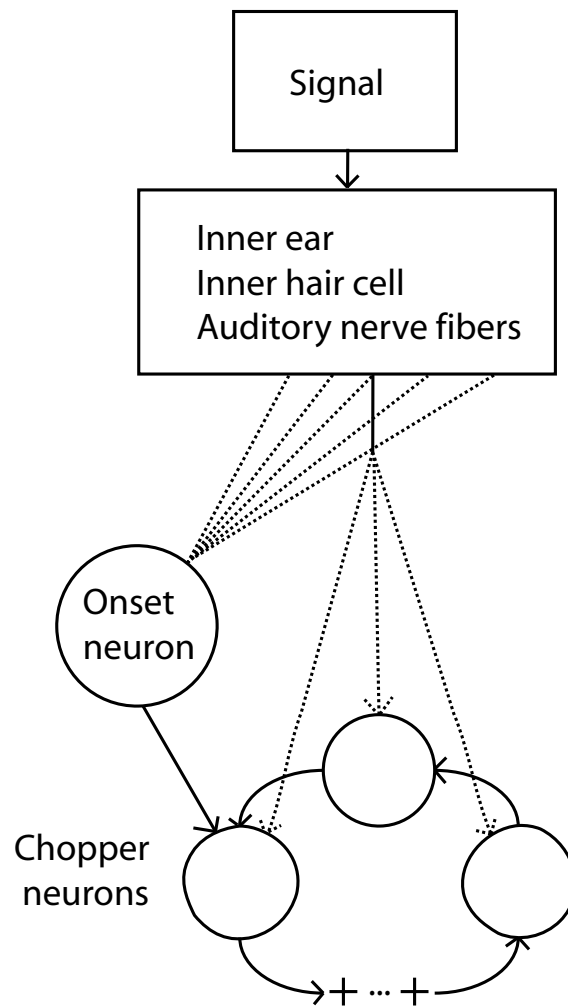


Figure 4.2: Scheme of the simulation topology I (“circular oscillator”). The signal is processed by a model of the inner ear, inner hair cells, and auditory nerve fibers. In the next processing step, 5 inputs from the nerve converge on each chopper neuron, the onset neuron receives its broadband input from the auditory nerve and excites one chopper neuron. The chopper neurons are arranged serially in a circle and can excite each other.

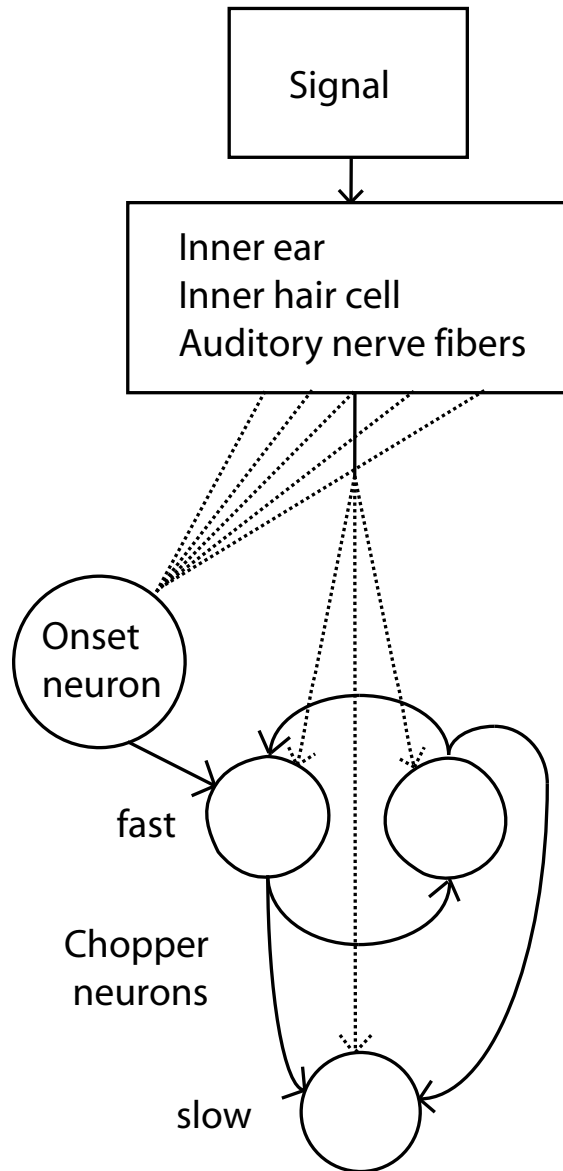


Figure 4.3: Scheme of the simulation topology II (“multi-oscillator”). The signal is processed by a model of inner ear, inner hair cells, and auditory nerve fibers. In the next processing step, 5 inputs from the nerve converge on each chopper neuron, the onset neuron receives its broadband input from the auditory nerve and excites one chopper neuron. Two (or three) fast chopper neurons are arranged in an unidirectional circle. They can excite each other, and project as a pace-maker to slower chopper neurons.

g_{Na}	1000 nS
g_{LTK}	200 nS
g_{lk}	2 nS
τ_E	0.1 ms
V_{Na}	55 mV
V_{LTK}	-70 mV
V_{lk}	-65 mV
V_E	0 mV
$V_{threshold}$	-62.2 mV
V_{rest}	-63.6 mV
C_m	12 pF

Table 4.1: Simulation parameters for the onset neuron.

Onset neuron

The onset neuron is a simplified version of the model that was proposed by Rothman and Manis (2003c) and is based on Hodgkin-Huxley equations. The model consists of a sodium (I_{Na}), a low-threshold potassium (I_{LTK}), an excitatory synaptic (I_E) and a leakage (I_{lk}) current. The time dependent conductance change g_E in response to an excitatory synaptic input is modelled as described in equation 4.8 (first proposed by Rall, 1967). Thus the change of the membrane potential is

$$C_m \frac{dV}{dt} = I_{LTK} + I_{Na} + I_{lk} + I_E, \quad (4.3)$$

with

$$I_{LTK} = \bar{g}_{LTK} \cdot w^4 z \cdot (V - V_{LTK}), \quad (4.4)$$

$$I_{Na} = g_{Na} \cdot m^3 h \cdot (V - V_{Na}), \quad (4.5)$$

$$I_{lk} = g_{lk} \cdot (V - V_{lk}), \quad (4.6)$$

$$I_E = g_E \cdot (V - V_E), \quad (4.7)$$

$$g_E = \bar{g}_E(t/\tau_E)e^{1-(t/\tau_E)}, \quad (4.8)$$

where C_m is the membrane capacitance and V the membrane potential. The reversal potential of K^+ , Na^+ , and of other ions is denoted by $V_{LTK,Na,\dots}$, the peak conductance of the LTK^- , Na^+ , and of other channels by $\bar{g}_{LTK,Na,\dots}$, the time constant by τ_E . The activation variables are w and m , and the inactivation variables are z and h .

The low threshold of the potassium current is the major cause of the onset behaviour (Rothman and Manis, 2003c, see Section 4.4.2). Simulation parameters of the onset neuron are listed in Table 4.1.

Chopper neurons

Chopper neurons are modelled as leaky integrate-and-fire neurons with synapses (Bleeck, 2000). The synapses are modelled as follows. Following an action potential in a presynaptic neuron, vesicles discharge transmitter into the synaptic cleft. The emission of vesicles (E , see equation 4.9) is simulated by use of a look-up table. The transmitter molecules are assumed to diffuse to the postsynaptic neuron. The decay of transmitter (T , see equation 4.10) is simulated by a leaky integrator. The probability of open channels for certain ions increases as the concentration of transmitter in the cleft becomes higher. Different ions constitute either excitatory or inhibitory postsynaptic currents (PSC, see equation 4.11). A hyperbolic tangent function simulates the conductance. A time delay with adjustable jitter (parameters: mean and standard deviation) that stands for the overall transmitter diffusion time was integrated in the simulation (equation 4.12). The synapse model is described by

$$E(t) = \begin{cases} E_{max} \cdot \frac{t}{t_{max}/2} & \text{if } 0 < t \leq t_{max}/2 \\ E_{max} \cdot (1 - \frac{t}{t_{max}/2}) & \text{if } t_{max}/2 < t < t_{max} \\ 0 & \text{else,} \end{cases} \quad (4.9)$$

$$\tau_{syn} \frac{dT(t)}{dt} = T(t) + E(t), \quad (4.10)$$

$$PSC(t) = w \cdot (\tanh(10 \cdot T(t) - 5) + 1)/2, \quad (4.11)$$

$$PSC_L(t + L) = PSC(t). \quad (4.12)$$

In the equations, $E(t)$ is the emission of vesicles, E_{max} the maximum emission, t_{max} the maximum emission time (0.2 ms). τ_{syn} denotes the time constant of the synapse, $T(t)$ the transmitter concentration, $PSC(t)$ the postsynaptic current, $PSC_L(t)$ the postsynaptic current with latency, L the latency, and w the weight of the synapse.

The soma of the simulated chopper neuron is based on a leaky integrate-and-fire model. The incoming postsynaptic currents from the synaptic inputs are integrated and build up a postsynaptic potential while a leakage current diminishes the input. If the potential reaches a defined threshold, a spike is elicited and the potential is set to zero. An absolute and relative refractory period (exponentially decreasing) ensures that spike generation is suppressed or needs stronger input for a selectable period of time. Therefore, the change of the soma potential is described by

	τ [ms]	Weight [a.u.]
Soma c.n.	0.33	
Syn. from c.n.	0.25	0.7
Syn. from o.n.	0.1 - 1.3	0.5 - 20
Syn. from a.n.	0.77	0.09 - 0.15
Abs. r.p.	0.6-2 ms	
Rel. r.p.	0-0.2 ms	

Table 4.2: Simulation parameters for the model of the chopper neurons (c.n.: chopper neuron, o.n.: onset neuron, a.n.: auditory nerve, Abs. r.p.: absolute refractory period, Rel. r.p.: relative refractory period. Both periods refer to the soma). The model is a leaky integrate-and-fire model and consists of a soma and synapses. The time constant refers to the leakage currents of the soma and synapses. The weights of the auditory nerve synapses are summed.

$$\tau_{som} \frac{dPSP(t)}{dt} = PSP(t) + R \cdot PSC(t) \quad \text{with} \quad (4.13)$$

$$PSP(t) = 0 \quad \text{if } PSP > thrs(t), \quad (4.14)$$

and the elicited action potentials (APs) are

$$AP(t) = \begin{cases} 1 & \text{if } PSP > thrs(t) \\ 0 & \text{else,} \end{cases} \quad (4.15)$$

where $PSP(t)$ is the postsynaptic potential, τ_{som} the time constant of the soma, R the resistance of the membrane, and $thrs(t)$ the threshold, which depends on the absolute and refractory periods.

Simulation parameters are displayed in Table 4.2. In real chopper neurons it is expected to find a distribution of the refractory period around 0.8 ms in the case of the fast chopper neurons. The time constant of the soma is set to a relatively low value to ensure fast chopping. The slow chopper neurons of multi-oscillator can have longer time constants because their chopping frequency is much lower. The summed weight of the synapses of the nerve is on average 8 times lower in the simulations than the weights of the synapses of the chopper and onset neuron. An excitatory postsynaptic potential just depolarizes the membrane slightly in order to enable chopping. This weak auditory nerve input does not mean that the overall response of the chopper neuron is low because the network plays also an important role. The refractory time matches the adjusted interval of chopping.

4.4 Results

4.4.1 Simulation of auditory nerve fibers

Fig. 4.4 shows the response of auditory nerve fibers (ANFs) to the “standard SAM”. The values along the left y-axis indicate the cochlear frequency channels, the right y-axis shows the mapping of the frequencies to their cochlea location according to Greenwood (1990). Fig. 4.4 demonstrates that the modulation and the carrier frequencies are encoded by the response of the auditory nerve. The modulation of the signal is encoded by the ANFs, provided their response is not saturated. In Fig. 4.5a, the result of 50 responses of the auditory nerve at CF = 600 Hz can be seen. The signal is the “standard SAM” (Fig. 4.1). The APs of the ANFs reflect the modulation and the carrier frequency. As expected, the fine-structure of this response shows only the positive half-waves of the incoming signals. Fig. 4.5a shows the PSC of 5 synapses. The response to the modulation frequency of 100 Hz is obvious, while the response to the carrier frequency is slightly blurred. This is due to the combination of the adjusted time constants of the synapses, carrier frequency, and modulation frequency. Within a modulation cycle the membrane voltage shows a phase of de- and repolarization (Fig. 4.5c).

4.4.2 Simulation of onset neurons

I modified a model of VCN onset cells with several potassium channels and different thresholds (Rothman and Manis, 2003c). In order to decrease the number of parameters and calculation time of the simulation, I reduced the number of channels without influencing the predominant onset behaviour. Each onset neuron in the simulations (characterized by its CF) receives a Gaussian weighted input ($W(channel)$, equation 4.16) of auditory nerve fibers, which is described by

$$W(channel) = \frac{1}{\sigma\sqrt{2\pi}} \cdot e^{-\frac{1}{2}\left(\frac{\Delta_{ch}}{\sigma}\right)^2}, \quad (4.16)$$

where Δ_{ch} denotes the distance to CF in number of channels (the curve is centered at CF of the onset neuron).

The variation of σ changes the width of the integration of frequency channels from the cochlea. Fig. 4.6 shows the distribution of the weights of the channels next to CF for $\sigma = 8$ and $\sigma = 16$ (σ has no dimension).

Real onset neurons may integrate the input over approximately one-third of the tonotopic array of the auditory nerve fibers (Palmer et al., 1996; Oertel et al., 2000; Golding et al., 1999). At low levels, the fibers with CF at the carrier frequency can carry periodicity information by synchronization. At higher levels, these fibers saturate and

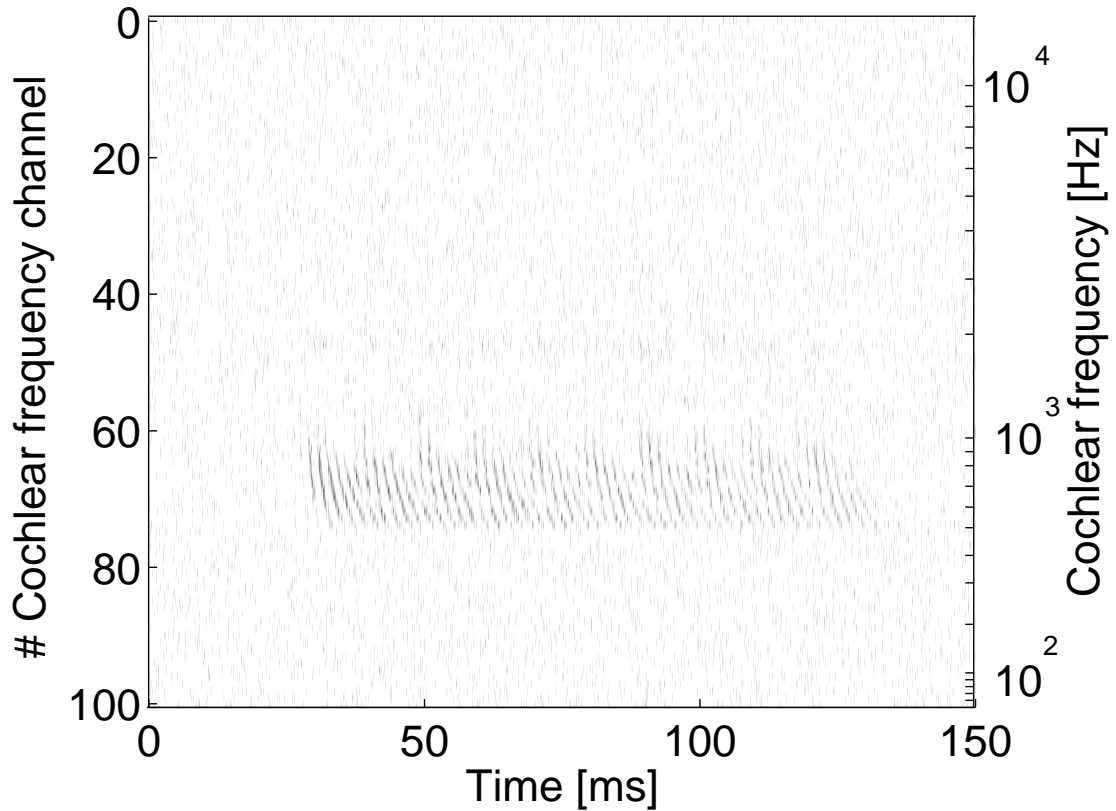


Figure 4.4: Response (APs) of the auditory nerve fibers to the “standard SAM”. On the left side, the frequency channels are indicated, and on the right side the corresponding frequencies are indicated. The frequency mapping of the channels is nearly logarithmic (Greenwood, 1990). Each channel can have several APs at the same time because it represents several nerve fibers. The number of APs is encoded by the darkness of the markers at a given location. The stimulus starts at 25 ms, has a duration of 100 ms and a level of 11 dB SPL. Obviously, the carrier and the modulation frequency are coded by APs within the range of about 10 frequency channels (65-75). The remaining channels show only spontaneous activity.

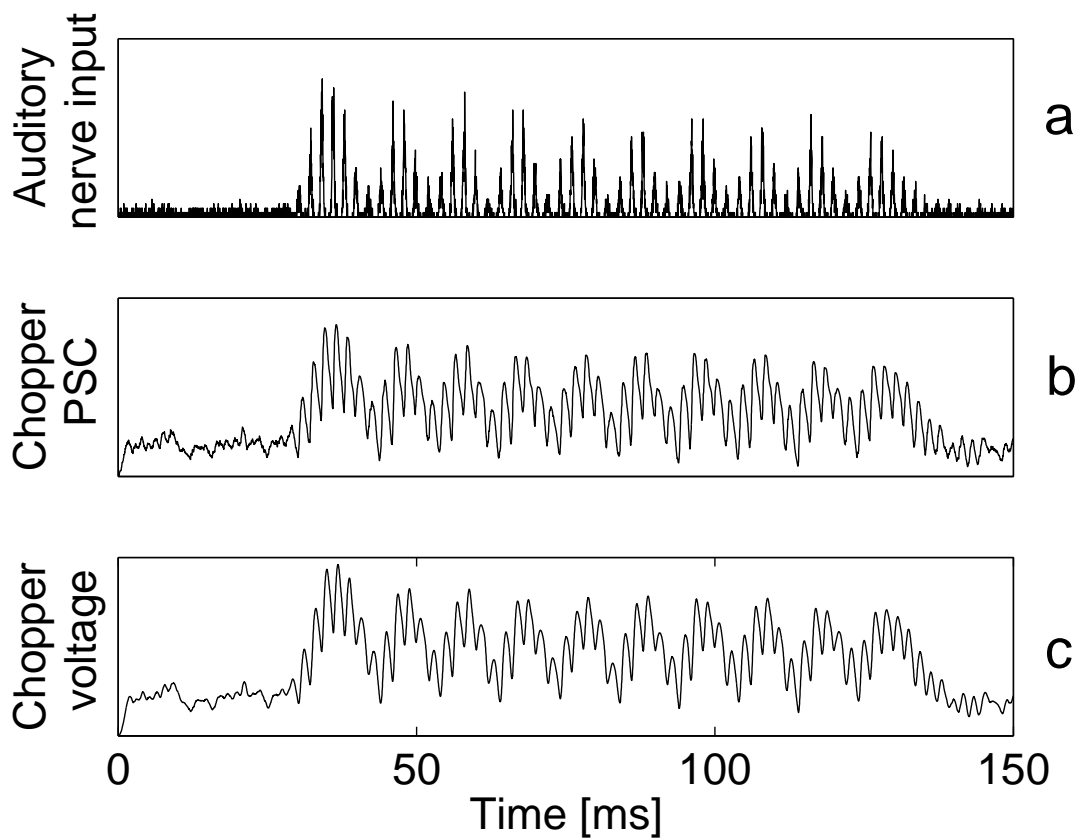


Figure 4.5: Transfer of the modulation frequency from the auditory nerve to a chopper neuron. The graphs show the response to 50 repetitions of the signal. a: Response of a cochlear frequency channel (nerve fiber) at $CF = 600$ Hz after stimulation with “standard SAM”. b: PSC of 5 synapses, c: Membrane voltage of chopper neuron. The membrane voltage is smoother than the PSC of the synapses due to the integration-function of the membrane.

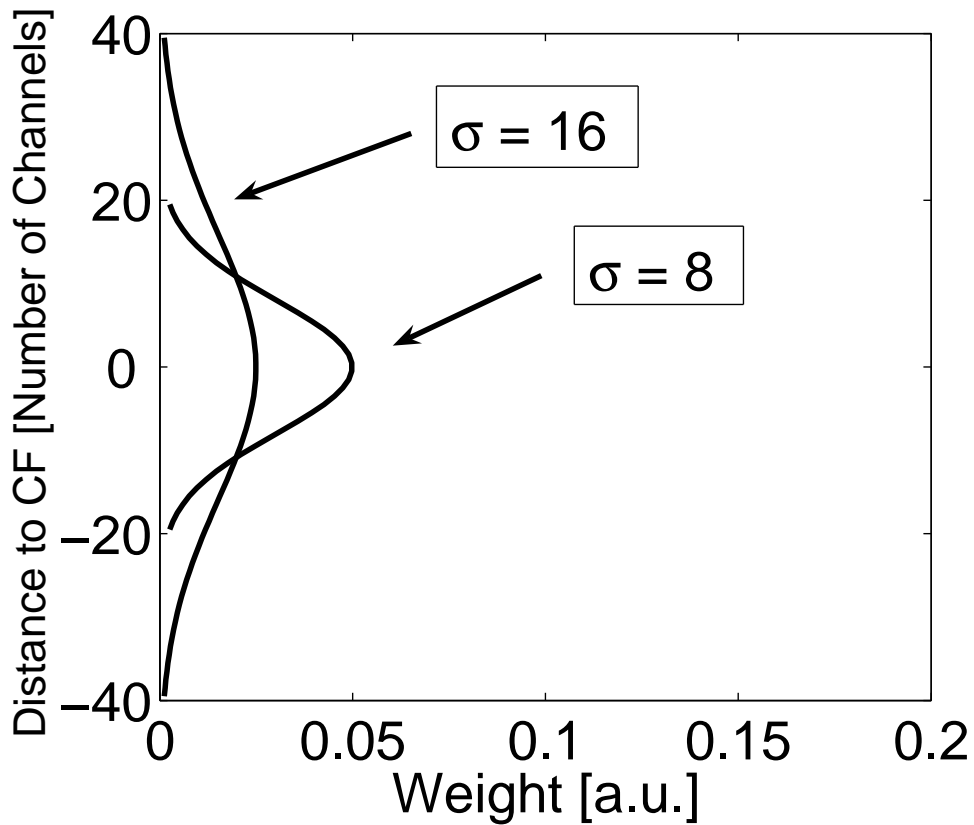


Figure 4.6: The onset neurons receive their input from a wide range of frequency channels. In my simulation the input from the channels is weighted with a Gaussian shape. The shape is centered at CF of the onset neuron. The simulations are calculated for two different values of the Gauss-curve parameter sigma. The y-axis shows the channel range of the incoming fibers (at CF the channel number is 0), the x-axis shows the weight.

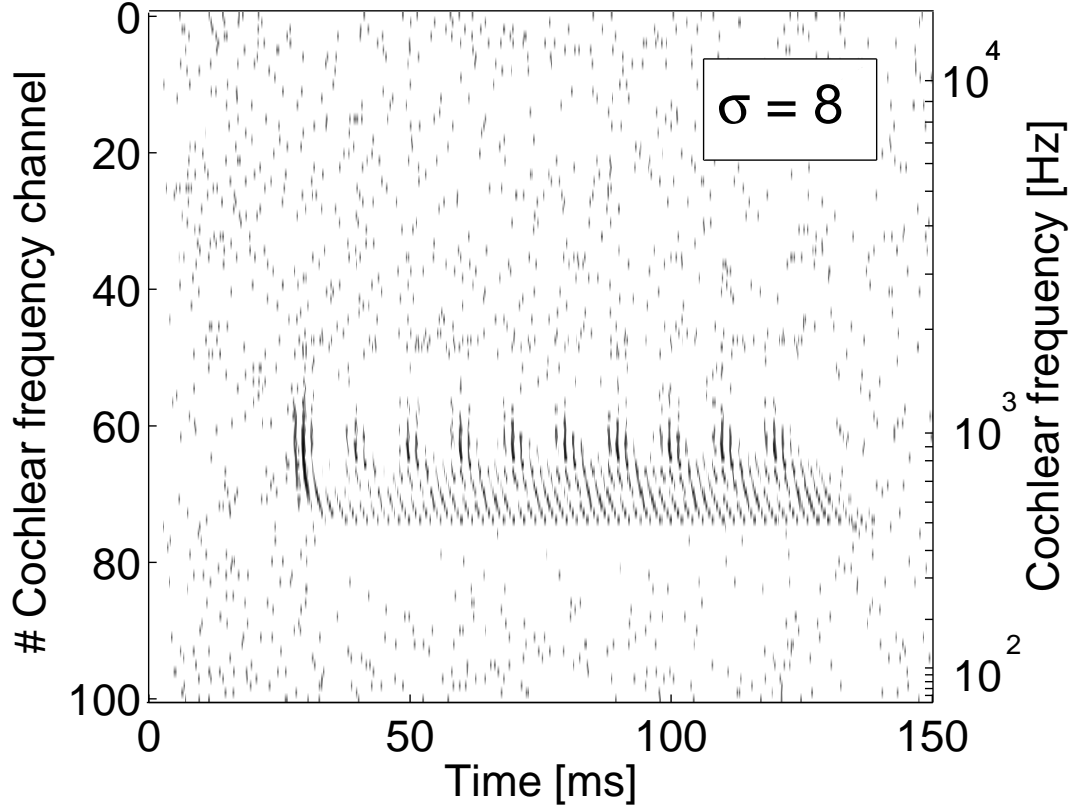


Figure 4.7: Result of 50 simulations of the response (APs) of onset neurons to the input of auditory nerve fibers of Fig. 4.4 (response to “standard SAM”). The number of APs is encoded by the darkness of the markers at a given location. Every horizontal line shows the response of one onset neuron in time, which receives input from Gaussian weighted frequency channels (Fig. 4.6). The center of the Gaussian shaped window is given by the left y-axis.

therefore cannot synchronize any longer while adjacent fibers with CF close to the carrier frequency start to synchronize. The onset neuron utilizes this information by integrating the activity of these fibers. With increasing level, the distance of those nerve fibers that can encode periodicity properly from those with CF at the carrier frequency increases. Their broad spectral integration input range therefore enables onset neurons to encode periodicity over a wide dynamic range up to the level where all its fibers are saturated.

In Fig. 4.7, the sum of 50 simulated responses of onset neurons ($\sigma = 8$) integrating over 100 frequency channels can be seen. With the applied input level, the APs of channels 60-73 are strongly phase locked to the modulation frequency.

4.4.3 Circuit of auditory nerve, onset- , and chopper neurons

The combined action of all components of this model provides a mechanism that generates stable oscillations that are triggered at the beginning as well as by each modulation cycle. The onset neuron is able to start the intrinsic oscillations, provided the membrane voltage of the chopper neuron is sufficiently depolarized by the input of the auditory nerve fibers. As a result, in spite of the broad tuning of the onset neurons, a narrow frequency tuning comparable to that of an auditory nerve fiber is preserved in chopper neurons. On the other hand, even if the auditory nerve fiber which provides input to the chopper neuron is saturated, periodicity may still be encoded because the input of the onset neuron comes from adjacent non-saturated frequency channels. As a consequence, this combination of inputs, which includes different filter mechanisms, has the features that are needed to conserve relevant temporal information concerning amplitude modulation as well as tuning to CF over a large range of intensity.

4.4.4 Comparison of the simulation results with properties of real chopper neurons

The model introduced in the last sections provides simulation data that are highly compatible with physiological data (e.g. Blackburn and Sachs, 1989; Frisina et al., 1990a). As spikes from the auditory nerve have a statistical component, the Monte-Carlo method is used for the purpose of comparing my simulation with this data. The following section compares physiological data from chopper neurons with the statistical properties of my simulations.

Regularity analysis of pure tone response

Blackburn and Sachs (1989) classified AVCN neurons using regularity analysis of interspike intervals. Important parameters of this analysis were the mean and the standard deviation (Fig. 4.8b). Introducing the coefficient of variation allows for a comparison of different units of chopper neurons and different stimulus levels. The CV is the ratio of the standard deviation to the mean of the interspike interval and is computed as a function of time. Sustained chopper neurons are a subtype of chopper neurons classified by their small CV, indicating highly regular interspike intervals. Fig. 4.8a shows the PSTH of such a sustained chopper (Blackburn and Sachs, 1989) with 4 to 5 response maxima. The neuron was stimulated with short tone bursts of 25 ms duration with a 1.6 ms rise and fall time. The frequency of the tone bursts (2.89 kHz) was at the CF of the neuron, 30 dB above its threshold. The regularity analysis shows a mean interspike interval of about 2 ms, a standard deviation of nearly 0.25 ms and a resulting CV of about 0.15. These values are stable in time. The result of my simulation with the circular oscillator, which in this case includes 5 chopper neurons (see Section 4.3.2),

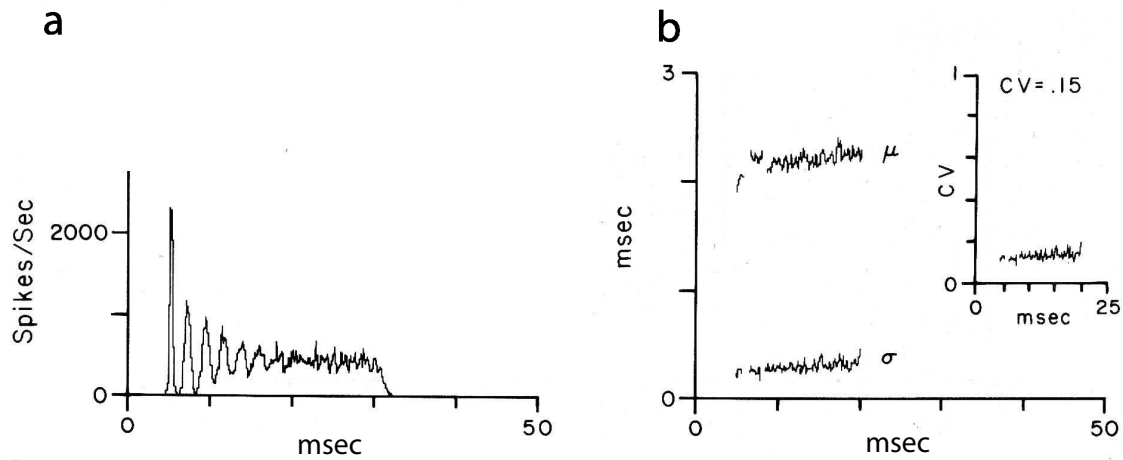


Figure 4.8: PSTH and regularity analysis of a sustained chopper neuron in the CN of the cat. a: PSTH, x-axis in ms, 4-5 peaks of the intrinsic oscillations are clearly visible. b: mean interval μ , standard deviation σ , coefficient of variation CV. Stimuli are short tone bursts (25 ms, 1.6 ms rise and fall time) with frequency at the CF of the chopper neuron (2.89 kHz), 30 dB above threshold (from Blackburn and Sachs, 1989).

is shown in Fig. 4.9. The properties of the simulation, such as firing rate, number of peaks, and ratio of peak heights are nearly the same as in the electrophysiological results. Even the regularity analysis could be matched to the analysis of the in vivo recording. For this purpose a jitter (standard deviation 0.26 ms) had to be added to each synaptic delay of the 5 interconnected chopper neurons to fit the CV. In the simulation the CV has a mean value of 0.14 (0.15 in the in vivo recording). Fig. 4.10 shows the simulation results of the multi-oscillator (see Section 4.3.2). Again, firing rate and ratio of peak heights match physiological properties. The number of peaks is increased and the regularity analysis shows smoother results and a lower CV (0.07). The jitter (the same as in circular oscillator) is added only to the synaptic delay of the interconnections of the fast chopper neurons.

Synchronization at different sound pressure levels

To verify the conclusion of the previous chapter that chopper neurons need to receive input from both the auditory nerve and onset neurons in order to conserve both the dynamic range of periodicity encoding and frequency tuning, I simulate responses of auditory nerve fibers, onset neurons with different integration widths, and chopper neurons with and without input from an onset neuron. For the simulation of the chopper neurons, two chopper neurons are arranged in a circular network. To quantify the degree of synchronization, the vector strength (see e.g. Langner, 1992) is calculated for the simulations. For perfect synchronization, VS equals 1, for no synchronization, VS equals 0. Without the input from the onset neuron, the weights of the synapses of

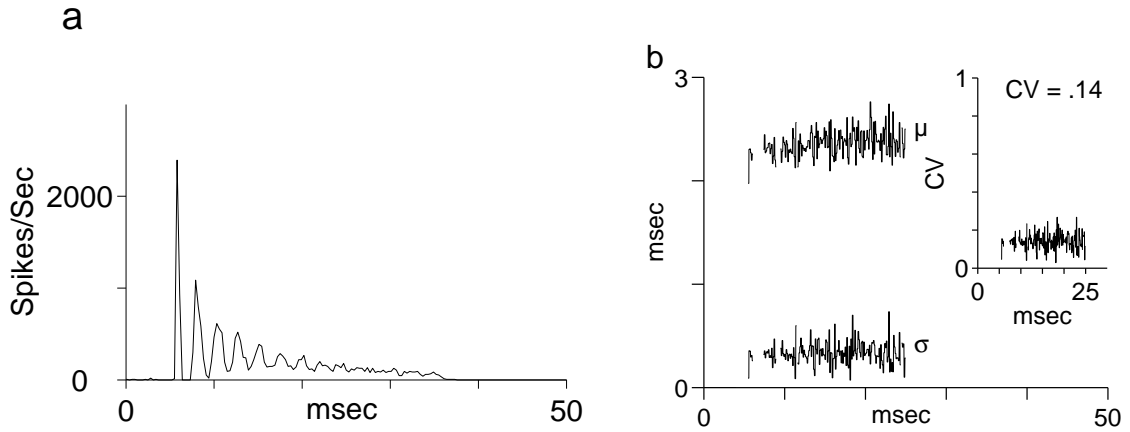


Figure 4.9: Response of a simulated chopper neuron (circular oscillator). Stimulus parameters are the same as in the physiological experiment (Fig. 4.8). a: Response to 500 stimuli are calculated and summed up (binwidth: 0.3 ms). Four to 5 peaks are clearly visible. The response parameters match the physiological data of Fig. 4.8. Random input from the auditory nerve and jitter of the synaptic delay leads to progressive blurring of the spike pattern. b: μ , σ and CV of the simulation. The graphs match the physiological data of Fig. 4.8.

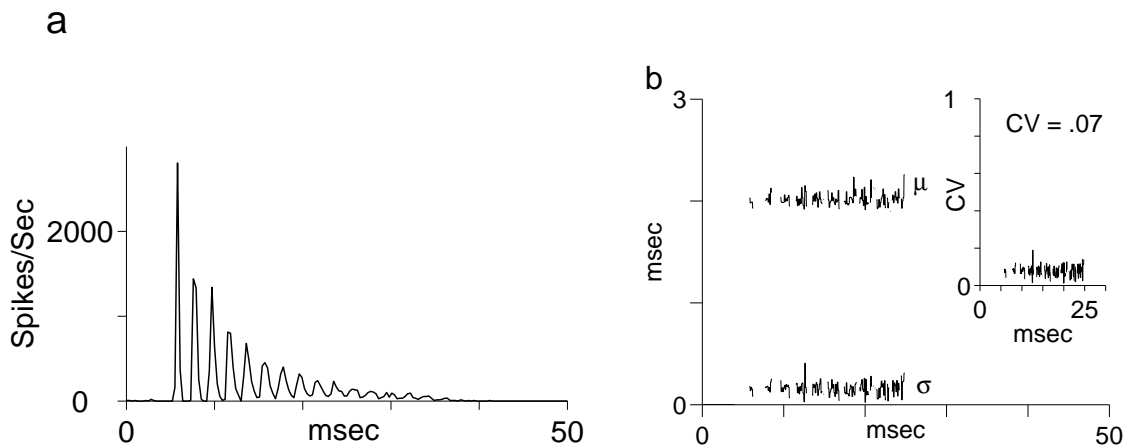


Figure 4.10: Response of simulated chopper neuron (multi oscillator). Stimulus parameters are the same as in the physiological experiment (Fig. 4.8). a: Response to 500 stimuli are calculated and summed up (binwidth: 0.3 ms). The response shows more peaks than the physiological data of Fig. 4.8. b: μ , σ and CV of the simulation.

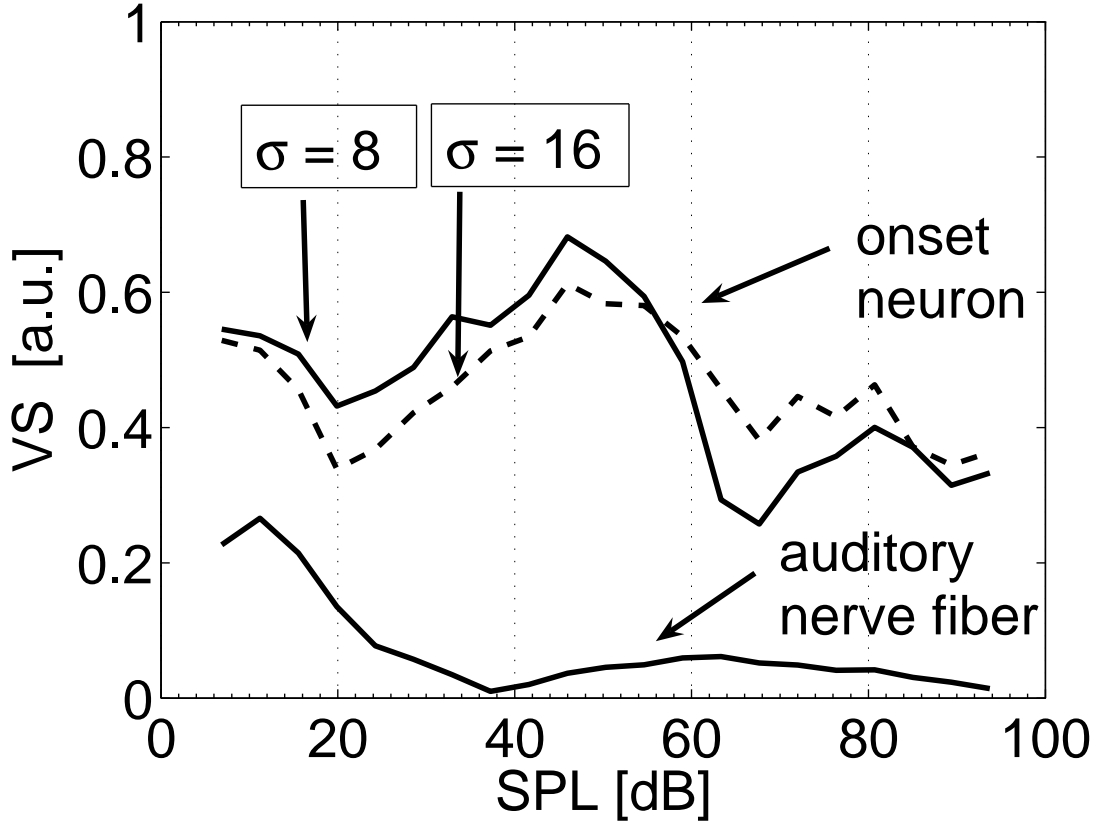


Figure 4.11: Comparison of VS of the simulation of auditory nerve fibers and two onset neurons at different SPL (response to “standard SAM”). The onset neurons have different bandwidths and show robust synchronization over a wide dynamic range.

the auditory nerve have to be increased to enable chopping.

Simulation of auditory nerve fiber and onset neuron with different integration widths The simulation of a nerve fiber with a CF at the carrier frequency of the AM signal (CF = 600 Hz, 50 repetitions) shows that the synchronization to the modulation ($f_m = 100$ Hz) is small and nearly vanishes above 40 dB SPL (Fig. 4.11). Because of its broader bandwidth, the onset neuron encodes periodicity much better than an auditory nerve fiber (see above; Fig. 4.11). For a smaller bandwidth ($\sigma = 8$), the synchronization is better at low levels, while for a broader bandwidth ($\sigma = 16$), synchronization is better at high levels (above 50 dB SPL). As explained above, nerve fibers away from CF may not yet be saturated and therefore can encode periodicity information by synchronization.

Simulation of chopper neurons with and without input from an onset neuron Real chopper neurons have a high frequency resolution, and encode periodicity information over a wide dynamic range (Frisina et al., 1990a). These are two conflicting demands. While frequency tuning requires narrow band input, periodicity is best encoded by broadband frequency integration. In this model, the solution for this problem is the combined input from both the auditory nerve and an onset neuron. Fig. 4.12 shows the VS of simulations of chopper neurons with and without onset neuron input. The different bandwidths of the onset neurons result in chopper responses showing the same effect as onset neurons, as discussed in the previous paragraph. Moreover, comparison of the simulation of chopper neurons with and without onset neuron input supports the theoretical conclusions of the previous chapter. Without input from an onset neuron, the encoding of periodicity breaks down at levels above 20-30 dB SPL. By contrast, the input of an onset neuron enables the encoding of periodicity information over a large dynamic range. The PSTHs in Fig. 4.13 show the responses of a chopper neuron synchronized to the modulation frequency at three different values of VS (in the case of integrating an input from an onset neuron). At higher level the neuron shows a transition from a continuous to a more onset-like response pattern (Fig. 4.12, arrows at a, b, and c), a behaviour which can also be observed in the responses of real chopper neurons (see Fig. 22 in Frisina et al., 1990a). It is remarkable that in spite of the input from the onset neuron, the output (Fig. 4.13d) is mainly related to the input of the auditory nerve and therefore shows nearly the same saturation behaviour. As expected, the interspike intervals generated by the chopper neurons closely correspond to twice the synaptic delay of the two chopper neuron network (Fig. 4.14).

4.5 Discussion

4.5.1 Comparison of the model with previous computer models

In order to explain the response properties of chopper neurons, previous simulations of chopper neurons relied exclusively on membrane properties (e.g. Wiegrebe and Meddis, 2004; Hewitt et al., 1992; Arle and Kim, 1991; Banks and Sachs, 1991). Although these models can reproduce PSTHs of chopper neurons, regularity of intrinsic oscillations (mean, standard deviation and coefficient of variation), and tuning to frequencies and periodicities of chopper neurons, they can not reproduce the dynamic ranges of the spike rate and periodicity encoding or the preference for multiples of 0.4 ms in the interspike intervals of chopper neurons. Moreover, it is difficult to see how these models could be used to explain the occurrence of the same time constant of 0.4 ms as observed in different species. The first attempt to introduce discretized and limited oscillations intervals is therefore based on spike-to-spike oscillations. The connections between the chopper neurons are presumed to be chemical synapses with a delay of 0.4 ms (Fig.

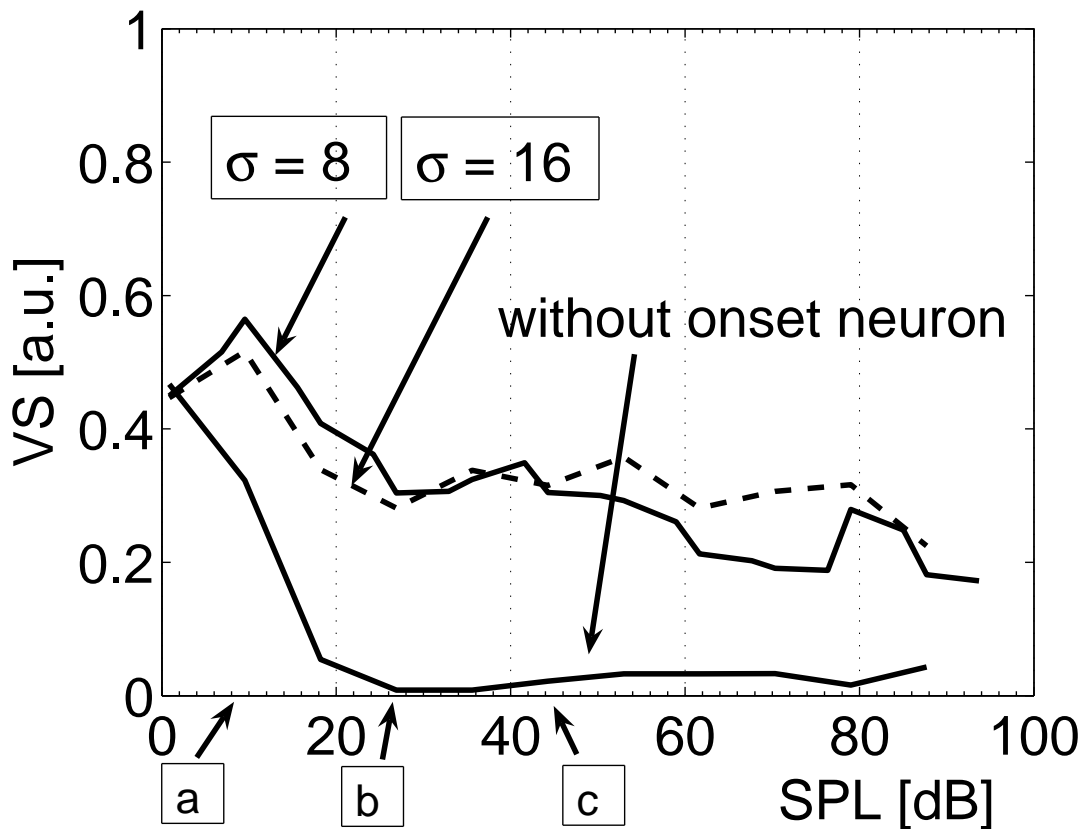


Figure 4.12: Comparison of VS of responses to AM of different chopper simulations at different SPL (response to “standard SAM”). Chopper neurons with input from an onset neuron ($\sigma = 8$, $\sigma = 16$) synchronize to AM signals over a wide dynamic range. By contrast, synchronization deteriorates above 20 dB SPL without input from an onset neuron.

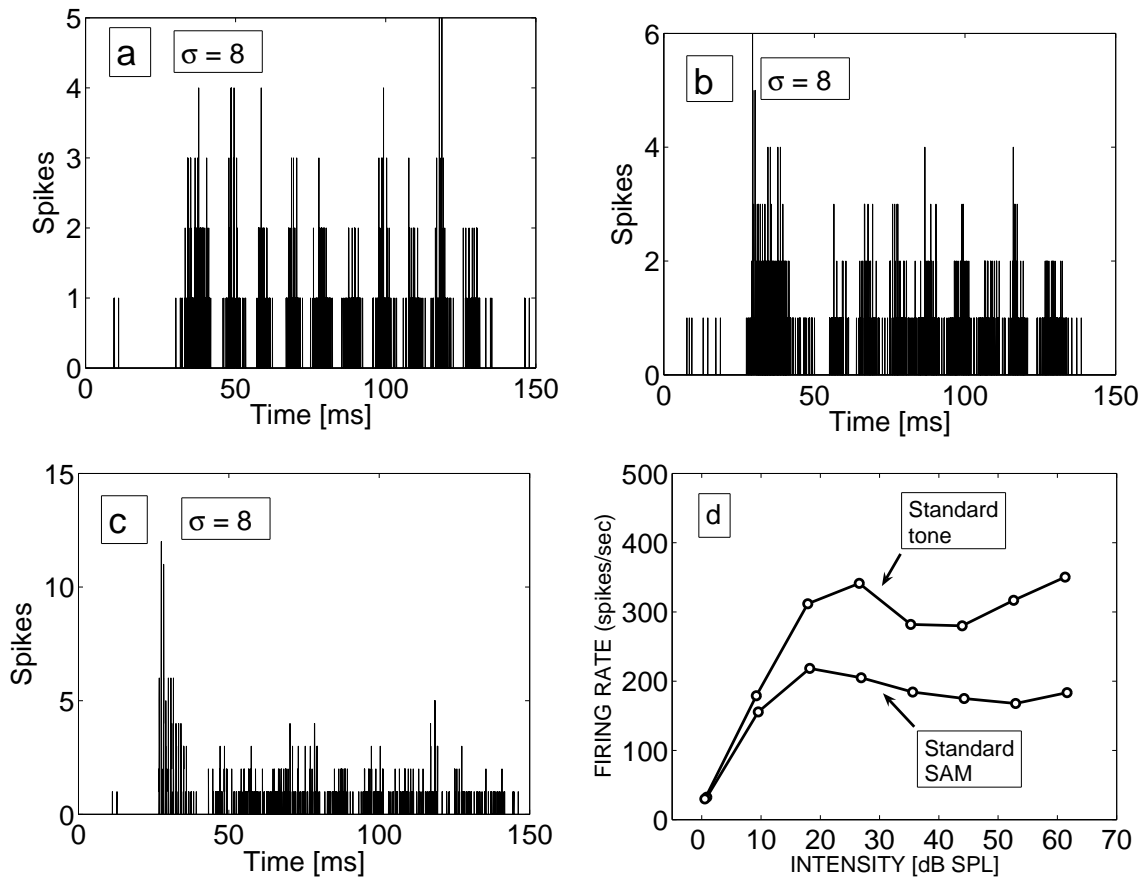


Figure 4.13: PSTHs of simulated chopper neurons ($\sigma = 8$) at point a (10 dB), b (27 dB) and c (45 dB) of SPL of Fig. 4.12. At higher levels the neurons show a more onset-like response pattern, a transition also observed in real chopper neurons (Frisina et al., 1990a). d: Firing rate vs. intensity of simulated chopper neurons (response to “standard SAM” and “standard tone”).

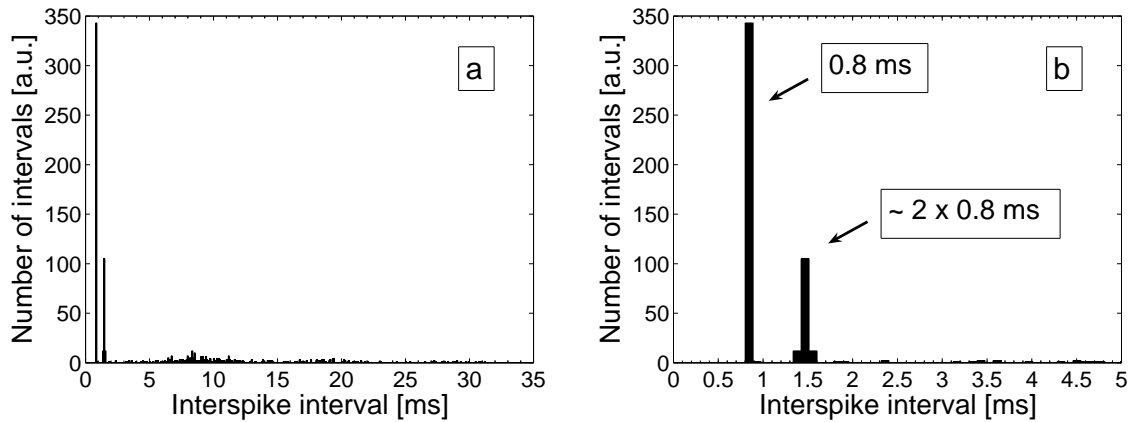


Figure 4.14: Interspike histograms of the response of simulated chopper neurons. SPL is 10 dB. a: The interspike intervals have only two prominent peaks. b: Enlargement of a. The two peaks are at 0.8 ms (the chopper interval) and at about twice 0.8 ms.

4.2). As a result, the simulations show chopping with constant interspike intervals (Figs. 4.9, 4.10). Although the model is appropriate for the simulation of the main properties of chopper neurons, its disadvantage is that the generation of first order intervals which are multiples of 0.4 ms would require an increasing number of neurons, as interspike intervals become larger. Moreover, these neurons would have the same chopping frequency but would be distinguished by different phase information. Since it is not known if and how this phase information could be used, another more effective model consisting of a reduced number of neurons in chopper circuits is introduced and tested (Fig. 4.3).

4.5.2 Regularity and periodicity analysis

In vivo properties of chopper neurons, such as the mean and the standard deviation of interspike intervals, and the CV, could be simulated after adding a jitter (standard deviation 0.26 ms) to the synaptic delay of the simulation (Figs. 4.8, 4.9, 4.10). This appears physiologically plausible because synaptic transmission, like every other diffusion mechanism, has a component of Brownian molecular movement. For this model, the jitter results in PSTHs that are blurred in time. The responses of irregular choppers can be explained by the assumption of a stronger input from the nerve. This time dependent input is transmitted into time dependent ISIs.

Physiological data show that the modulation frequency of SAM is encoded in one frequency channel with a small dynamic range of 30-40 dB (Frisina et al., 1985). This raises the question of how chopper neurons achieve their total dynamic range of about 90 dB. The answer suggested by this model is that chopper neurons receive input from onset neurons which integrate over a wide frequency range (Palmer et al., 1996; Oertel

et al., 2000; Golding et al., 1999). In my simulation, this integration window was selected to be Gaussian shaped (Section 4.4.2, Fig. 4.6). However, the optimal range and shape of the integration window for encoding periodicity information has to be studied in further simulations. The simulation presented here shows that the difference between the synchronization of the nerve and the onset neuron is considerable. The auditory nerve carries information tonotopically, whereas the onset neuron with its broadband integration utilizes temporal information from many frequency channels at the expense of spectral information. In line with physiological data (Frisina et al., 1990a), the dynamic range of the onset neuron for periodicity coding is much larger than that of the nerve (Fig. 4.11) and enables phase coding even at the highest levels investigated (90 dB SPL). The “hierarchy in enhancement”, observed by Frisina et al. (1990a), is optimally transformed in this model of chopper neurons. A simulated chopper neuron responds when input from the auditory nerve indicates activity in a frequency channel and when it is triggered by an onset neuron, which codes periodicity and transients. The simulations also demonstrate the importance of the width of the frequency channel integration. Variation of the width shows that the frequency channel integration can be adapted for encoding periodicity at low or high levels (Fig. 4.11, compare $\sigma = 8$ and $\sigma = 16$) or other stimulus conditions.

The chopper neuron simulations show a dramatic difference between the results obtained with and without input from an onset neuron. Dynamic ranges differ by at least 70 dB. (Fig. 4.12). Since the effect of different widths of frequency channel integration for the onset neurons is transferred to the chopper neurons (Figs. 4.11, 4.12, compare $\sigma = 8$ and $\sigma = 16$), the adjustment of the integration width has also consequences for the subsequent processing steps.

The way in which the firing rate of the simulated chopper neurons (Fig. 4.13d) depends on the input from the auditory nerve, is compatible with the results of Frisina et al. (1990b). The firing rates of the simulated choppers in response to the “standard SAM” and the “standard tone” (Fig. 4.13d) differ despite the same sound level. This may be explained by the fact that in the case of a SAM the energy is distributed over the carrier frequency and sidebands, whereas in the case of a tone the energy is concentrated on one frequency component (see equation 4.2). The interspike interval histograms of the simulated chopper neurons (Fig. 4.14) show that the chopper period is conserved even for modulated signals. Therefore, the output of the chopper neuron could serve as an intensity-independent time reference for a subsequent temporal analysis, as was proposed in a model for pitch estimation (Langner, 1981, 1983, 1992). The model consists of an oscillator, a frequency reducer, and a coincidence neuron. Chopper neurons (stellate cells) in the VCN were presumed to be correlatives of oscillator units.

The previous chapter presents the different degrees of synchronization in the nerve, the onset neuron, and the chopper neuron for different levels. My simulation results match these data, including the dynamic ranges of the chopper neuron and the nerve (Figs. 4.11, 4.12).

Overall, the conclusion is that the described physiological properties of chopper neurons can be explained by connections as implemented in this model. In particular, spike

intervals that are multiples of 0.4 ms can be reproduced by a network of interconnected chopper neurons. My simulations show that input from an onset neuron is needed for chopper neurons to express a wide dynamic range of periodicity coding, in spite of their narrow frequency tuning. As already mentioned in previous chapter, lateral inhibition could indeed enhance frequency tuning in the presence of a broadband input, but tuning curves of chopper neurons seem to show no or only little lateral inhibition (Bourk, 1976; Caspary et al., 1994). In spite of their connections to onset neurons, the dynamic range of the pure tone response of the simulated chopper neurons is determined solely by the input from the auditory nerve. This input is mainly responsible for starting and stopping the response of the choppers and therefore can solve the problem addressed by Ferragamo et al. (1998a) concerning interconnected chopper neurons: “This circuit raises the question whether the mutual excitation in choppers could be self-sustaining and how chopper responses are terminated”.

It is difficult to see how the described features could be realized in models of chopper neurons that are based exclusively on membrane properties without interconnections and input from an onset neuron.

4.6 Conclusions

1. A model for chopper neurons is proposed which is composed of a circular network of neurons activating each other via chemical synapses characterized by a synaptic delay of 0.4 ms. All of these neurons receive input from the auditory nerve, but one neuron in the network receives an additional input from an onset neuron.
2. In contrast to previous models, the present model can explain the preference for multiples of 0.4 ms in oscillations of chopper neurons. It has also the advantage of explaining their large dynamic range of periodicity encoding in spite of their narrow frequency tuning.
3. Like the previous models, the present model is able to simulate interspike intervals of spike trains of the chopper responses with high precision.
4. The simulation can explain essential properties of real chopper neurons by input from onset neurons.

Chapter 5

Spectral integration in a simulation of onset and chopper neurons in the cochlear nucleus

5.1 Abstract

Chopper neurons in the cochlear nucleus have unique temporal and spectral properties, which cannot be fully explained by currently popular models (e.g. Banks and Sachs, 1991; Hewitt et al., 1992; Wiegrebe and Meddis, 2004). Therefore, a new model (Bahmer and Langner, 2006a) was suggested based on the assumption that chopper neurons receive input from onset neurons and from the auditory nerve, thereby combining different forms of auditory signal analysis. As a result of the interaction of broadband input from onset neurons and narrowband input from the auditory nerve, chopper neurons are characterized by a remarkable combination of sharp frequency tuning and faithful periodicity coding. My simulations show that the width of the spectral integration is crucial for both the precision of periodicity coding and the resolution of single components of sinusoidal amplitude modulated sine waves. While a small integration width enables chopper neurons to resolve frequency components, it is a disadvantage for encoding periodicity information at high levels and vice versa. Therefore, one may hypothesize that it would be expedient if the hearing system was able to adapt spectral integration of onset neurons to varying stimulus conditions. Furthermore, a preference for different integration widths in different subjects may account for a corresponding dichotomy found in pitch perception (Schneider et al., 2005).

5.2 Introduction

Chopper neurons in the cochlear nucleus are a major input to the inferior colliculus, the prominent processing station in the midbrain, and a major source of tonotopic information. This may be the reason why chopper neurons have outstanding physiological properties, such as their large dynamic range of periodicity encoding combined with their narrow tuning. In order to explain how these conflicting demands can be fulfilled by a single type of neuron, it is proposed that in addition to their input from the auditory nerve chopper neurons receive input from onset neurons (Bahmer and Langner, 2006a). By means of these inputs, chopper neurons may combine two different aspects of first-order signal processing. While their input from auditory nerve fibers comes from a narrow frequency range (Ferragamo et al., 1998a), the input from onset neurons provides integration over a wide range of frequencies. It was shown that onset neurons may integrate over approximately one-third of the tonotopic array of the cochlea (Palmer et al., 1996; Oertel et al., 2000; Golding et al., 1999).

The results of my simulation of chopper neurons that are activated by onset neurons show that it may be of advantage if auditory processing could adapt the width of the spectral integration for a coding of periodicity information at different levels (see also Bahmer and Langner, 2006b). This conclusion is supported by a quantification of the influence of the integration width of onset neurons on the tuning and the periodicity encoding of the chopper neurons in this model. For this purpose I compare the simulated responses of nerve fibers and chopper neurons to sinusoidal amplitude modulated sine waves (SAM) at different widths of integration. It is conceivable that the width of the integration window must also have consequences for consecutive auditory processing steps and especially for different modes of pitch perception. For example, when asked to judge the pitch of narrow-band harmonic sounds, some subjects indicate the fundamental pitch (f_0), while others perceive the pitch of a low harmonic component (spectral pitch f_{SP}). It is remarkable that these individual differences are correlated with differences in the relative size of the left and right auditory cortices (Schneider et al., 2005). On the basis of my simulations, it is hypothesized that this dichotomy in pitch perception may be related to different widths of spectral integration of onset neurons in different subjects.

5.3 Methods

The environment used in my simulation was MATLAB. Essential parts of this model are: the inner ear with the basilar membrane, the hair cells, and the auditory nerve. Resonators provide the correct activation of the membrane (for a detailed description see Bahmer and Langner, 2006b). The frequency-place transition of the cochlea is mapped nearly logarithmically by 100 simulation channels (Bahmer and Langner, 2006b; Greenwood, 1990), where a channel with a high number is activated by a low

frequency and a channel with a low number (at the base of the cochlea) is activated by a high frequency.

The neuron models are a Hodgkin-Huxley-like model (Rothman and Manis, 2003c) for the onset neuron and leaky integrate-and-fire (LIF) models for the chopper neurons. The models were described in detail previously (Bahmer and Langner, 2006b). The integration window of the onset neurons is gaussian shaped with different widths, 2, 4, 8, and 16, which are classified as σ of the gaussian formula and indicate an integration of 10, 20, 40, and 80 channels of the nerve response, respectively. Pure tones and SAM were used as stimuli. SAM consisted of a carrier frequency (cf) and two sidebands (lower and upper harmonics), which together carry the same amount of energy as the carrier frequency. The graphs of the simulated nerve and chopper responses in Fig. 5.1 are normalized for comparison (corresponding spike rates are listed in the figure caption).

5.4 Results

Responses of the auditory nerve and chopper neurons were simulated to investigate and to compare the effect of the spectral integration of onset neurons and the convergence of information from the nerve and the onset neuron on the tuning properties, the nonlinear behaviour, and the periodicity encoding of chopper neurons.

5.4.1 Tuning and nonlinear effects of the simulated chopper neurons

The model of the chopper neurons was stimulated with three different SAM (carrier frequency (cf) 400, 500, and 600 Hz, modulation frequency (mf) 100 Hz) at 40 dB SPL. The transition of the carrier frequency from 400 to 600 Hz with the same modulation frequency of 100 Hz covers the transition from resolved to unresolved harmonics. The simulation results of the corresponding nerve responses can be seen in Fig. 5.1 in the first row. The values in percent indicate the resolution of the lower harmonics (lh) and is calculated by $(peakmax_{lh} - peakmin_{lh})/peakmax_{lh}$. Therefore, the decreasing numbers in the first row in Fig. 5.1 mark the change from resolved to unresolved lower harmonics, which corresponds to the less peaky curves.

Rows 2-5 of Fig. 5.1 show the response of the simulated chopper neurons with input from onset neurons with increasing integration widths of 2, 4, 8, and 16, which correspond to σ of the gaussian formula. It is remarkable that most of the responses of the chopper have a higher resolution than the corresponding nerve response (width 2, 4 for all cf; width 8, 16 for cf 400 and 500 Hz.). In particular, the response of the chopper neuron with onset integration window 2 at a carrier frequency of 600 Hz shows an enhanced resolution of 40% of the lower harmonic. With increasing width of the integration

window, the resolution decreases. This change is exceptionally strong at a carrier frequency of 600 Hz. For the tested bandwidths and modulation frequency of 100 Hz it needs a carrier frequency of 600 Hz or more to undercut the resolution of the nerve. At low harmonic ratios of carrier and modulation frequencies (<6) the model circuit of onset and chopper neuron enhances the resolution in spite of the spectral integration by the onset neuron.

The different resolutions in the response of the nerve and the simulated chopper neurons are not only due to network properties, but also to nonlinear interactions of the frequency components in the cochlea. To investigate these nonlinear effects, simulations of responses to particular SAM signals are compared with the superposition of the corresponding pure tone responses (total sound pressure level 40 dB SPL, pure tone at carrier minus 6 dB, pure tone at sidebands minus 12 dB for equal amount of energy). As a typical example, the simulated responses with integration widths of 2 and 16 at cf 600 Hz are plotted together with the corresponding superimposed pure tone responses (bold and dashed lines in Fig. 5.2a, b). In addition, to quantify the nonlinear effects, the pure tones responses are fitted by weighting each pure tone response to the response to SAM (dotted line in Fig. 5.2a, b). In order to compensate for the nonlinear effects for a width of 2, the fitting weights have to be 0.7, 1, 1.45, for a width of 16 the fitting weights are 1.1, 1, 1.35 (see figure caption for details). The superimposed pure tone response peaks differ more from the corresponding SAM response in the case of a narrow integration window than in the case of the broader integration window, which means that the nonlinear effects are greater for the narrow than for the broad integration window. It is remarkable that the non-linearities also result in shifts of the spectral representation. In the case of the narrow integration (Fig. 5.2a) the maximum of the response curve representing the upper harmonic (700 Hz) is shifted to higher frequencies, whereas the maximum due to the lower harmonic is shifted to lower frequencies, in comparison to the corresponding pure tone responses. This effect is not present for the broad integration window (Fig. 5.2b).

5.4.2 Periodicity representation of the simulated chopper neurons

The input from the onset neuron provides precise periodicity information, which is especially important at high levels (see discussion). Therefore, responses of chopper neurons receiving input from onset neurons with different integration windows at different levels were simulated. To quantify the periodicity encoding, the vector strengths (VS, for details see e.g. Bahmer and Langner, 2006b) of the responses were calculated (Fig. 5.3). At low levels (40 dB SPL) an increase of the integration width results in a decrease of VS. At high levels (70 and 80 dB SPL) the VS decreases until the integration window reaches a width of 8; from a width of 8 to 16 the VS increases.

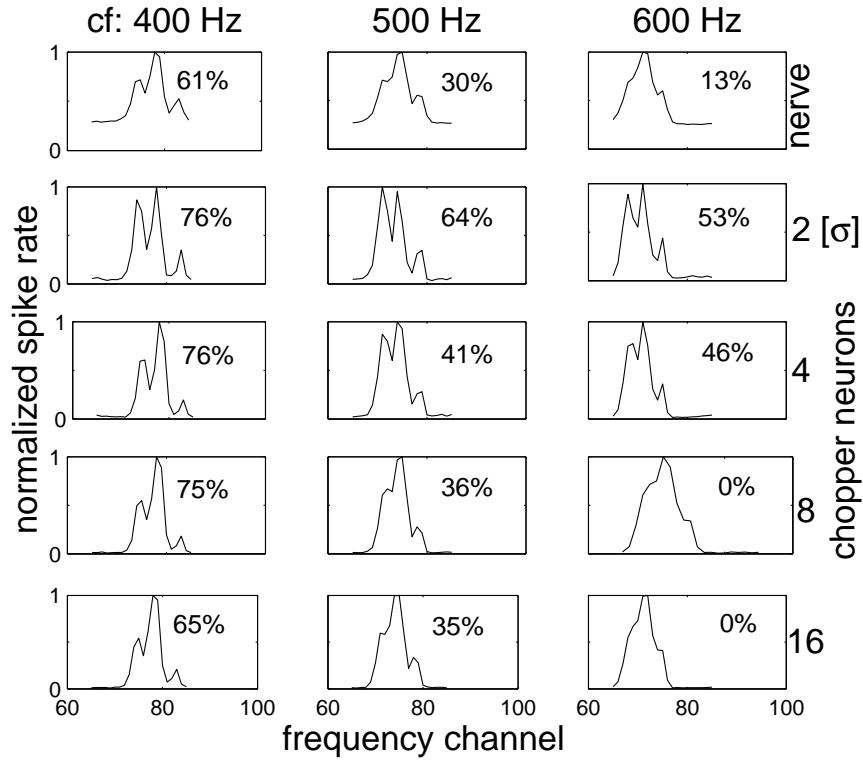


Figure 5.1: Simulation of nerve (first row) and chopper responses (2nd to 5th row) to SAM (cf 400 Hz first column, cf 500 Hz second column, and 600 Hz third column; mf 100 Hz for all). The choppers receive input from onset neurons with integration widths $\sigma = 2, 4, 8,$ and 16 (2nd to 5th row). The values in percent indicate the resolution of the lower harmonics (lh) $[(peakmax_{lh} - peakmin_{lh})/peakmax_{lh}]$. Frequency channels correspond to Greenwoods map (Greenwood, 1990, see text). The spike rates are normalized for comparison (corresponding spike rates for cf 400, 500, 600 Hz: nerve: 99, 108, 113; choppers width 2: 93, 94, 105; choppers width 4: 121, 99, 119; choppers width 8: 176, 174, 173; choppers width 16: 217, 211, 212).

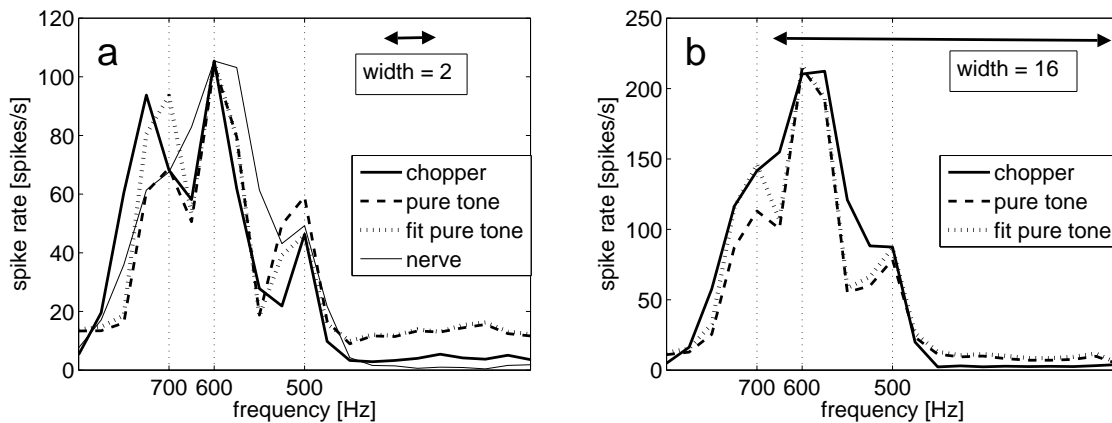


Figure 5.2: Quantifying the nonlinear effects of two chopper model responses with integration width 2 (**a**) and 16 (**b**), cf 600 Hz. The corresponding widths σ of the gaussian shaped integration windows are indicated by the lengths of the double arrows. The frequency indication on the x-axis is due to the maximum responses in the simulated nerve channels. Responses to SAM and corresponding pure tone responses are compared.

a: *Bold curve:* SAM response of a chopper simulation with input integration width 2. *Dashed curve:* Corresponding superimposed pure tone chopper responses. *Dotted curve:* Fit of the superimposed pure tone response to the SAM response; weights 0.7 for 500 Hz, 1 for 600 Hz, 1.45 for 700 Hz. *Light curve:* Corresponding superimposed pure tone nerve responses.

b: *Bold curve:* SAM response of a chopper simulation with input integration width 16. *Dashed curve:* Corresponding superimposed pure tone chopper responses. *Dotted curve:* Fit of the superimposed pure tones to the SAM response; weights 1.1 for 500 Hz, 1 for 600 Hz, 1.35 for 700 Hz.

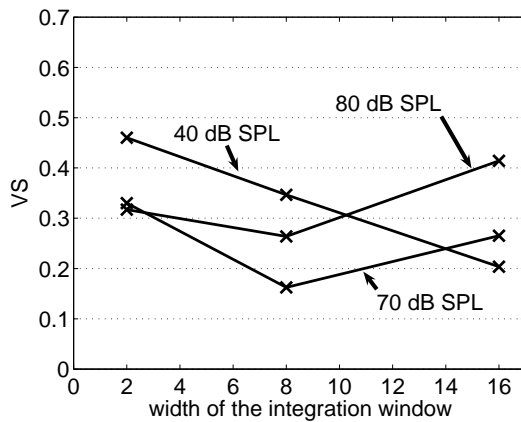


Figure 5.3: Vector strength (VS) of the responses of simulated chopper neurons with different integration widths at different levels. VS was calculated in the frequency channel of the cf.

5.5 Discussion

5.5.1 Tuning of the simulated chopper neurons

In Fig. 1 the SAM responses of simulated chopper neurons which receive input from onset neurons with different integration windows show a change in their resolution of the harmonics. As expected their resolution is better with a narrow than with a broader integration window. The reason is that broader integration windows of onset neurons at neighbouring CF overlap more, which smears the frequency information provided by the onset neurons to the chopper neurons. Looked at the other way round, decreasing the width of the integration window results in sharper tuning of the chopper neuron. In some cases, the simulated chopper neurons show a 40% enhancement in their resolution of harmonics compared to the resolution of the nerve. An explanation for this enhancement is the fact that two inputs - from the nerve and the onset neuron - act in this case as two multiplicative filters: the neuron will produce an output only if both inputs were active at the same time, if only one input or none were active, no output will be produced. This results in a sharper tuning.

5.5.2 Periodicity representation of the simulated chopper neurons

The results depicted in Fig. 5.3 demonstrate the dependency of the VS of the chopper neuron on the width of the integration window and on the level. A theoretical explanation (Fig. 5.4a-c) for these results is as follows: at low levels the nerve fiber, which projects to the chopper neuron, can provide the periodicity information that is neces-

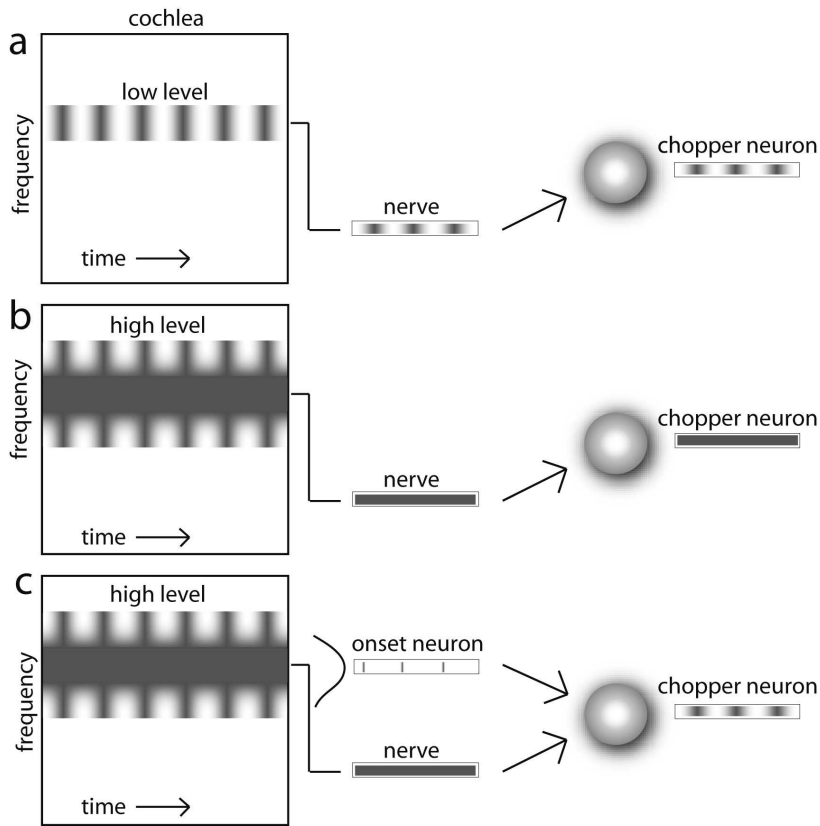


Figure 5.4: Illustration of periodicity encoding of simulated chopper neurons at low and high levels.

sary to synchronize the chopper response (Fig. 5.4a). A broader integration window would result in less synchronized responses because noise from off-CF channels would decrease VS (Fig. 5.3, declining curve at 40 dB SPL). However, at high levels the inputs from the nerve fiber saturate, and as chopper neurons receive input only from narrowly tuned fibers, periodicity information will be lost (Fig. 5.4b). On the other hand, at high levels periodicity information can still be transferred from non-saturated off-CF channels via the integration window of the onset neuron (Fig. 5.4c). The simulation results show that a narrow integration window is always an advantage for spectral coding. In contrast, a broad integration window is advantageous for periodicity coding at high levels, while for low levels a narrow integration window may be better. This is due to two other opposing effects: the correlation of synchronized activity in different channels is higher when the channels are in close proximity, on the other hand a broad integration window also includes non-saturated channels.

5.5.3 Explanation for a dichotomy of pitch perception?

Considering the high dynamic range of our acoustic environment and the fact that the auditory system has to deal with both narrow and broadband signals, one might hypothesize that it would be advantageous if the hearing system were able to adapt the spectral integration of onset neurons to different stimulus conditions.

Schneider et al. (2005) found narrow and broadband adaptations in the pitch perception of different subjects. The pitch of a harmonic sound in some objects may be dominated by periodicity information, in others by certain resolved harmonics. This model might provide an explanation for this phenomena at an early stage of auditory signal processing. The hypothesis is that the correlative of the perception of the fundamental is a dominance of onset neurons with broad integration windows, while a preference for the perception of the harmonics is a dominance of narrow integration windows. The broad integration allows for a better encoding of the periodicity of a signal at high levels but shows a worse resolution of each harmonic component, while the narrow integration shows a worse ability to encode periodicity over a large dynamic range but results in a good resolution of components. The preference for the width of the integration might be an inherited intrinsic property of the neurons or, perhaps more likely, the result of an individual learning process: in the maturation of the auditory system the formation of task specialized neuronal structures could adapt to the acoustic environment. One could also postulate mechanisms that to some extent dynamically control the integration window of onset neurons, depending on the stimulus or the processing task. The adaptation of the window could be accomplished by level dependent lateral inhibition or by inhibition from higher processing centers. It is even possible that frequency channels which contribute to the integration process could be selected via presynaptic inhibition.

5.6 Conclusions

- In my simulation, variation of the integration widths of onset neurons results in variation of the spectral resolution of chopper neurons. Smaller widths result in a higher resolution of frequency components.
- Variation of the integration widths of onset neurons also results in variation of the periodicity encoding of chopper neurons. Narrow integration widths lead to better periodicity encoding at low levels. At high levels broader integration widths lead to better periodicity encoding, which results in a conflicting demand at high levels for adapting the width of the integration to tuning or to encoding periodicity.
- The pitch dichotomy of individual preferences for either periodicity pitch or the pitch of spectral components of harmonic sounds can be explained by assuming adaptations of the width of the integration to either spectral or temporal coding.

Chapter 6

Networks of Hodgkin-Huxley-like neuron models for the simulation of oscillating neurons in the cochlear nucleus

6.1 Abstract

Hodgkin-Huxley-like (HH) models for chopper neurons (e.g. Rothman and Manis, 2003c) that are not interconnected in a neuronal network show properties which are not in line with physiological findings. For example, the response of the single models is strongly dependent on the input strength, whereas real chopper neurons have a response which is relatively independent of level changes (Pfeiffer, 1966; Blackburn and Sachs, 1989). In the model, such independence on the input can be achieved by interconnected networks of HH-like neurons.

Simulated responses of the HH-like model of Rothman and Manis (2003c) show that short ISI as found in real chopper neurons cannot be provided by the model. In order to achieve these short ISIs, I optimized the time constants of this model with genetic algorithms. In addition, ISIs of chopper neurons show a preference for multiples of 0.4 ms. Therefore, a two-neuron interconnected network consisting of the optimized HH-like neuron models was built with a synaptic delay of 0.4 ms. With this small circuit it is then possible to build a more complex network that is activated by the simultaneous input of an onset neuron and auditory nerve and that can provide ISIs, which are multiples of 0.4 ms.

6.2 Introduction

In Chapter 4 a network of leaky integrate-and-fire (LIF) neurons was introduced in order to simulate chopper neurons. In this chapter the LIF neuron models are substituted by HH-like models. A possible candidate for this purpose - the HH-like chopper model of Rothman and Manis (2003c) - is tested for its physiological relevance and its usability in the network introduced previously.

6.2.1 Special features of chopper neurons in the VCN

It is still an open discussion which role chopper neurons play in pitch perception. Chopper neurons can indeed represent the fundamental frequency of complex sounds and of iterated rippled noise and can enhance the representation of SAM in comparison to their auditory nerve fiber input (Winter et al., 2003; Frisina et al., 1990a; Rhode and Greenberg, 1994). But they lack to span the whole range of periodicity frequencies of human pitch perception. In the PAN model of Langner (1981) described in Chapter 2 the choppers need no tuning to a modulation frequency for their functional role in the periodicity analysis, but the described enhancement of modulation frequency (Winter et al., 2003; Frisina et al., 1990a; Rhode and Greenberg, 1994) might improve the temporal processing. The enhancement can be achieved in the simulations by integrating HH-like models in the PAN model. The integration of HH-like models can furthermore help to understand data of electrophysiological recordings of single chopper neurons and data from pitch perception experiments. Chopper neurons in the VCN are outstanding because of their constant interspike intervals (ISI) and their relative independence of the ISI despite changing level (Pfeiffer, 1966; Blackburn and Sachs, 1989; Wiegrebe and Winter, 2001). For Winter et al. (2003) the importance of level independence at such a low level of auditory processing was considered unclear. But for the PAN model the independence of ISIs is important as the output of the choppers represent a time reference, which has to be robust. Such robust level independent interspike intervals were also found in the IC which receive its main input from chopper neurons in the VCN (Langner and Schreiner, 1988). Therefore, to some extent the level independence which is found in the CN is transferred to higher processing centers.

6.2.2 VCN neuron models

Stellate and bushy cells of the VCN have already been described by several HH-like and compartment models (e.g. Banks and Sachs, 1991; Wang and Sachs, 1995; Arle and Kim, 1991; Hewitt et al., 1992). HH-like models are the most detailed models concerning the dynamic properties of the membrane currents. The currents are modeled by means of mathematical equations that describe their progression in time (see Chapter 2). The equations are highly complex and nonlinear. Because of this high complexity,

the time for computer simulations is high in comparison to LIF models (see Chapter 2). On the other hand, the advantage of the HH-like model is, that more detailed effects like tuning to modulations can be tested properly (e.g. Wiegrebe and Meddis, 2004). Furthermore, focusing on the time progression of channel variables in a simulation can help to gain insight in the mechanism of channel interplay.

The advantage of the LIF model is that some characteristics like the refractory period of the neuron model is easy to adjust by setting a time constant. The refractory period determines the maximum firing rate of a cell. The refractory period in the HH-like models is a complex function of many channels. Because of this, changing the refractory period is a multidimensional nonlinear problem, which can be solved by the use of so-called “genetic algorithms”. These algorithms are described in the methods section of this chapter and in a more detailed way in Chapter 10.

A further subtype of the neuron models is the multi-compartment neuron model in contrast to a point neuron. In the case of a point neuron the complex spatial dimensions are neglected and the soma is simulated as a spheroid, whereas the compartment model subdivides the cell into soma, dendrites, and axon which can again consist of many compartments in which the ion flows are simulated. Calculation time increases with the number of the compartments. Banks and Sachs (1991) presented a VCN stellate cell model which consists of a somatic and axonal compartment, which integrate active channels coupled to a passive dendritic tree, which was modified by Wang and Sachs (1995). Altogether, the described stellate models were successful in that they replicated many of the response characteristics of stellate cells in vitro and in vivo. For example, during a depolarizing current pulse, the models exhibited repetitive firing and when stimulated with auditory-nerve-like synaptic input, the models exhibit a response in their poststimulus time histograms (PSTHs) which is similar to the response of real chopping cells in vivo. The models show constant interspike intervals for one stimulus level, match regularity analysis of chopper neurons and were also successful in replicating responses to more complex stimuli (Arle and Kim, 1991; Hewitt et al., 1992; Wang and Sachs, 1995).

The most detailed analysis and modeling of current kinetics of VCN neurons is presented by Rothman and Manis (2003c).

6.2.3 The HH-like “Rothman chopper”

Many studies have shown that VCN neurons differ in their intrinsic electrical properties and especially the K^+ currents they express (Manis and Marx, 1991). Rothman and Manis (2003a) examined the K^+ currents using whole cell voltage clamp technique on isolated VCN cells from adult gerbils. The K^+ currents are important in controlling spike shape, spike rate, spike adaptation, and regularity of discharge. Especially, the high-threshold delayed-rectifier-like K^+ current (I_{HT}) has been found in both bushy and stellate cells (Manis and Marx, 1991). T-stellate cells are the anatomical correlate of the chopper neurons. The I_{HT} allows spiking at high frequency because of its fast

time constants and activation at high voltages. This provides a fast repolarization of their action potential (Wang et al., 1998).

Rothman and Manis fitted HH-like equations to their data. For this purpose, they analyzed in detail the kinetics of three potassium currents of VCN cells, namely a rapidly activating current (I_A), a rapidly activating, slowly inactivating low-threshold current (I_{LT}), and a non-inactivating high-threshold current (I_{HT}). But only the I_{HT} is used in the chopper model of Rothman and Manis (2003c). The properties of this current will be described in the following.

Kinetic analysis of the high-threshold potassium current (I_{HT})

According to Rothman and Manis (2003a), all VCN cell types possess I_{HT} , however only the type I-c cell of their classification, which is their correlative to a stellate cell, appear to have the high-threshold potassium current I_{HT} as its only outward current at the membrane voltage $V > -80$ mV. They found also that the time course of activation of I_{HT} is more complex than expected from a single current and tried to fit their model to the current trace of the type I-c cell. The time course of activation of I_{HT} is described mathematically best by a sum of two arbitrary current components n and p rather than by one component alone (see Chapter 2 for explanation of activation and inactivation variables in the HH formalism). The variables n and p - a fast and a slow component - are both voltage and time dependent. In addition, they found that the best fit is by the expression $n^2 + p$ (Fig 6.1). The corresponding time constants τ_n of $n(t,V)$ is greater than τ_p of $p(t,V)$. The fast and slow component in the activation is apparent in all the VCN cells of their sample.

A comparison of the voltage dependent time constants between the model and the real data is depicted in Fig. 6.2A and B. In Fig. 6.2A the data and the mathematical fit of the fast time constant τ_n , and in Fig. 6.2B the data and the mathematical fit of the slow time constant τ_p is shown. The data from real cells clearly show great variability. Altogether, Rothman and Manis (2003b) found that the best numerical reconstruction of I_{HT} is given by

$$I_{HT} = \bar{g}_{HT} \cdot [\varphi n^2 + (1 - \varphi)p] \cdot (V - V_{HT}) \quad (\varphi = 0.85). \quad (6.1)$$

They left \bar{g}_{HT} , which is the maximum conductance, as a free parameter as the found that the magnitude varied from cell to cell. The fractional parameter φ was set to 0.85 and describes the ratio between activation and deactivation (Rothman and Manis, 2003b).

The simulation of the model current traces with \bar{g}_{HT} set to 150 nS can be seen in Fig. 6.2 C, D, and E. I_n plays the major role in the whole model response $I_n + I_p$ and the tail of the curves of I_n and I_p show that the decay of I_p at the signal ending is slower than that of I_n .

Rothman and Manis (2003b) stated that I_{HT} consists of two independent currents

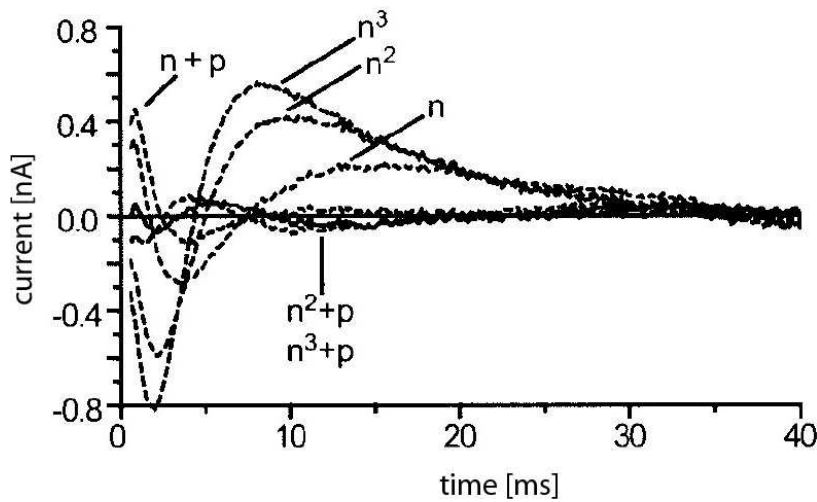


Figure 6.1: Fitting the time progression of the activation current by different mathematical expressions. The plot shows the difference curves between a real current trace of the activation of I_{HT} (straight line at current = 0 nA) and different fitting expressions which consist of the sum of two arbitrary activation variables n and p of the HH formalism (see Chapter 2 for details of the formalism). The variable n has different exponentials for fitting the curve. The term “ $n^2 + p$ ” fits the I_{HT} the best (redrawn from Rothman and Manis, 2003b).

because of to significantly voltage dependencies and different reversal potentials. They saw in the tail of the currents of I_{HT} that sometimes the fast component reversed sign before the slow component and vice versa. The influence of the slow component on the length of after-hyperpolarization was tested in the neuron model by removing the slow component (Rothman and Manis, 2003c). There was no change in interspike timing or shape of the action potentials and it was concluded that the slow component may contribute little to shaping the discharge pattern of VCN neurons because of its small magnitude and slow kinetics (Rothman and Manis, 2003b). The molecular identity of I_{HT} might be the so-called “KCNC1” channel which is expressed in bushy and stellate cells (Perney and Kaczmarek, 1997). Like I_{HT} , this channel shows a slow and fast activation component (Kanemasa et al., 1995).

As an example for the high variability of models in fitting the time constants of the high threshold current, different time-voltage curves are shown in Fig. 6.3. The high variability is sometimes due to different samples in the data collection. Rothman and Manis (2003c) hypothesized that differences in time constants do not lead to dramatic effects but have effects on subthreshold potentials.

Description of the sodium (I_{Na}) and the remaining currents

Rothman and Manis (2003c) modeled the fast-inactivating sodium current I_{Na} accord-

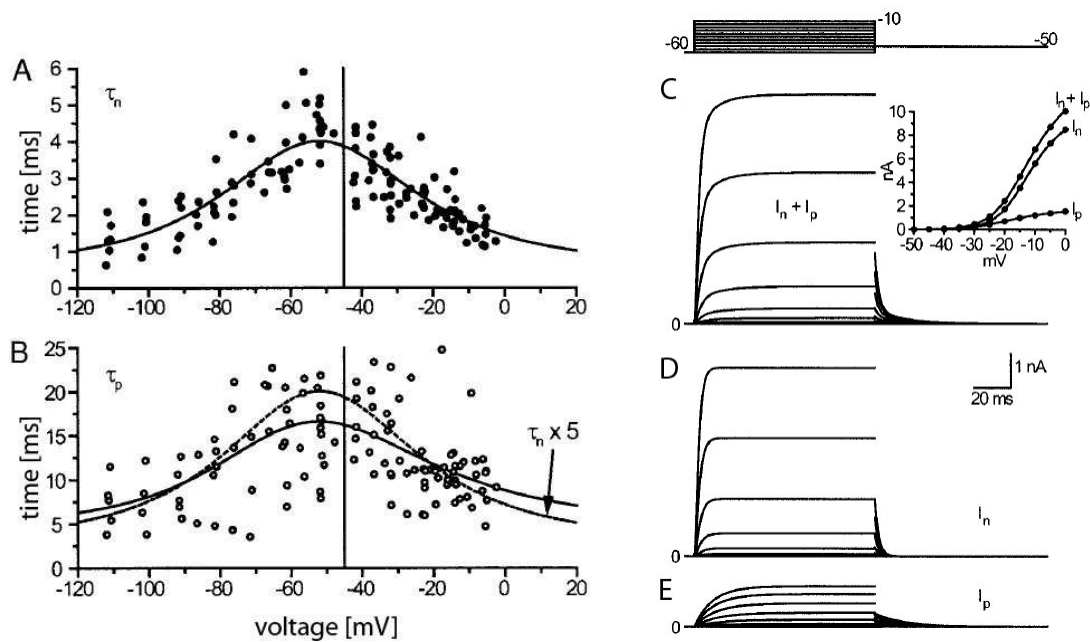


Figure 6.2: *Left:* Summary of activation and deactivation of I_{HT} . Activation ($V > -45$ mV) and deactivation ($V < -45$ mV) analysis of 16 Type I-c cells). A: data of fast time constants τ_n and fit. B: data of slow time constants τ_p and fit. dashed: the same line of A times 5 . The real data show a great variability. *Right:* Model I_{HT} . C: model response trace of I_{HT} ($g_{HT} = 150$ nS and $\varphi = 0.85$). Inset: steady-state I-V relations of I_n , I_p , and $I_n + I_p$ (\bullet). D and E: model I_n and I_p in isolation (redrawn from Rothman and Manis, 2003b).

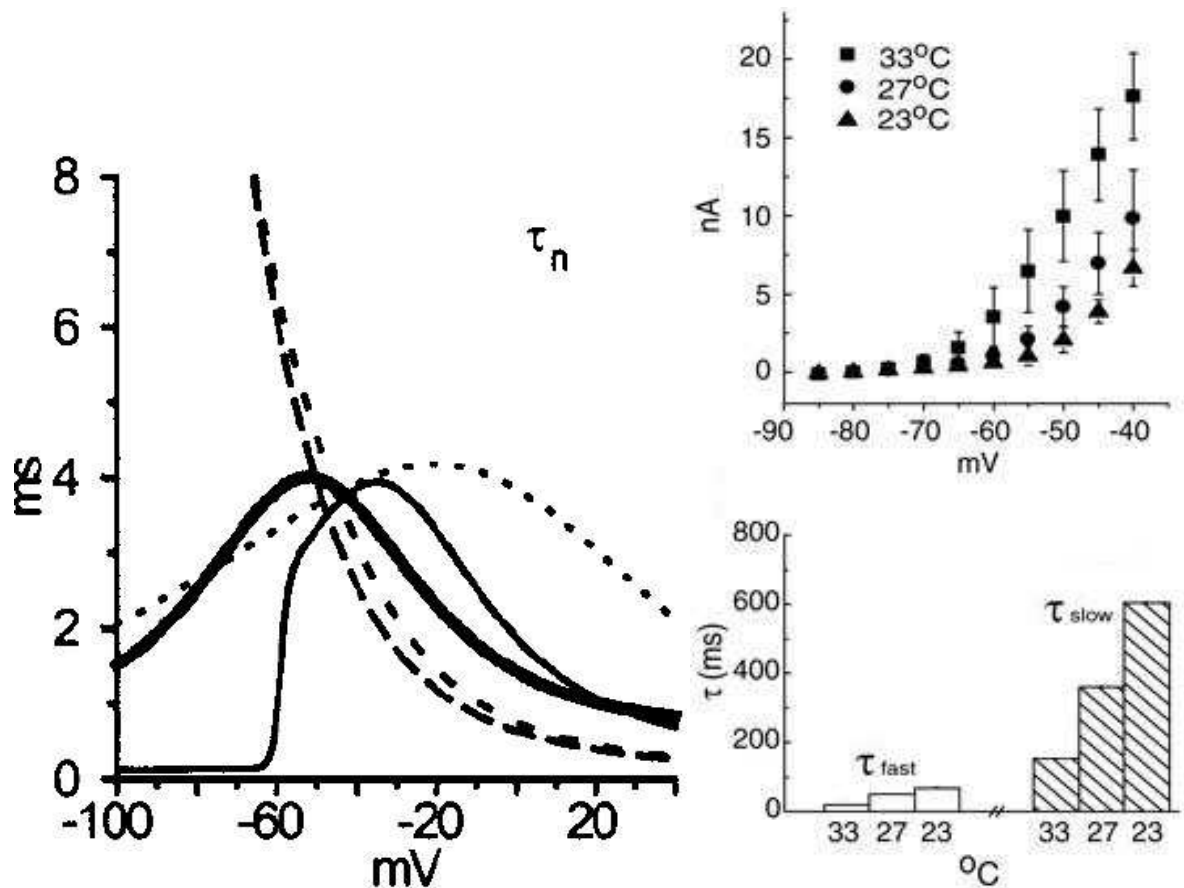


Figure 6.3: *Left*: Comparison of VCN time constants of the high-threshold current of different models. Thin lines represent different models, and bold lines represent the model of Rothman and Manis (2003c). Stellate cell model of Banks and Sachs (1991) (long dashed line), Wang and Sachs (1995) (short dashed line), Rothman et al. (1993) (thin line), Perney and Kaczmarek (1997) (dotted line). Time constants τ_n represent values at 22 $^{\circ}\text{C}$ (redrawn from Rothman and Manis, 2003c). *Right*: Temperature dependence of the conductance (*top*) and time constants (*bottom*) of a K^+ channel of octopus cells in the VCN (redrawn from Cao and Oertel, 2005).

ing to other voltage-clamp studies in mammalian neurons (Costa, 1996; Belluzzi et al., 1985).

The hyperpolarization-activated cation current I_h was found to be expressed in the majority of VCN neurons (Rothman and Manis, 2003a) and was modeled after other voltage-clamp studies from auditory (Banks et al., 1993; Fu et al., 1997; Forsythe and Stanfield, 1996) and nonauditory neurons (Huguenard and McCormick, 1992; Travagli and Gillis, 1994). Rothman and Manis (2003c) decreased the rate constant by a factor of 3 when investigating the model at higher temperatures. Cao and Oertel (2005) measured the dependence of the conductances and time constants on the temperature of low voltage and high voltage K^+ channels and found remarkable differences between the time constants at 22°C and 33°C (see Fig. 6.3, right). They found a Q10-factor in some cases up to 4. If the temperature increases by 10°, the velocity of a reaction changes by multiplying it with the Q10 factor. Interestingly, they described that although activation and inactivation was in both cases sensitive to temperature, the peak currents of the high-voltage activated channel did not change significantly with temperature. Furthermore, they stated that their "experiments indicate that electrophysiological properties of neurons are distorted when recordings are made at reduced temperature".

6.2.4 Substituting LIF neurons by HH-like neurons in the Multi-oscillator

The models described above simulate single chopper neurons that show oscillations due to membrane properties. A LIF model of chopper neurons that shows oscillations due to network properties and is based on anatomical and physiological properties of real chopper neurons is proposed in Chapter 3. This circuit was tested successfully in Chapter 4 with LIF neuron models.

In order to test other aspects of the model like tuning to modulation or the interplay between the time constants of the synaptic delay and the channels, the LIF neuron models are substituted with HH-like models.

The HH-like model of Rothman and Manis (2003c) is capable of simulating VCN chopper neurons. Therefore, the model will be tested for its physiological relevance and its usability in the previously introduced topology. The question raises which parameters of the model are important and which have to be adjusted to fit in the proposed circuit of two chopper neurons and how these new parameters can be interpreted.

The chapter is organized as follows:

In Section 6.3 the used models and methods are outlined. In Section 6.4 the results are presented. Section 6.5 discusses the major points, Section 6.6 concludes the chapter with the central claims.

6.3 Methods

6.3.1 NEURON and Matlab

The program NEURON is a common simulation environment in computational neuroscience. It contains a collection of physiological relevant neuron models (“ModelDB”), in which Rothman and Manis (2003) have implemented their model of stellate cells. In this chapter, the model was tested and the simulation results were analyzed and visualized by importing the data files from NEURON into Matlab.

For the modification of the model, it was implemented in Matlab source code and the differential equations are numerically realized by the Euler method in Matlab. In the following, the implementation of the neuronal models and the genetic algorithm for the modification of the model is described.

6.3.2 Neuronal modeling

HH-like models

The chopper model of Rothman and Manis (2003c) is based on HH equations. The model contains a sodium current (I_{Na}), a high-threshold potassium current (I_{HT}), a cation current (I_h), a leakage current (I_{lk}), an excitatory synaptic (I_E) current, and an external electrode current source (I_{ext}). The time dependent conductance change g_E in response to an excitatory synaptic input is modeled as described in equation 6.8 (first proposed by Rall, 1967).

Thus the change of the membrane potential is

$$C_m \frac{dV}{dt} = I_{Na} + I_{HT} + I_h + I_{lk} + I_E - I_{ext}, \quad (6.2)$$

with

$$I_{Na} = g_{Na} \cdot m^3 h \cdot (V - V_{Na}), \quad (6.3)$$

$$I_{HT} = \bar{g}_{HT} \cdot [\varphi n^2 + (1 - \varphi)p] \cdot (V - V_{HT}), \quad (\varphi = 0.85), \quad (6.4)$$

$$I_h = \bar{g}_h \cdot r \cdot (V - V_h), \quad (6.5)$$

$$I_{lk} = g_{lk} \cdot (V - V_{lk}), \quad (6.6)$$

$$I_E = g_E \cdot (V - V_E), \quad (6.7)$$

$$g_E = \bar{g}_E(t/\tau_E)e^{1-(t/\tau_E)}, \quad (6.8)$$

where C_m is the membrane capacitance and V the membrane potential. The reversal potential of K^+ , Na^+ , and of other ions is denoted by $V_{HT,Na,\dots}$, the peak conductance of the $HT-$, Na^+- , and of other channels by $\bar{g}_{HT,Na,\dots}$, the time constant by τ_E .

g_{Na}	1000 nS
g_{HT}	150 nS
g_{lk}	2 nS
g_h	0.5 nS
τ_E	0.1 ms
V_{Na}	55 mV
V_{HT}	-70 mV
V_{lk}	-65 mV
V_E	0 mV
$V_{threshold}$	-38.3 mV
V_{rest}	-63.9 mV
C_m	12 pF

Table 6.1: Simulation parameters for the chopper neuron. See text for description.

The activation variables are w , m , and r , and the inactivation variables are z and h . Simulation parameters of the chopper neuron are listed in Table 6.1.

Leaky-integrate-and-fire models

To output various ISIs that are multiples of 0.4 ms, the circuit of two chopper neuron models triggers several LIF neuron models that have different refractory periods. The LIF neurons are modeled as neurons with synapses (Bleack, 2000). The synapses and the soma are modeled as follows. After an action potential from a presynaptic neuron a synapse discharges vesicles filled with transmitter in the synaptic cleft. The emission of vesicles is simulated with a look-up table. The transmitter molecules diffuse to the postsynaptic neuron. The decay of transmitter is simulated by a leaky-integrator. The probability of open channels for certain ions increases with higher concentration of transmitter in the cleft. Different ions constitute either excitatory or inhibitory postsynaptic currents. A hyperbolic tangent function simulates the conductance. A time delay with adjustable jitter (parameters: mean and standard deviation) which stands for the overall time for diffusion of transmitter can be integrated in the simulation. The soma of the chopper neurons is based on a leaky-integrate-and-fire model. The incoming postsynaptic currents (PSCs) from the synaptic inputs are integrated and build up a postsynaptic potential (PSP). A leakage current diminishes the input. If the potential reaches a defined threshold a spike is elicited and the potential is set to zero. An absolute and a relative refractory period (exponentially decreasing) ensures that spike generation is suppressed or needs stronger input for a period of time. The model parameters are given in Tab. 6.2

	τ [ms]	Weight [a.u.]
Soma c.n.	0.33	
Syn. from c.n.	0.25	0.7
Syn. from o.n.	0.1 - 1.3	0.5 - 20
Syn. from a.n.	0.77	0.09 - 0.15
Abs. r.p.	0.6-2 ms	
Rel. r.p.	0-0.2 ms	

Table 6.2: Simulation parameters for the model of the chopper neurons (c.n.: chopper neuron, o.n.: onset neuron, a.n.: auditory nerve, Abs. r.p.: absolute refractory period, Rel. r.p.: relative refractory period. Both periods refer to the soma). The model is a leaky integrate-and-fire model and consists of a soma and synapses. The time constant refers to the leakage currents of the soma and synapses. The weights of the auditory nerve synapses are summed.

6.3.3 Genetic algorithm in Matlab

The previously introduced HH-like equations are highly nonlinear. As one of the aim is to optimize the equations for a faster generation of spikes, an adequate mathematical tool for the optimization of the nonlinear equations has to be used. Whereas most of direct and gradient search methods fail in optimization of nonlinear problems, genetic algorithms are designed for a fast search for an optimized solution of nonlinear problems. These algorithms imitate genetic evolution by combination of “genes” of so-called “individuals”. The combination process is partly random. The individuals are scored by a fitness function and the ones with the highest score survive and can combine again their genes and produce offsprings. These processes are iterated to find the optimal individuals (see Section 10.5 for details).

Here, combinations of some coefficients of time constants and of conductances of the HH-like equations of Rothman and Manis (2003c) form the individuals which were optimized by the genetic algorithm. The fitness function is the mean ISI of the output of the model. If the number of the spikes were less than 20 the function were set to one, to prevent a break-off of the spike generation before the input ends. The population contains 20 individuals, which were uniformly distributed. The initial range of the individuals for variation of conductances (g_{Na^+} , g_{K^+}) and time constants (τ_m , τ_h , τ_p , τ_d) of the activation/inactivation variables is set from 0 to 1 and from 0.9 to 1.1, respectively. The following parameters are explained in full length in Section 10.5. Fitness scaling was due to a rank order, the selection function stochastically uniform, reproduction factors were elite count 2 and crossover fraction 0.8, mutation was Gaussian (scale 1, shrink 1), crossover function was a scattered, forward migration (fraction 0.2, interval 20), stopping criteria was either 100 generations or 50 stall generations in the conductance optimization or fitness limit of 0.8 or 50 stall generations in the time constants optimization.

clamp @	first cell	second cell
delay	5 ms	10 ms
duration	100 ms	100 ms
temperature	33° C	
connection	first with second cell	
weights	0.03	
delays	1 ms	

Table 6.3: Simulation parameters for the network of two chopper models of Fig. 10.2

6.4 Results

6.4.1 Patch clamp simulations of a single “Rothman chopper”

Rothman and Manis (2003c) proposed a HH-like model of onset and chopper neurons in the cochlear nucleus. The results of their paper (Rothman and Manis, 2003c) can be reproduced in NEURON. The implemented type I-c model (chopper neuron) simulates the response to a current clamp. In my simulation, the currents are varied from 0 to 200 pA and the corresponding voltage responses are saved. The voltage responses were analyzed in Matlab and the ISIs were plotted versus the input strength (Fig. 6.4). A strong dependence of the ISIs on the input strength can be clearly seen. In addition, the corresponding spike rate is plotted in the figure. The maximum of the spike rate curve marks the beginning of the refractory period which inhibits spiking. Therefore, the spike rate declines after the maximum. The ISIs approach asymptotically 2 ms with stronger input. In contrast, some real chopper neurons show smaller ISIs (e.g. 1.4 ms in Young et al., 1988). Moreover, the dynamic range of the spike rate of real chopper neurons is about 200-300 spikes/s in average Frisina et al. (1990a). If this physiological dynamic range is applied to the simulation of of Fig. 6.4, the corresponding ISIs in the simulation would span a range of about 5 to 23 ms, whereas real ISIs differ much less with varying level (e.g. Frisina et al., 1990b)

6.4.2 Patch clamp simulations of a network of two “Rothman choppers”

As it is presumed here that a network can stabilize ISIs in the presence of changing input strength, a network consisting of two chopper neurons, which are equally connected, was built up in NEURON. The corresponding graphical user interfaces of NEURON are depicted in the Appendix (Section 10.4). The choppers models are connected with synapses with an exponential decay of transmitter. The value of the synaptic weights and delays are displayed in Tab. 6.3.

Fig. 6.5 shows the result of the simulation. In contrast to the simulation of the single

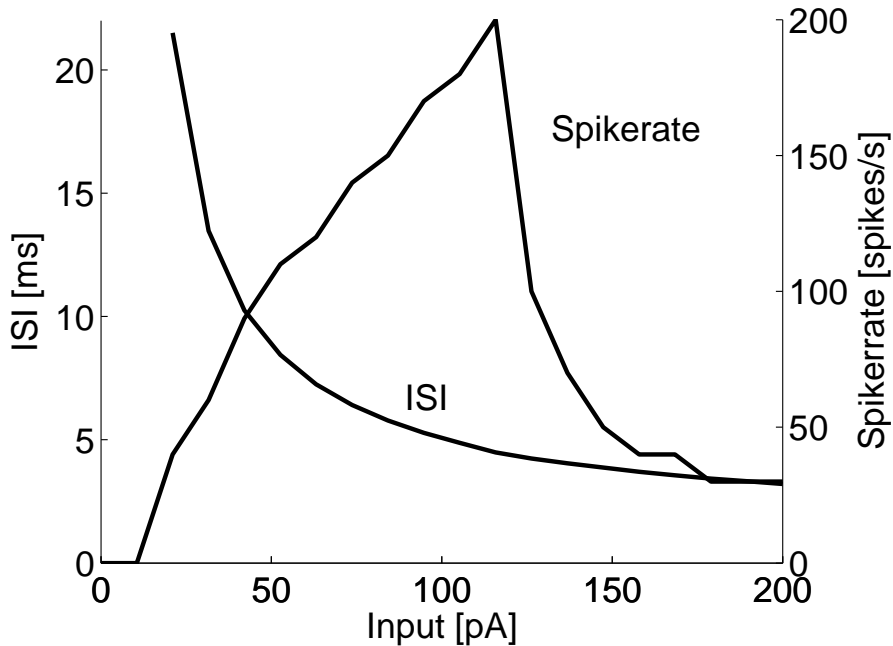


Figure 6.4: Single Rothman and Manis model: Dependence of the ISI on the input strength

neuron, the ISIs do nearly not vary when the input strength changes. The variation of the ISIs of the simulation is in the range of 0.1 milliseconds. The spike rate switches at 40 pA from 0 to 250 spikes/sec abruptly.

6.4.3 “Acceleration” of the “Rothman chopper” using genetic algorithms (GA)

As described above, the model of Rothman and Manis (2003c) cannot produce ISIs that are smaller than 2 ms. Furthermore, evidence was found that the smallest ISI is 0.8 ms (see Chapter 3). Therefore I tried to change the membrane model of Rothman and Manis (2003c) in such a way that it can produce ISIs of 0.8 ms. The membrane model of the chopper cell consists of a sodium current, a high threshold potassium current, a cation current, a leakage current, an external electrode current, and in parallel a membrane capacity of the cell (see method for details). The current is determined by the conductances of the specific ion channel. In the HH-like description of the cell the potassium and sodium channel behaviour is determined by activation and inactivation variables. The behaviour of the cation channel in this model is only determined by one activation variable. These variables are dependent on both membrane voltage and time. The time dependence is due to relaxing time constants, which are again membrane

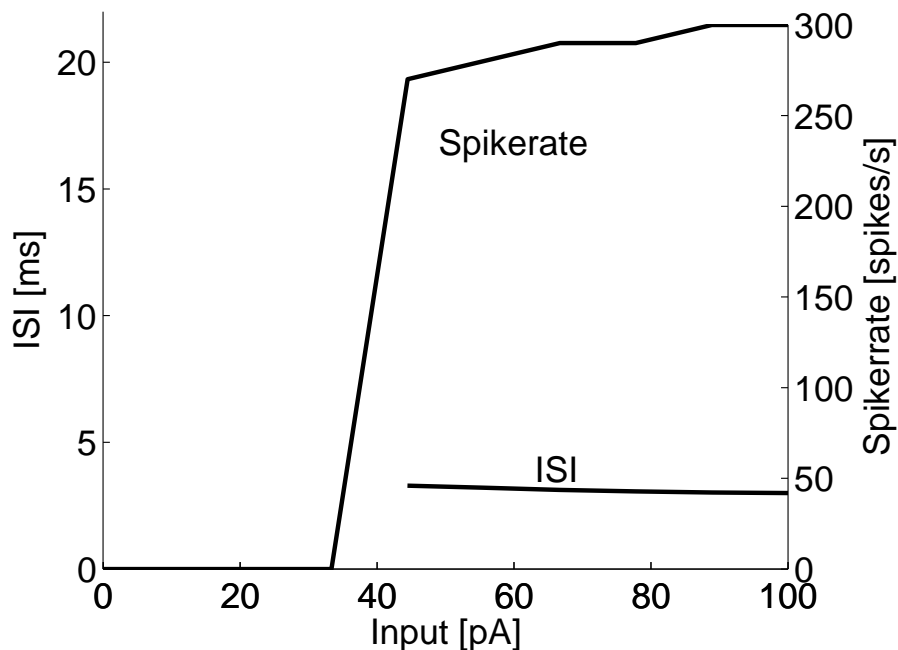


Figure 6.5: Network of Rothman and Manis model: Dependence of the ISI on the input strength.

voltage dependent. For this complexity, the optimization problem was divided into two subproblems: The first optimization was targeted on the maximum conductances, the second optimization on the time constants. Optimization focuses on the sodium and potassium channels at the same time because the interplay of both channels is important in order to maintain generation of action potentials of the cell.

Minimization of ISI by optimization of the conductances of the sodium and potassium channel

The smallest ISIs that can be achieved depend strongly and in a quasi-linear way on the capacity of the cell: decreasing of the capacity leads to decrease of the ISIs. Anatomically, reducing the capacity can stand for reducing the dimension of the cell provided that the specific capacity of the membrane remains the same. The dependency on the conductance and activation variables is more complex. Therefore, in the first optimization, capacity was set to a fixed value, the genetic algorithm (GA) was started, which optimized the maximum conductances of the sodium and potassium channel, the best results for the conductances to achieve a minimum ISI were selected, and this process was iterated with a smaller fixed capacity (temperature was set to 38°, the input strength to 180 pF, which is slightly beneath the maximum input at which the cell stops firing because of refractory period in order to achieve the smallest possible

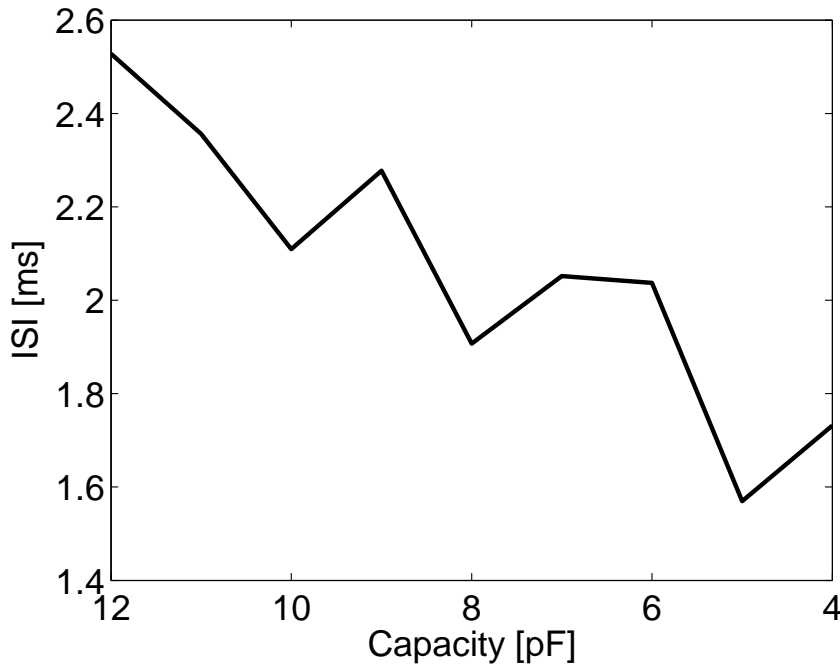


Figure 6.6: Single Rothman and Manis model: Optimization of conductances with GA: The best ISI with varying capacity

ISI). The best ISIs (convergence of the GA) for fixed capacities are plotted in Fig. 6.6 (see methods for details). As expected in general smaller values of the capacity leads to smaller minimal ISIs. In the simulated range of the capacity the ISI shows a minimum at 5 pF. The calculation was stopped after 4 pF because smaller values seem to correlate to unrealistic size of the neurons (see discussion for details). This optimization procedure produces a minimum ISI of about 1.6 ms. The corresponding factors for the conductances are shown in Fig. 6.7. In this figure, it is remarkable that the curve progression of the ISI is mainly determined by the progression of the factor of the potassium current.

Minimization of ISI by optimization of the time constants of the sodium and potassium channel

In the second optimization, time constants of the activation/inactivation variables of the sodium and potassium channel were optimized (see methods). Again capacity was set to a fixed value and the GA was iterated as described above. The results are depicted in Fig. 6.8. In contrast to the optimization of the maximum conductances, the optimization of the time constants converges to smaller ISIs at the same capacity. The first best ISI of this optimization reaches already the best value of all in the previous optimization. At 5 pF the goal of an ISI of 0.8 is achieved and as at 4 pF the ISI is

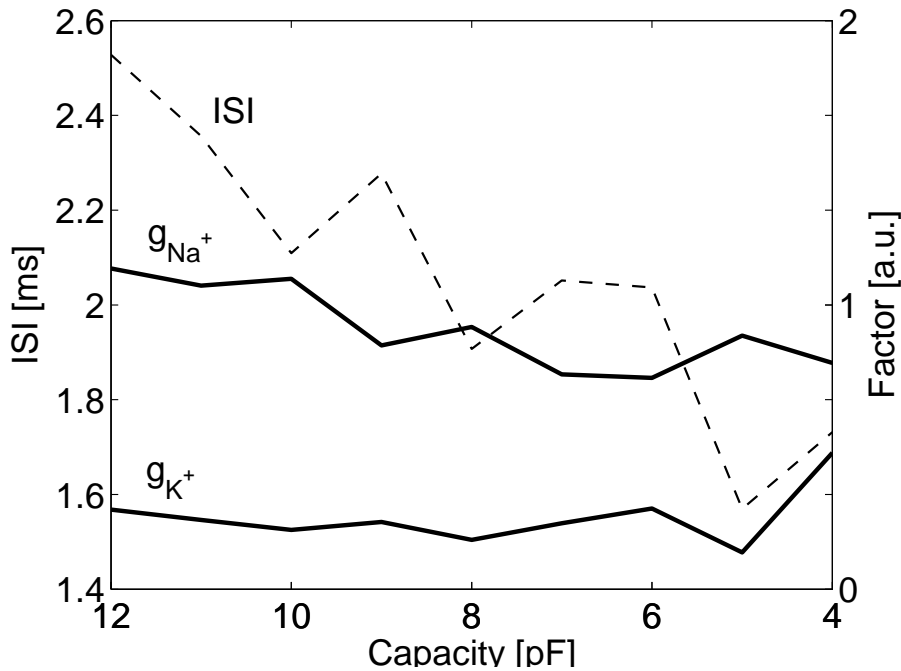


Figure 6.7: Single Rothman and Manis model: The best conductance-individuals with varying capacity

only slightly better, the algorithm was stopped. The corresponding factors of the time constants of the sodium and potassium channels are shown in Fig. 6.9. Interestingly, only the time constant τ_n , which is the time constant of the activation variable of the potassium channel, shows a globally decreasing progression. This is plausible because if the activation of the potassium channel is faster the refractory period will be shorter. But it is difficult to draw further conclusion concerning the remaining time constants as the dependencies are too complex.

6.4.4 The “fast Rothman chopper” in the Multi-oscillator

The membrane chopper model with a refractory period of 0.8 can be utilized in complex network of neurons. To test the functionality, the model is integrated in physiologically inspired networks.

Two “fast Rothman choppers” in a small circuit with input from onset neuron and from auditory nerve

After optimization of the model of Rothman and Manis (2003c) to achieve an ISI of 0.8 ms, it can be now a part of a network consisting of two choppers with a synaptic delay

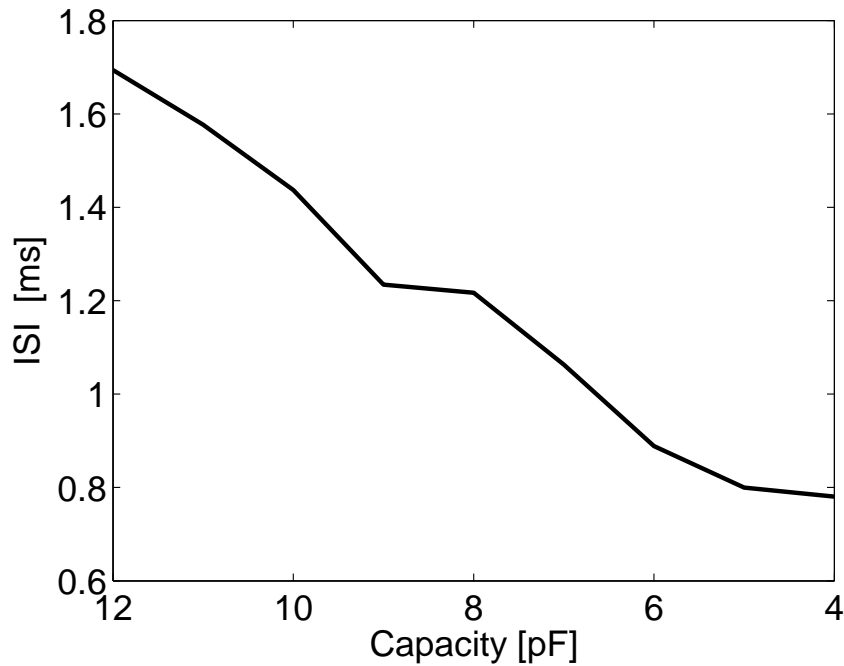


Figure 6.8: Single Rothman and Manis model: Optimization of time constants with GA: The best ISI with varying capacity

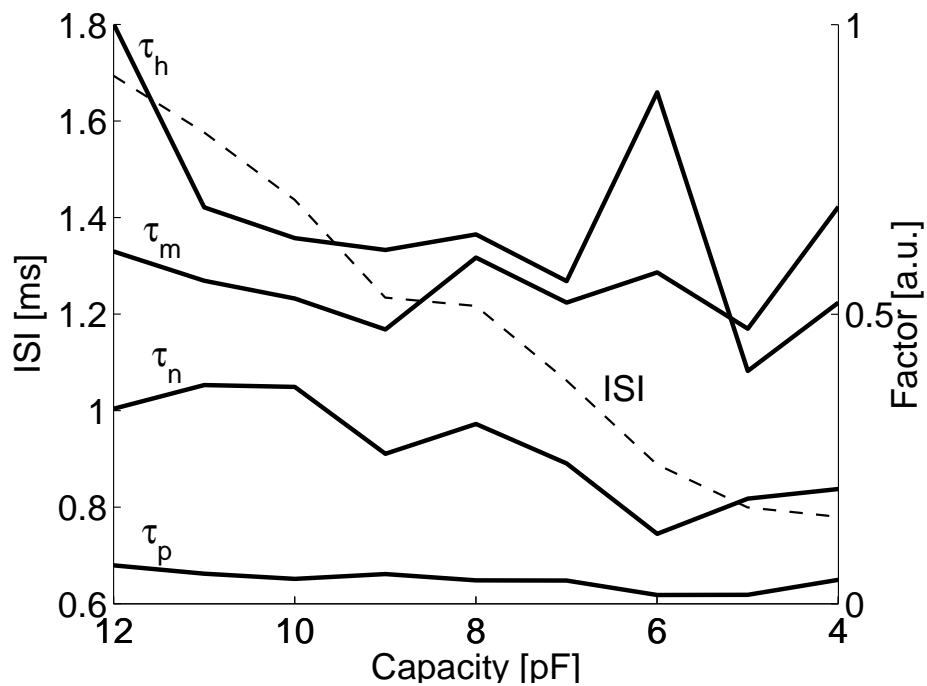


Figure 6.9: Single Rothman and Manis model: The best time-constant-individuals with varying capacity.

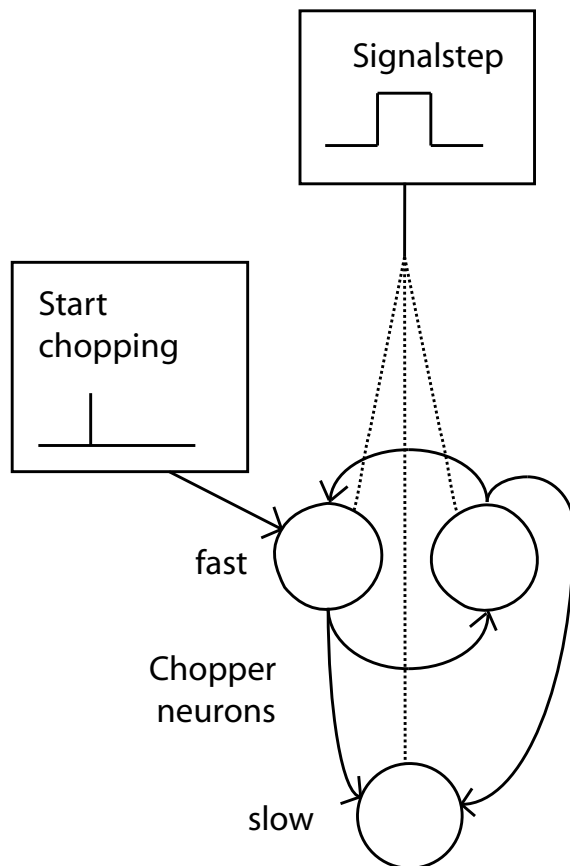


Figure 6.10: Physiologically inspired topology of chopper neurons with input from onset and ANF.

of 0.4 ms and can elicit spikes in a regular fashion. Evidence for the synaptic delay of 0.4 ms is given in Chapter 3. Further physiological and anatomical evidence (Chapter 3) lead to the simulation paradigm (see Fig. 6.10) that is described in Chapter 4. The difference to the simulation topology of Chapter 4 is that the nerve input and the input of the onset neuron are modeled as a signal step and one spike simultaneously with the beginning of the nerve signal step, respectively. The first input depolarizes the membrane of the chopper neurons but does not initiate spikes, because the weights of the input is adjusted in such a way that the change cannot trigger a spike. Instead, chopping is initialized by an additional spike of the onset neuron. The fast neurons act as a pace-maker with a clock-rate of 0.4 ms and project to slower chopper neurons which, due to their larger refractory period, skip shorter intervals while leaving intervals which are multiples of 0.4 ms. With this topology, the number of neurons required for long ISI and the redundancy of phase information is diminished in comparison to a simple circular network (see Chapter 4).

The simulation of the fast chopper neurons in the network (Fig. 6.11, left) shows that spiking starts with the input of the nerve and the onset neuron and stops with one

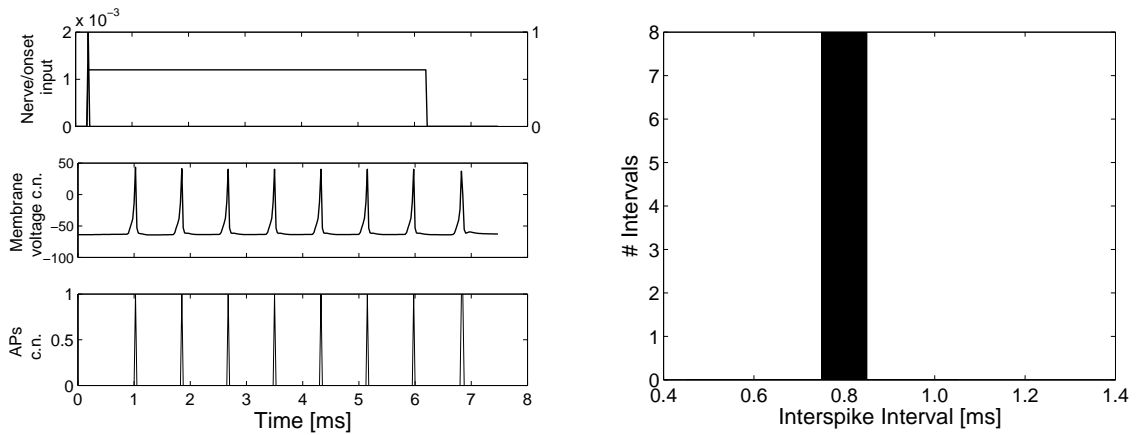


Figure 6.11: *Left:* Response of one fast chopper neuron in the physiologically inspired topology. *Right:* Histogram of the ISIs of the response of the fast chopper neuron.

additional spike after the end of the nerve input. The spikes show regular interspike intervals (Fig. 6.11, right). The histogram shows that the ISIs have a duration of 0.8 ms.

In Fig. 6.12 details of the simulation of a slow LIF chopper neuron with a refractory period of about 1.2 ms are depicted. The slow chopper neuron skips two of three incoming spikes, which have a delay of 0.4 ms. This results in ISIs of the slow chopper neuron of 1.2 ms.

A bank of chopper neurons producing different multiples of 0.4 ms

The fast chopper neurons which are connected as described above operate as a pace-maker and can also project to a variety of slower chopper neurons (Fig. 6.13). This yields a bunch of interspike intervals, which can be utilized for example for further time analysis.

The simulation of such a bank of slow LIF chopper neurons is shown in Fig. 6.14. The slow chopper neurons receive input from the same fast HH-like pace maker and have different refractory periods. The histograms show that the generated ISIs are multiples of 0.4 ms, which is the clock rate of the pace maker.

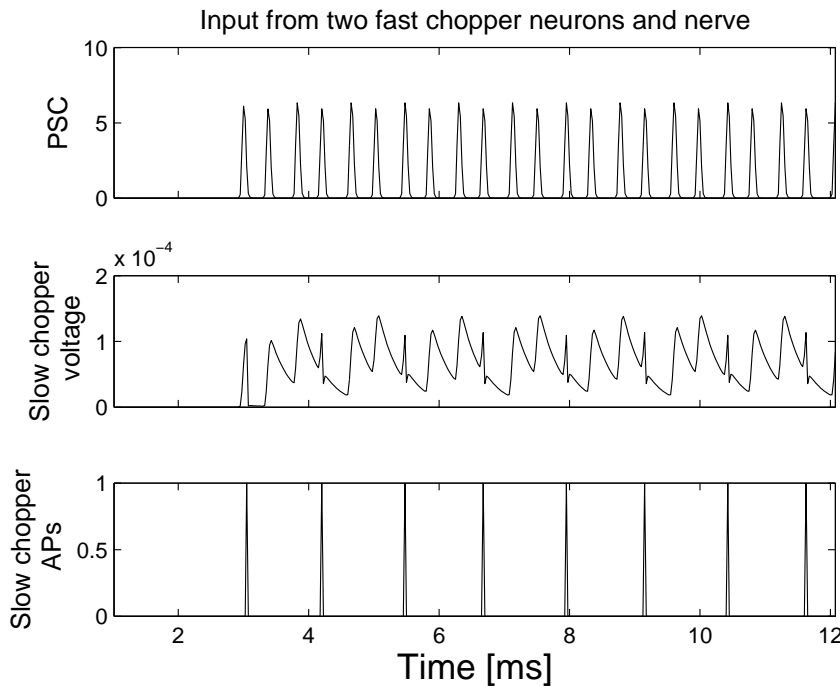


Figure 6.12: The pace maker circuit projects to a chopper neuron that filters multiples of 0.4 ms, which are appropriate to the refractory period.

6.5 Discussion

6.5.1 Simulations of single chopper neurons and networks of chopper neurons

The results of the original model of Rothman and Manis (2003c) for a single chopper neuron show that the results do not cover the physiological response range of real chopper neurons. The model is developed from measurements of real choppers and matches their sample. But obviously the sample is a subgroup of the entire chopper population and the model is fitted to the average of their sample (Rothman and Manis, 2003b). Furthermore, the temperature in their simulations (33°C) was not set to a physiological value. A strong dependence of the ISI on the input strength might be also apparent in isolated cells, but the small variation of the ISI apparent in vivo recordings seems to be a feature of the interconnected cells.

All of the HH-like models (including the model of Rothman and Manis, 2003c) show an increase of the spike rate and a decrease of the ISI until the refractory period is reached. Therefore, in order to explain the particular dynamic of the spike rate and the relatively independence of the ISI of chopper neurons despite level-changes, other mechanisms like stabilization of ISIs by neuronal networks can be taken into account. The simulation of the two-chopper network shows that it is possible to achieve the

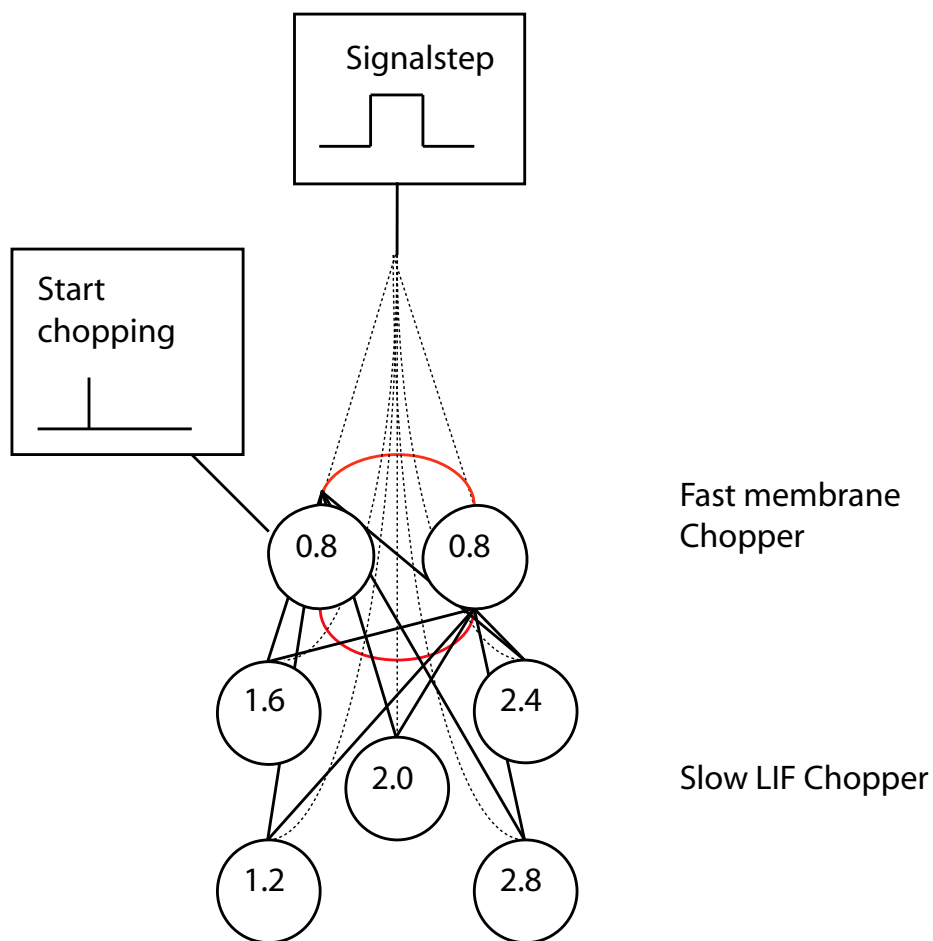


Figure 6.13: A bank of chopper neurons providing multiples of 0.4 ms by reducing a high-frequency input from a pacemaker mikro-circuit.

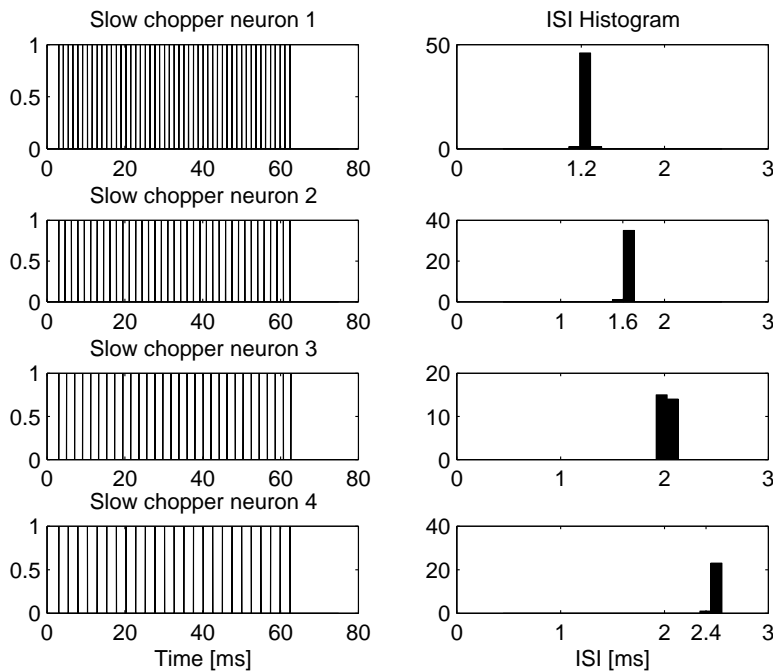


Figure 6.14: Different multiples of 0.4 ms can be provided by a small number of chopper neurons, which receive an input from the same pacemaker.

independence of the ISI from the input strength. The step-like increase of the spike rate in the simulation discussed in Section 6.4.4 seems not very physiological and is due to the highly precise synaptic delay. In a more physiologically approach, a small jitter would be added to the delay of the synapses with the consequence that some spikes would fall into the refractory period. As a result the step-like spike rate curve would be then smoothed out.

6.5.2 The optimization of the model using Genetic Algorithms

The HH-equations contain many parameters which can be used for optimization. Although genetic algorithms (GA) are capable to search in a high-dimensional parameter room, the number of the parameters should be as low as possible to reduce calculation time and to find fast reasonable solutions. The parameter, capacity of the neuron model, was taken out of the optimization loops of the GA because it has strong and nearly linear effect on the ISI that are generated: the lower the capacity the faster the cell generates spikes. The decrease of the capacity is equivalent to an decrease of the dimension of the cell. In the simulations of Rothman and Manis (2003c) the membrane capacity of 12pF yields a radius of 21 μm (neuronal specific membrane capacity of 0.9 $\mu\text{F}/\text{cm}^2$). In my simulation the “fast Rothman chopper” holds a capacity of 4 pF. The

corresponding surface is $444 \mu m^2$ and hence the radius of the (spherical) cell

$$r = \sqrt{444 \mu m^2 / \pi} \approx 12 \mu m.$$

This seems to be a physiological value as in the sample of Rothman and Manis (2003a) the shortest diameters range from 16 to 30 μm and in the sample Josephson and Morest (1998) the smallest cell areas are $128 \mu m^2$, which is equal to a radius of 6.4 μm .

A further way to lower the dimension of the parameter room in the optimization was to sort the parameters into groups. These groups are time constants and conductances and each of them were optimized at the same time. I chose to multiply these parameters by a factor because variation of them is equal to changing the temperature of a cell. This modification conserves the ability of the channels to generate action potentials and conserves the general response characteristics of the channels. Tests of the variation of the activation/inactivation progression curve $x_\infty(V)$ results in a severe change of the property of channel response characteristics and stops the generation of action potentials. Therefore this curve was not altered.

The optimization of the time constants resulted in the following multiplicative factors: $\tau_n \times 0.2036$, $\tau_p \times 0.0191$, $\tau_m \times 0.5576$, and $\tau_h \times 0.3667$ (“fast Rothman chopper”, refractory period 0.8 ms, see Section 6.4.4). The accuracy of the factors is given by four digits because small changes of the factors sometimes leads to deterioration of generating spikes. On one hand, the factors for the three time constants $\tau_{n,m,h}$ can be physiologically interpreted by an increase of the temperature: The temperature of the simulation in Rothman and Manis (2003a) was set to $33^\circ C$, whereas the temperature in vivo is about $38^\circ C$ and therefore time constants are smaller. Moreover, the Q10 value of these specific channels was found to be in a range of 2-4 (Cao and Oertel, 2005, see Fig. 6.3, right), which gives an even stronger decrease of the time constants than with the standard Q10 factor of 2 (see reaction-velocity-temperature rule by van `t Hoff). On the other hand, Rothman and Manis (2003b) fitted their model to data by averaging time constants and conductances that show high variability (see Section 6.2). As shown in Fig. 6.2 A, the time constant τ_n sometimes varies by a factor of 4 (see data point at about -110 mV), in Fig. 6.2 B τ_p by a factor of 4-5 (data point at about -75 mV). That means that the original data already contain much lower time constants than they used for their model, which in turn means that the optimized time constants of my model partly fall in the range of the measured data.

The fourth factor for τ_p , which is the slow component of the activation function (see Section 6.2.3), seems to be very small, but due the fact that discrepancies in the I_{HT} activation time constants of different models are great (see Section 6.2.3), the integration of the slow component in the model seems to be still unclear. Rothman and Manis (2003b) stated that the fast and slow component are probably due to independent channels, and therefore the slow channel might not be expressed in the fast chopper cells.

6.5.3 The “fast Rothman chopper” in the Multi-oscillator

The test of the optimized model with input from an onset neuron (a spike at the beginning of the signal) and from the nerve (a step-like signal) shows that it is plausible to assume that the choppers can excite each other. They oscillate with a period of 0.8 ms and a phase delay of 0.4 ms (Fig. 6.11). With the optimized model it is possible to integrate the HH-like model in the topologies proposed in Chapter 4. Also properties like tuning to a frequency (see Section 6.2, Winter et al., 2003; Frisina et al., 1990a; Rhode and Greenberg, 1994) can be incorporated in the model.

Furthermore, a slow chopper neuron can be triggered by the fast pacemaker choppers with the result that it oscillates with a period that is a multiple of 0.4 ms (Fig. 6.12). The model allows that a whole population of slower chopper neurons can be triggered by the pace maker circuit (Figs. 6.13, 6.14), which means a synchronization of a large network. The whole network requires only an input from the onset neuron at the peripheral pacemaker chopper neurons. This is in line with anatomical properties of stellate cells (chopper neurons) and octopus cells (onset neurons), which are adjacent in the VCN.

6.6 Conclusions

- Single HH-like chopper models (e.g. from Rothman and Manis, 2003c) show a strong dependency of ISI when changing the input strength. They do not show any preference for multiples of 0.4 ms, which is in contrast to physiological data.
- In contrast, networks of HH-like chopper neurons with a synaptic delay of 0.4 show this preference and an independence of ISI when changing the input strength.
- The HH-like model of chopper neurons by Rothman and Manis (2003c) does not account for short ISIs of real chopper neurons. The model has been modified with genetic algorithms to generate ISIs as short as 0.8 ms.
- This “fast Rothman chopper” has been successfully integrated in the multi-oscillator proposed in Chapter 4.
- An enlarged network which is synchronized by a circuit of two “fast Rothman choppers” can account for a preference of ISIs for multiples of 0.4 ms as found in physiological data (Chapter 3).

Chapter 7

Particular Issues

In this chapter particular issues are laid down that are not discussed in the previous chapters but were objective of discussions with other scientists. These issues may be relevant for further examinations.

7.1 Input to chopper neurons from onset units: Octopus or D-stellate cells?

The two inputs of the chopper neuron model which is described in Chapter 3 are supposed to come from the auditory nerve and an onset neuron. Octopus cells in the VCN are proposed as anatomical correlate to the onset units in the periodicity model (Langner, 1981). Ferragamo et al. (1998a) have shown that t-stellate cells (related to chopper neurons) receive input from d-stellate cells which are referred to onset-choppers. It was stated that the model seems plausible if onset units are d-stellate cells (Greenberg, S., pers. communication). There are some differences between d-stellate and octopus cells concerning their contribution to the enhancement of the dynamic range of chopper neurons. First d-stellate cells provide an inhibitory input. In our simulations the dynamic range has been enhanced by excitatory input that cannot simply be substituted by inhibition. In the majority of cases, inhibition is accompanied by a temporal delay and differs from excitation in the temporal contribution to spike generation and suppression, respectively.

Second, onset neurons (octopus cells) show the largest dynamic range of AM coding (up to 90-115 dB in Frisina et al., 1990b). It is hard to understand why this specialized property of onset neurons would not be used. Furthermore, octopus cells are adjacent to chopper neurons and in the proposed model of this work only a small portion of chopper neurons need input from onset neurons to be activated and activate a large network of subsequent chopper neurons.

7.2 Functional role of inhibition of D-stellate cells

As discussed in the previous section, d-stellate cells are less suitable to enhance AM encoding than octopus cells. However, it has been shown that t-stellate cells do indeed receive inhibitory input from d-stellate cells (Ferragamo et al., 1998a). There are several possible functional roles for this input.

Inhibition could mute effectively t-stellate cells in order to avoid accidentally self-excitation (without a spike from the onset neuron) or stop oscillations triggered by onset neurons. Furthermore, the combination of inhibitory and excitatory input might enhance the signal detection and provide a means of gain control by reducing the noise by inhibition (Josephson and Morest, 1998; Caspary et al., 1994).

On the other hand, Caspary et al. (1994) found that blockade of inhibitory inputs increased discharge rate primarily within the excitatory response area. That implies that temporal responses of chopper neurons show no or little change in the bandwidth of their response.

Furthermore, simulation of stellate cells showed that increasing number of inhibitory input increases regularity of firing (Josephson and Morest, 1998; Banks and Sachs, 1991).

7.3 Is the nerve input necessary for the Multi-oscillator?

The multi-oscillator, which was introduced in Chapter 4, consists of a small pacemaker circuit of two fast neurons and a reducer consisting of slow neurons. The pacemaker circuit may oscillate with a period of 0.8 ms in response to input from auditory nerve and an onset neuron. The pacemaker projects to slower neurons which oscillate with a period that is a multiple of the pace maker's clockrate of 0.4 ms. All of the chopper neurons of the multi-oscillator receive also an input from the auditory nerve, as it is in vivo. For the fast neurons this input enables chopping; it is a condition for starting and stopping the chopper neurons and necessary in a self-exciting network (Bahmer and Langner, 2007). But, in the context of the model this does not seem to be necessary for the slow chopper neurons because the functional role is substituted by the projection of the fast neurons. On the other hand, if an additional inhibition of chopper neurons is included (see above: functional role of inhibition of d-stellate cells) the input seem reasonable again: If inhibition mutes the circuit, the onset neuron could not start the chopper neurons. With the excitatory input from the nerve the inhibition is compensated and the onset neuron is able to start the oscillation of the chopper neurons. Integration of inhibition seems reasonable to enhance dynamic processing as mentioned above.

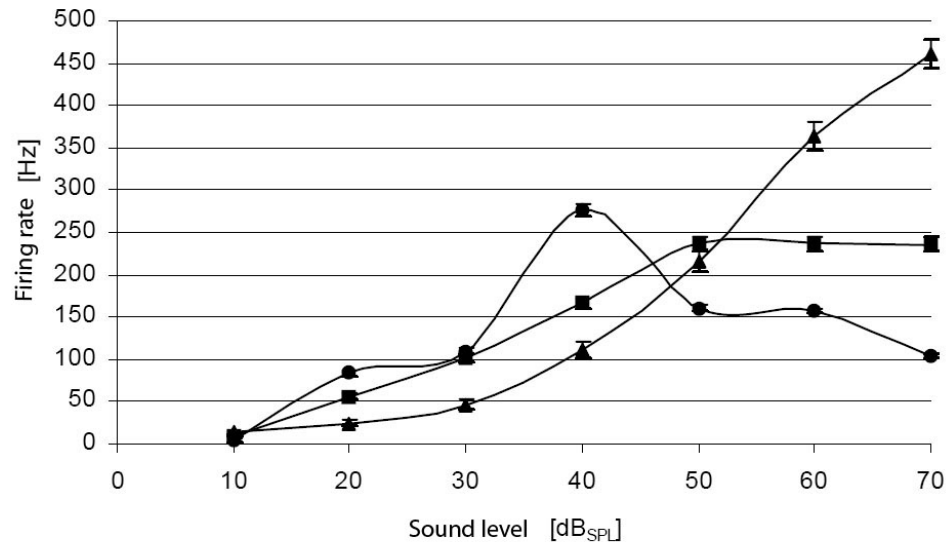


Figure 7.1: Three classes of rBMF function response patterns (level dependent firing rate at best modulation frequency) of IC neurons • - with optimum; ■ - saturating; ▲ - monotone (modified from Zschau, 2006).

7.4 Comparison of particular simulation results with experimental results

The simulation results in Chapter 4 and 5 show that the integration of the onset neuron over a wide frequency range has consequences for the periodicity encoding of the subsequent neurons. The level dependent progression of the synchronization curve of the onset neuron shows an optimum which depends on the width of the integration of the onset neuron. The influence of level and depth of modulation on the periodicity processing in the IC can be found in Zschau (2006), Diploma work at TU Darmstadt. As neurons in the auditory midbrain can encode periodicity information into their spike rate (Langner and Schreiner, 1996), it was hypothesized that the mechanism that causes the optimum in the level dependent VS in the CN neurons (see Chapter 4,5) is transferred into the midbrain. In the sample of Zschau (2006) three classes of level dependent firing rate at best modulation frequency (rBMF) were found (Fig. 7.1). According to Zschau (2006), Semple and Kitzes (1985); Woolley and Casseday (2004); Ehret and Merzenich (1988); Ferragamo et al. (1998b) have described similar classes of response pattern with similar dynamic ranges in the rBMF.

One class (20% of the neurons) shows an optimum at 40 dB SPL in the response to SAM, which is in line with the simulation of the response of the onset neuron in Chapter 4 to SAM. The other two classes show a saturating (42% of the neurons) and a monotone

(38%) increasing slope. Saturation started at 40-60 dB over the threshold.

The three classes differ not only in the shape of rBMF curve but consequently also in their dynamic ranges (Fig. 7.2). “Optimum” cells show a dynamic range between 50 and 90 dB, “monotone” cells in average 90 dB, and “saturation” cells in average 55 dB. Similar results are described in Woolley and Casseday (2004). In addition to the explanation of the “optimum” cell response in Chapter 4, the “saturation” and “monotone” cells response in the IC could be explained by a very large integration window of the onset neuron, but different level of spontaneous activity of the nerve fibers.

The same basic mechanism for both cell types is as follows: At low levels periodicity encoding increases with sound level because more frequency channels contain periodicity information. But at a certain level fibers at CF start to saturate and cancel the effect of providing periodicity information from fibers which start to fire at the same time. Therefore encoding of periodicity information remain constant stationary from this level.

In addition to the “saturation cell”, the “monotone cell” may receive input from onset neurons that integrate over nerve fibers with high spontaneous activity. The high noise of the not activated fibers is substituted by signal information with higher level. As noise is progressively diminished in the input of the onset neuron, periodicity information is enhanced.

Altogether the three groups might be subclasses of each other. The monotone curve may be the first part of the saturation curve which may be the first part of the optimum curve. If this is true, the difference could be determined by the width of the integration window and the spontaneous activity of the integrated nerve fibers.

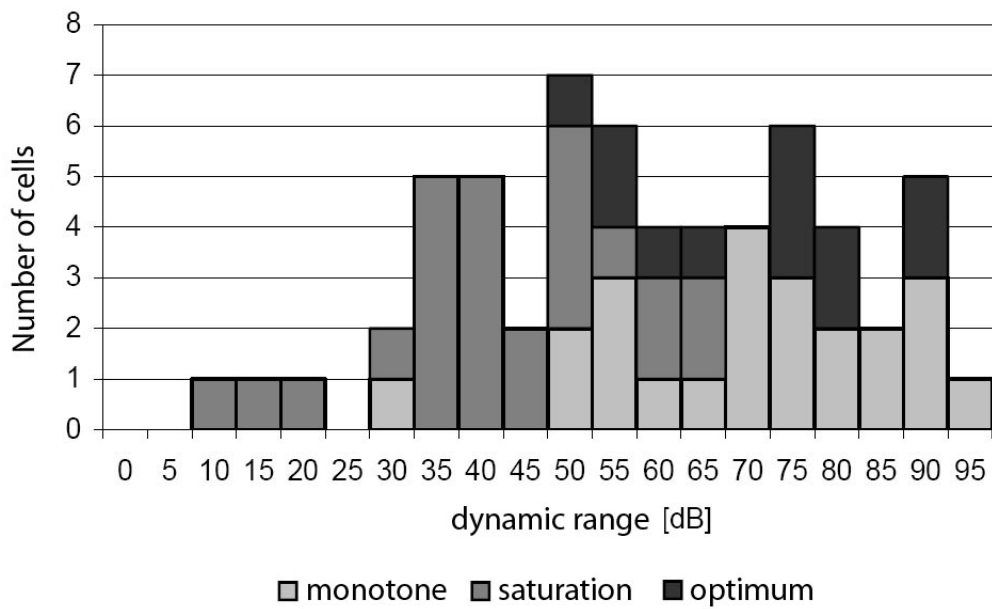


Figure 7.2: The three classes of Fig. 7.1 differ in their dynamic range in rBMF (modified from Zschau, 2006).

Chapter 8

General Discussion and Outlook

Each previous chapter of this thesis contains a discussion section. In addition, this general discussion summarizes the previous results in a broader context of the issues mentioned in the general introduction. This chapter is divided in two parts. The first part focuses on the physiological relevance of the simulation models and results, the second part shows the perspectives of these models.

8.1 General Discussion

8.1.1 Biological background for the Circular Oscillator and the Multi-oscillator

Evidence for a time constant of 0.4 ms emerges in recordings of neurons in the IC (Langner, 1981, 1983; Langner and Schreiner, 1988), in psychoacoustical experiments (Langner, 1981), and in recordings in the CN in Young et al. (1988). Consequently, a neuronal model for a temporal correlation analysis was suggested as a basis for pitch perception. This model included multiples of 0.4 ms as preferred intervals for intrinsic neuronal oscillations (Langner, 1983, 1992). Obviously, an explanation is required for the observation that the same time constant is apparent in different measurements and in various species such as man, Guinea fowl, and cat.

The high dynamic range of periodicity encoding as well as the rate function of chopper neurons can not be understood unless one assumes that their input comes from nerve fibers that code only a narrow frequency range and that onset neurons may activate chopper neurons.

Onset neurons show the best periodicity encoding in the VCN. Provided that they are able to trigger chopper neuron oscillations, they could enhance the periodicity encoding of chopper neurons. The input of onset neurons from a broad frequency range permits periodicity encoding even if single auditory nerve fibers saturate. Since chopper neurons

code periodicity similarly and they are located close to onset neurons, it seems reasonable to assume that they could receive an input from onset neurons. These neurons may be octopus cells. However, an actual connection between octopus cells and chopper neurons has not yet been demonstrated. As a consequence of the above conclusions, the topology of the simulation is as follows:

- To ensure the preference for multiples of 0.4 ms, chopper neurons are arranged in a circular network. The minimum number of two chopper neurons in this network corresponds to the proposed minimum refractory period of 0.8 ms.
- Chopper neurons receive input from both auditory nerve fibers and onset neurons.

In order to explain the response properties of chopper neurons, previous simulations of chopper neurons relied exclusively on membrane properties (e.g. Wiegrefe and Meddis, 2004; Hewitt et al., 1992; Arle and Kim, 1991; Banks and Sachs, 1991). Although these models can reproduce PSTHs of chopper neurons, regularity of intrinsic oscillations (mean, standard deviation and coefficient of variation), and tuning to frequencies and periodicities of chopper neurons, they can not reproduce the dynamic ranges of the spike rate and periodicity encoding or the preference for multiples of 0.4 ms in the interspike intervals of chopper neurons. Our first attempt to introduce discretized and limited oscillations intervals is based on spike-to-spike oscillations. The connections between the chopper neurons are presumed to be chemical synapses with a delay of 0.4 ms. As a result, the simulations show chopping with constant interspike intervals.

8.1.2 Regularity and periodicity analysis

In vivo properties of chopper neurons, such as the mean and the standard deviation of interspike intervals, and the coefficient of variation (CV), could be simulated with our model. The interspike interval histograms of the simulated chopper neurons show that the chopper period is conserved even for modulated signals. Therefore, the output of the chopper neuron could serve as an intensity-independent time reference for a subsequent temporal analysis, as was proposed in a model for pitch estimation (Langner, 1981, 1983, 1992).

In spite of their connections to onset neurons, the dynamic range of the pure tone response of the simulated chopper neurons is determined solely by the input from the auditory nerve. This input is mainly responsible for starting and stopping the response of the choppers and therefore can solve the problem addressed by Ferragamo et al. (1998a) concerning interconnected chopper neurons: “This circuit raises the question whether the mutual excitation in choppers could be self-sustaining and how chopper responses are terminated”.

Physiological data show that the modulation frequency of SAM is encoded in one frequency channel in the nerve with a small dynamic range of 30-40 dB (Frisina et al., 1985). This raises the question of how chopper neurons achieve their total dynamic

range of chopper neurons of about 90 dB. The answer which is suggested by our model is that chopper neurons receive input from onset neurons which integrate over a wide frequency range (Palmer et al., 1996; Oertel et al., 2000; Golding et al., 1999). In our simulation, this integration window was selected to be Gaussian shaped. However, the optimal range and shape of the integration window for encoding periodicity information is unknown and has to be studied in further simulations. The simulation presented here shows that the difference between the synchronization of the nerve and the onset neuron is considerable. The auditory nerve carries information tonotopically, whereas the onset neuron with its broadband integration utilizes temporal information from many frequency channels at the expense of spectral information. In line with physiological data (Frisina et al., 1990a), the dynamic range of the onset neuron for periodicity coding is much larger than that of the nerve and enables phase coding even at the highest levels investigated (90 dB SPL). The chopper neuron simulations show a dramatic difference between the results obtained with and without input from an onset neuron. Dynamic ranges differ by at least 70 dB.

8.1.3 Effects of changing the width of the frequency channel integration

The simulations also demonstrate the importance of the width of the frequency channel integration. Variation of the width shows that the frequency channel integration can be adapted for encoding periodicity at low or high levels.

Since the effect of different widths of frequency channel integration for the onset neurons are transferred to the chopper neurons, the adjustment of the integration width has also consequences for the subsequent processing steps.

The simulation results show that a narrow integration window is always an advantage for spectral coding. In contrast, a broad integration window is advantageous for periodicity coding at high levels, while for low levels a narrow integration window may be better. This is due to two other opposing effects: the correlation of synchronized activity in different channels is higher when the channels are in close proximity, on the other hand at high levels a broader integration window may also include non-saturated channels.

The SAM responses of simulated chopper neurons which receive input from onset neurons with different integration windows show a change in their resolution of the harmonics. As expected their resolution is better with a narrow than with a broader integration window. The reason is that broader integration windows of onset neurons at neighbouring CF overlap more, which smears the frequency information provided by the onset neurons to the chopper neurons. The other way round, decreasing the width of the integration window results in sharper tuning of the chopper neuron. In some cases, the simulated chopper neurons show a 40% enhancement in their resolution of harmonics compared to the resolution of the nerve (Chapter 5). An explanation for

this enhancement is the fact that two inputs - from the nerve and the onset neuron - act in this case as two multiplicative filters: the neuron will produce an output only if both inputs were active at the same time, if only one input or none were active, no output will be produced. This results in a sharper tuning.

Considering the high dynamic range of our acoustic environment and the fact that the auditory system has to deal with both narrow and broadband signals, one might hypothesize that it would be advantageous if the hearing system were able to adapt the spectral integration of onset neurons to different stimulus conditions.

Schneider et al. (2005) found narrow and broadband adaptations in the pitch perception of different subjects. The pitch of a harmonic sound in some objects may be dominated by periodicity information, in others by certain resolved low harmonics. The proposed multi-oscillator might provide an explanation for this phenomenon at an early stage of auditory signal processing: The correlative of the perception of the fundamental results from a dominance of onset neurons with broad integration windows, while a preference for the perception of the harmonics results from a dominance of narrow integration windows. The broad integration allows for a better encoding of the periodicity of a signal at high levels but shows a bad resolution of each harmonic component, while the narrow integration shows a bad ability to encode periodicity over a large dynamic range but results in a good resolution of components. Therefore, the described filtering mechanism determined by the shape of the integration window of the onset neuron at a low level of auditory nuclei is transferred to processing of the auditory system at a high level. An analogue example of such a filtering mechanism is the principle of tonotopy which is found throughout the auditory system commencing with the frequency filter mechanism of the cochlea. Cheveigné (2000) therefore called the auditory system a “separation machine”. A preference for a width of integration might be an inherited intrinsic property of the auditory system or, perhaps more likely, the result of an individual learning process: in the maturation of the auditory system the formation of task specialized neuronal structures could adapt to the acoustic environment. One could also postulate mechanisms that to some extent dynamically control the integration window of onset neurons, depending on the stimulus or the processing task. The adaptation of the window could be accomplished by level dependent lateral inhibition or by inhibition from higher processing centers. It is even possible that frequency channels which contribute to the integration process could be selected via presynaptic inhibition. These dynamic control mechanism could help to understand the “Cocktail-party effect”.

8.1.4 Periodicity coding despite saturation of nerve fibers?

As shown in Chapter 4 it is necessary for periodicity coding of chopper neurons that input from non-saturated nerve fibers project to chopper neurons. But in some cases auditory nerve fibers show to some extent periodicity coding despite saturation (Frisina et al., 1996; Winter et al., 2003). Therefore, chopper neurons might not need an

additional input from onset neurons to enhance their dynamic range of AM coding (Wiegrebe, L., pers. communication). In order to enhance the dynamic range of chopper neurons up to 90 dB, an input must provide a high synchronous response for at least a dynamic range of 90 dB. In contrast, data of Frisina et al. (1996) shows much smaller synchronous response to AM from 30 dB over threshold and in this paper it is stated that the reduction in AM responsiveness with sound level correlates with the limited dynamic range of nerve fibers concerning the rate-intensity function. Therefore, despite that the nerve fibers show to some extent AM coding at saturation (30-40 dB over threshold), this fact cannot explain the large dynamic range of AM coding of chopper neurons of up to 90 dB.

8.1.5 Experimental basis for the time constants in VCN neurons

The results of Chapter 6 show that it is possible to simulate the topology proposed in Chapter 3 and 4 not only with LIF models but also with a modified HH-like model of stellate cells. The modification performed by genetic algorithms was discussed for its physiological pertinence (see Chapter 6). Calculations and comparison gave evidence that the modified model can be in the physiological range. The conductances and time constants of the VCN channels were discussed (Oertel, D., pers. communication). The results of Cao and Oertel (2005) are in some ways contradicting to the findings of Rothman and Manis (2003b) concerning the fittings of the conductances. It was stated (Oertel, D., personal communication): “It is not always easy to decide how to fit exponentials to currents. People usually try fitting a single exponential first. If the fit is terrible, they go to two exponentials. The fit is invariably better but is it good enough? Those are to some extent arbitrary judgments.”

8.1.6 The “fast Rothman chopper” in the Multi-oscillator

The test of the optimized model with input from onset neuron and from the nerve shows that it is plausible to assume that the choppers can excite each other and oscillate with a period of 0.8 ms and a phase delay of 0.4 ms. It is possible to integrate the optimized HH-like model in the topologies proposed in 4 and properties of chopper neurons like tuning to a frequency (see Section 6.2, Winter et al., 2003; Frisina et al., 1990a; Rhode and Greenberg, 1994) can be incorporated.

Furthermore, a slow chopper neuron can be triggered by the fast pace maker choppers and oscillates with a period that is a multiple of 0.4 ms. Even a whole population of slower chopper neurons can be triggered by the pace maker circuit, which means a synchronization of a large network. The whole network requires only an input from the onset neuron at the peripheral pacemaker neurons, which is in line with anatomical properties of stellate cells (chopper neurons) and octopus cells (onset neurons), which

are adjacent in the VCN.

8.2 Outlook

In this section, extensions of the multi-oscillator (Chapter 3 and 4) and of the periodicity model (Chapter 2 and 3) for further simulations are outlined.

8.2.1 Implementation of inhibition

As described above, chopper neurons receive broadband inhibitory input, which is assumed to play a role rather in gain control than in frequency tuning (see above). For this purpose, an additional neuron with a negative weight can be integrated in the topology. Several questions arise: In which way will the input from the auditory nerve overcome the inhibition and which role plays timing in encoding modulation as inhibitory input is delayed? Can the inhibitory input enhance AM coding? Is it possible to mute a network of several interconnected neurons by inhibition to prohibit undesired self-activation by spontaneous activity?

8.2.2 Large networks containing the Multi-oscillator

The multi-oscillator, which is discussed in Chapter 4, is a prototype for a building block in a large network. The small pace maker enslaves all the subsequent neurons which are supposed to be perhaps hundreds of neurons that are connected. Inhibition as described above will therefore play an important to prohibit self-excitation and enhance exact timing.

Large networks can have some special operation modes. Anninos (1972) showed in a simulation that a large network consisting of 200-1000 neurons fires at times that are integer multiples of the synaptic delay. The networks were specified by a number of parameters like the ratio of inhibitory neurons in the network, cell connections, and similar properties. It was found that the neurons of the network can show self-maintaining cyclic modes with a fixed period (multiples of the synaptic delay), which can be altered in the period by an external input. Surprisingly, evidence was found that the nets cycling modes do not depend on the detailed structure of the net.

Considering these results, it would be interesting to simulate such large networks, which are triggered by the pace maker of the multi-oscillator. Consequently, several questions arise: How robust will this network be? What will be the effects of the inhibitory regulation? Which effects has an external input like the nerve input? Simulations can perhaps help to understand the structure of the VCN and the intra- and interconnections of chopper neurons.

8.2.3 Pure tone and AM processing

The periodicity model from Langner (Langner, 1981, 1983, 1992; Rees and Langner, 2005), which is described in Chapter 2 and 3, gives a basis for the explanation for pitch perception. It is a model, which correlates the carrier and modulation frequency of a harmonic complex signal. The oscillator is triggered by the modulation and elicits several spikes for coding every modulation. These spikes coincide with spikes from integrated responses to the carrier. As a result a coincidence occurs when multiples of the carrier period fit into the modulation period.

But what happens if the signal is a pure tone? In this case, no modulation is apparent and the oscillator is only triggered by the signal onset. Therefore the oscillator should send spikes for at least one period of the pure tone, so that again one spike of the oscillator and one spike of the delayed pure tone can coincidence.

These are two modes of the model and the pure tone mode has to be tested in further simulations. Especially the interplay between the inhibitory input and the excitatory input from the onset neuron in the pure tone mode has to be analyzed.

8.2.4 Integration of the results in the periodicity model from Langner

The periodicity model described in Chapter 2 and 3, is an abstract model of a neural network in the central auditory system. As the nerve input and the inhibition of the chopper neurons apparently play an important role for encoding modulation frequency the model has to be completed by these inputs. Inhibition has been already integrated in a newer version of the model, to enable the coincidence neuron to respond only to a distinct relation between the modulation and the carrier frequency and not to higher harmonic relations. As it is known that this inhibition is delayed, it seems that in this case at the beginning of the processing the neurons let pass a higher amount of information and with time the information amount is “sharpened”. It is interesting if this principle can be echoed in further simulations of chopper neurons including inhibition.

Chapter 9

Summary

The aim of this work was to test a new model for oscillating neurons (chopper neurons) in the cochlear nucleus of the auditory system.

In **Chapter 3** is shown that multiples of 0.4 ms are apparent in intrinsic oscillations in the auditory system and in pitch shift experiments. The existence of a time constant of 0.4 ms is explained by the assumption of a minimum chemical synaptic delay of this size between chopper neurons. The large dynamic range of periodicity coding, the small dynamic range of pure tone response, and the sharp frequency tuning of chopper neurons can be explained as a functional result of simultaneous projections from both the auditory nerve fibers and onset neurons to chopper neurons.

As a consequence, the topology of the simulation described in the following **Chapter 4** is as follows: To ensure the preference for multiples of 0.4 ms as observed in physiological and psychophysical experiments, chopper neurons are arranged in a circular network. The minimum number of two chopper neurons in this network results in a chopper period of 0.8 ms which corresponds to the proposed minimum refractory period of 0.8 ms. In the topology, chopper neurons receive input from both auditory nerve fibers and onset neurons. Simulations of the model show that in contrast to previous models, the present model can explain the preference for multiples of 0.4 ms. The model has also the advantage of explaining their large dynamic range of periodicity encoding of chopper neurons in spite of their narrow frequency tuning.

Like the models investigated previously by other authors, the present model is able to simulate interspike intervals of spike trains of the chopper responses with high precision. Moreover, the simulation can explain essential properties of real chopper neurons by input from onset neurons.

As discussed in **Chapter 5**, the simulations show that variation of the integration widths of onset neurons results in a corresponding variation of the spectral resolution of chopper neurons with smaller widths resulting in a higher resolution of frequency components. Variation of the integration widths of onset neurons also results in varia-

tion of the periodicity encoding of chopper neurons. Narrow integration widths lead to better periodicity encoding at low levels. At high levels broader integration widths lead to better periodicity encoding. Therefore it is a conflicting demand at high levels for to adapt the width of the integration to tuning or to encoding periodicity. The observed pitch dichotomy of individual preferences of human subjects for either periodicity pitch or the pitch of low spectral components of harmonic sounds (Schneider et al., 2005) can be explained by assuming adaptations of the width of the integration to either spectral or temporal coding.

In contrast to physiological data, Hodgkin-Huxley(HH)-like models of single chopper neurons (e.g. from Rothman and Manis, 2003c) show a strong dependency of their interspike intervals when changing the input strength and do not show any preference for multiples of 0.4 ms. Simulations in **Chapter 6** show that networks of HH-like chopper neurons with a synaptic delay of 0.4 ms do exhibit this preference and their chopper intervals are independent of changing the input strength. The HH-like model of chopper neurons by Rothman and Manis (2003c) does not account for short oscillating intervals of real chopper neurons. The model has been modified with genetic algorithms to generate oscillating intervals as short as 0.8 ms. This “fast Rothman chopper” has been successfully integrated in the multi-oscillator proposed in Chapter 4. An enlarged network which is synchronized by a circuit of two “fast Rothman choppers” can account for a preference of ISIs for multiples of 0.4 ms as found in physiological data.

Zusammenfassung in deutscher Sprache

Das Ziel dieser Arbeit war, ein Modell für oszillierende Neurone (Chopperneurone) in der ersten Station der Hörbahn (Nucleus cochlearis) zu entwickeln und zu testen.

In **Kapitel 3** werden Vielfache von 0.4 ms in intrinsischen Oszillationen im auditorischen System und in sog. “pitch shift” Experimenten beschrieben. Die Zeitkonstante von 0.4 ms wird durch die Annahme einer kleinsten chemischen synaptischen Verzögerung erklärt. Die in physiologischen Experimenten beschriebene hohe dynamische Breite der Periodizitätskodierung, die geringe dynamische Breite in der Antwort auf einzelne Töne und das präzise Tuning von Chopperneuronen kann durch die gleichzeitige Projektion von sowohl auditorischen Nervenfasern als auch von sog. Onsetneuronen verstanden werden.

Daraus ergibt sich die Topologie des Choppermodells in **Kapitel 4** folgendermassen: Um die Präferenz für Vielfache von 0.4 ms sicherzustellen, bilden die simulierten Chopperneurone ein kreisförmiges Netzwerk. Die kleinste Anzahl von zwei Chopperneuronen in diesem Netzwerk entspricht der geforderten minimalen Refraktärzeit von 0.8 ms. Die simulierten Chopperneurone erhalten einen Eingang von Nervenfasern und Onsetneuronen. Simulationen dieses Modells zeigen, dass das hier vorgestellte Modell im Gegensatz zu den bisherigen Modellen, die Präferenz für Vielfache von 0.4 ms von Chopperneuronen erklären kann. Das Modell ist zusätzlich noch in der Lage, die hohe Dynamik der Periodizitätskodierung bei gleichzeitigem präzisiertem Tuning verständlich zu machen. Darüber hinaus kann das Modell, wie die bisherigen Modelle auch, Interspike-Intervalle präzise simulieren.

In **Kapitel 5** wird in Simulationen von Chopperneuronen gezeigt, dass die Änderung der Integrationsbreiten der projizierenden Onsetneurone eine Veränderung der spektralen Auflösung der Chopperneurone nach sich ziehen. Werden die Integrationsbreiten schmaler, wird die Auflösung von Frequenzkomponenten besser. Außerdem verändert die Breite auch die Periodizitätskodierung. Schmale Integrationsbreiten führen zu einer besseren Periodizitätskodierung bei niedrigen Lautstärken. Bei hohen Lautstärken führt eine breite Integration zur besseren Kodierung. Das ist die Ursache dafür, dass bei hohen Lautstärken sich die Adaptation der Integrationsbreite an das Tuning und die Adaptation an die Periodizitätskodierung entgegenstehen. Die beobachtete Zweideutigkeit der Tonhöhenempfindung, die bestimmt ist durch entweder die Einhüllende oder durch eine niedrige spektrale Komponente eines harmonischen Klanges (Schneider et al., 2005), kann durch die Annahme erklärt werden, dass die Integrationsbreite der Onsetneurone an spektrale oder zeitliche Kodierung angepaßt ist.

Im Gegensatz zu physiologischen Daten zeigen Hodgkin-Huxley-artige Modelle von einzelnen Chopperneuronen (z.B. von Rothman and Manis, 2003c) eine starke Abhängigkeit ihrer Interspike-Intervalle bei Veränderungen der Eingangsstärke und zeigen keine Präferenz der Interspike-Intervalle für Vielfache von 0.4 ms. Simulationen in **Kapitel 6** zeigen, dass Netzwerke Hodgkin-Huxley-artiger Neurone mit einer synaptischen Verzögerung von 0.4 ms diese Präferenz und eine Unabhängigkeit von der Eingangsstärke aufweisen. Mit dem Hodgkin-Huxley-artigen Choppermodell von Rothman and Manis (2003c) können die kurzen Interspike-Intervalle von physiologischen Chopperneuronen nicht simuliert werden. Daher wurde das Modell mit Hilfe von genetischen Algorithmen modifiziert, um Interspike-Intervalle von 0.8 ms zu erzeugen. Dieser “schnelle Rothman-Chopper” wurde erfolgreich in den “Multi-Oszillator” aus Kapitel 4 integriert. Die Präferenz physiologischer Interspike-Intervalle für Vielfache von 0.4 ms kann auch durch ein erweitertes Netzwerk, das durch zwei verschaltete “schnelle Rothman-Chopper” synchronisiert wird, erklärt werden.

Chapter 10

Appendix

10.1 Leaky integrate-and-fire neuron and synapses as Matlab function-file

10.1.1 Synapse

```
function [PSCout]=Synapse(dt,steps,leakage,weight,AP,mu,sigma)

persistent ltime
persistent transmitter
persistent buffer
persistent latencystep
global depletion2
if length(transmitter)==0
transmitter=0;
end
if length(ltime)==0
lzeit=length(depletion2)- steps +1;
latencystep=abs(round(normrnd(mu,sigma)/dt));
end
%-----Calculation-----
if AP ==1
ltime=1;
latencystep=abs(round(normrnd(mu,sigma)/dt));
end
transmitter=transmitter+depletion2(ltime)*dt;
transmitter=transmitter-transmitter*dt*leakage;
PSCin=weight*(tanh(abs(transmitter)*10 - 5)+1)/2;
```

```

ltime=ltime+1;
%-----Latency-----
if latencystep1>length(buffer)
buffer(latencystep+1)=PSCin;
else
buffer(latencystep+1)=buffer(latencystep+1)+PSCin;
end
PSCout=buffer(1);
buffer(1)=[];

```

The depletion in the synapse is a look-up table:

```

function depletion2=depletion(dt,steps);

lengthdep=0.0002; % 0.2ms
if dt>=lengthdep disp('dt has to be smaller than 0.0002!')
depletion=0;
else
stepstable=round(lengthdep/dt);
maxvalue=12e3;
x=1:stepstable/2;
table=x*(maxvalue/(stepstable/2));
depletion=[ table fliplr(x(1:end-1))*maxvalue/(stepstable/2) 0];
depletion2=[ depletion zeros(1,Schritte)];
end

```

10.1.2 Soma

```

function [APout]=Somanoise(dt,leakage,PSC,threshold,mu,sigma)

persistent ltime
persistent current
if nargin<4
global threshold
end
if length(current)==0
current=0;
end
%-----Threshold-----
noise=normrnd(mu,sigma)*0.0001;
threshold2=[threshold 0 zeros(1,ltime)]; % with buffer

```

```

if length(ltime)==0
ltime=length(threshold)+1; % outside refractory time
end
%-----Calculation-----
current=current+PSC*dt;
current=current-current*dt*leakage;
currentout=current;
if (current+noise)>threshold2(ltime) + 0.0001
APout=1;
current=0;
ltime=1;
else APout=0;
ltime=ltime+1;
end

```

The threshold for the soma is a look-up table:

```

function out=threshold(absrefrac,relrefrac,dt)

absz=zeros(1,round(absrefrac/dt));
absz(1,:)=10;
if relrefrac =0
below=round(relrefrac/dt);
x=linspace(0,14,below);
relz=(10)*exp(-x);
out=[absz relz];
else
out=absz;
end

```

10.2 Hodgkin Huxley Equations of the model of Rothman and Manis (2003c)

The model currents presented below have voltage and time dependencies similar to those of the original Hodgkin and Huxley model (1952). In these equations, currents are governed by an activation/ inactivation variable x whose rate of change is defined by the following first-order differential equation

$$\frac{dx}{dt} = (x_{\infty} - x)/\tau_x \quad (10.1)$$

where τ_s is the time constant of x , x_∞ is the steady-state value of x (i.e. the value of x when $t \gg x$), and x itself represents the activation/ inactivation variables a , b , c , w , z , n , p , m , h , and r in the following text. Although the formalism of the preceding equation is different from the original HH formalism in which activation/inactivation variables are expressed in terms of “open” and “close” rate constants α and β , they are nevertheless mathematically equivalent when $x_\infty = \alpha/(\alpha + \beta)$ and $\tau_x = 1/(\alpha + \beta)$. Reversal potentials are: $V_K = -70$ mV, $V_{Na} = +55$ mV, $V_h = -43$ mV, and $V_{lk} = -65$ mV.

Fast transient K^+ current

$$I_A = \bar{g}_A \cdot a^4 bc \cdot (V - V_k) \quad (10.2)$$

$$a_\infty = [1 + \exp(-(V + 31)/6)]^{1/4} \quad (10.3)$$

$$b_\infty = [1 + \exp((V + 66)/7)]^{-1/2} \quad (10.4)$$

$$c_\infty = b_\infty \quad (10.5)$$

$$\tau_a = 100 \cdot [7 \exp((V + 60)/14) + 29 \exp(-(V + 60)/24)]^{-1} + 0.1 \quad (10.6)$$

$$\tau_b = 1000 \cdot [14 \exp((V + 60)/27) + 29 \exp(-(V + 60)/24)]^{-1} + 1 \quad (10.7)$$

$$\tau_c = 90 \cdot [1 + \exp(-(V + 66)/17)]^{-1} + 10 \quad (10.8)$$

Low-threshold K^+ current

$$I_{LT} = \bar{g}_{LT} \cdot w^4 z \cdot (V - V_K) \quad (10.9)$$

$$w_\infty = [1 + \exp(-(V + 48)/6)]^{-1/4} \quad (10.10)$$

$$z_\infty = (1 - \zeta) \cdot [1 + \exp((V + 71)/10)]^{-1} \quad (\zeta = 0.5) \quad (10.11)$$

$$\tau_w = 100 \cdot [6 \cdot \exp((V + 60)/6) + 16 \cdot \exp(-(V + 60)/45)]^{-1} + 1.5 \quad (10.12)$$

$$\tau_z = 1000 \cdot [\exp((V + 60)/20) + \exp(-(V + 60)/8)]^{-1} + 50 \quad (10.13)$$

High-threshold K^+ current

$$I_{HT} = \bar{g}_{HT} \cdot [\varphi n^2 + (1 - \varphi)p] \cdot (V - V_K) \quad (\varphi = 0.85) \quad (10.14)$$

$$n_\infty = [1 + \exp(-(V + 15)/5)]^{-1/2} \quad (10.15)$$

$$p_\infty = [1 + \exp(-(V + 23)/6)]^{-1} \quad (10.16)$$

$$\tau_n = 100 \cdot [11 \exp((V + 60)/24) + 21 \exp(-(V + 60)/23)]^{-1} + 0.7 \quad (10.17)$$

$$\tau_p = 100 \cdot [4 \exp((V + 60)/32) + 5 \exp(-(V + 60)/22)]^{-1} + 5 \quad (10.18)$$

Fast Na⁺ current

$$I_{Na} = \bar{g}_{Na} \cdot m^3 h \cdot (V - V_{Na}) \quad (10.19)$$

$$m_{\infty} = [1 + \exp(-(V + 38)/7)]^{-1} \quad (10.20)$$

$$h_{\infty} = [1 + \exp((V + 65)/6)]^{-1} \quad (10.21)$$

$$\tau_m = 10 \cdot [5 \exp((V + 60)/18) + 36 \exp(-(V + 60)/25)]^{-1} + 0.04 \quad (10.22)$$

$$\tau_h = 100 \cdot [7 \exp((V + 60)/11) + 10 \exp(-(V + 60)/25)]^{-1} + 0.6 \quad (10.23)$$

Hyperpolarization-activated cation current

$$I_h = \bar{g}_h \cdot r \cdot (V - V_h) \quad (10.24)$$

$$r_{\infty} = [1 + \exp((V + 76)/7)]^{-1} \quad (10.25)$$

$$\tau_r = 10^5 \cdot [237 \exp((V + 60)/12) + 17 \exp(-(V + 60)/14)]^{-1} + 25 \quad (10.26)$$

Leak current

$$I_{lk} = \bar{g}_{lk} \cdot (V - V_{lk}) \quad (10.27)$$

10.3 Programs for NEURON and Matlab

The following script in NEURON is an iteration for different values of IClamp currents. It can be called from within a NEURON session (file → load mod-file). Before starting the script a Ro_Cell object has to be created within NEURON.

```
//Andreas Bahmer 25.1.06

objref icur
icur = new Vector (50, 100)
ncur = 2 // normal number of current steps
variable_domain(&ncur, 1, 50)
imax = 50
objref w // window, run control and plot window
objref rect, recv, reci, tempmatrix
rect = new Vector()
recv = new Vector()
reci = new Vector()
tempmatrix = new Matrix()
recv.record(&Ro_Cell[0].soma.v(0.5)) //assignment of the membrane voltage
rect.record(&t)//assignment of the time
```

```

//loop for different IClamp values and storage of membrane voltages for each
values
// in tempatrix

proc runhere(){
for i=0,ncur-1 {
icur.x[i] = i*imax/(ncur-1)
IClamp[0].amp=icur.x[i]/1000
IClamp[1].amp= icur.x[i]/1000
run()
tempmatrix.resize(ncur+1,rect.size()+1)
tempmatrix.setrow(i+1,recv )
tempmatrix.x[i+1][rect.size()]=icur.x(i)
}
tempmatrix.setrow(0,rect )
}
objref savdata
savdata = new File()
// saves tempmatrix in rothmanmat.txt (first two values are header)
proc matrix() {
n=tempmatrix.ncol
m=tempmatrix.nrow
savdata.wopen("rothmanmat.txt")
tempmatrix.fprint(savdata, "% g")
savdata.close()
}
w = new HBox()
w.intercept(1)
xpanel("")
xbutton("Run ", "runhere()")
xbutton("save matrix", "matrix()") //button for saving tempmatrix
xvalue("IV max (pA)", "imax", 200)
xvalue("# IV steps", "ncur", 2)
xpanel()
w.intercept(0)
w.map("Andreas Bahmer 06",400,50,200,200)

```

The following script-file in Matlab imports the Rothmanmat.txt file generated by the previous code in NEURON. The first two values in the file have to be removed by hand.

```

clear all
close all

```

```

data=load('rothmanmat.txt'); % erase first line (only 2 elements)
[m,n ]=size(data);
imagesc((1:n-1)*0.025,data(2:end,end),data(2:end,1:end-1))
xlabel('Time [ms]')
ylabel('Input [pA]')
colormap(1-gray)

%% Action potentials
ap=(data(2:end,1:end-1)>-20);
figure
imagesc((1:n-1)*0.025,data(2:end,end),ap)
colormap(1-gray)

%%-----Analysis

zeit=data(1,1:end-1)*0.001;
%% ap is data without time and input strength!!

for za1=1:m-1
clear isi isi2
isi=diff(zeit(find(ap(za1,:)))));
isi2=isi(find(isi>0.0001));
g(za1)=data(za1+1,end);
g2(za1)=mean(isi2);
g3(za1)=length(isi2);
end

figure
p1 = line(g,g2*1000,'Color','k');
ax1 = gca;
set(ax1,'XColor','k','YColor','k')
set(get(ax1,'YLabel'),'String','ISI [ms]')
ax2 = axes('Position',get(ax1,'Position'),...
'XAxisLocation','bottom',...
'YAxisLocation','right',...
'Color','none',...
'XColor','k','YColor','k');
p2 = line(g,g3*1/0.1,'Color','k','Parent',ax2);
ylabel('Spikerrate [spikes/s]')
xlabel('Input [pA]')

```

The following data is the complete setup of the two membrane chopper network model in NEURON (call: “forall psection()” in NEURON)

```

Ro_Cell[0].soma {nseg=1 L=19.5441 Ra=150
/*location 0 attached to cell 1*/
/* First segment only */
insert morphology {diam=19.5441}
insert capacitance {cm=0.9}
insert kht {ek_kht=-70 gkhtbar_kht=0.0125}
insert k_ion {}
insert na {ena_na=55 gnabar_na=0.0833333}
insert na_ion {}
insert leak {g_leak=0.000166667 erev_leak=-65}
insert ih {ghbar_ih=4.16667e-05 eh_ih=-43}
insert ExpSyn {tau=0.1 e=10}
insert IClamp {del=5 dur=100 amp=0.12}
}
Ro_Cell[1].soma {nseg=1 L=19.5441 Ra=150
/*location 0 attached to cell 2*/
/* First segment only */
insert morphology {diam=19.5441}
insert capacitance {cm=0.9}
insert kht {ek_kht=-70 gkhtbar_kht=0.0125}
insert k_ion {}
insert na {ena_na=55 gnabar_na=0.0833333}
insert na_ion {}
insert leak {g_leak=0.000166667 erev_leak=-65}
insert ih {ghbar_ih=4.16667e-05 eh_ih=-43}
insert ExpSyn {tau=0.1 e=10}
}

```

10.4 Graphical User Interface of NEURON simulations in Chapter 6

Figures 10.1-10.4 are screenshots of the graphical user interface in NEURON of simulations in Chapter 6. A reproduction of a simulation of a single chopper neuron from Rothman and Manis (2003c) can be seen in Fig. 10.1, Figs. 10.2-10.4 illustrate the implementation of two chopper neuron models of Rothman and Manis (2003c) in a network.

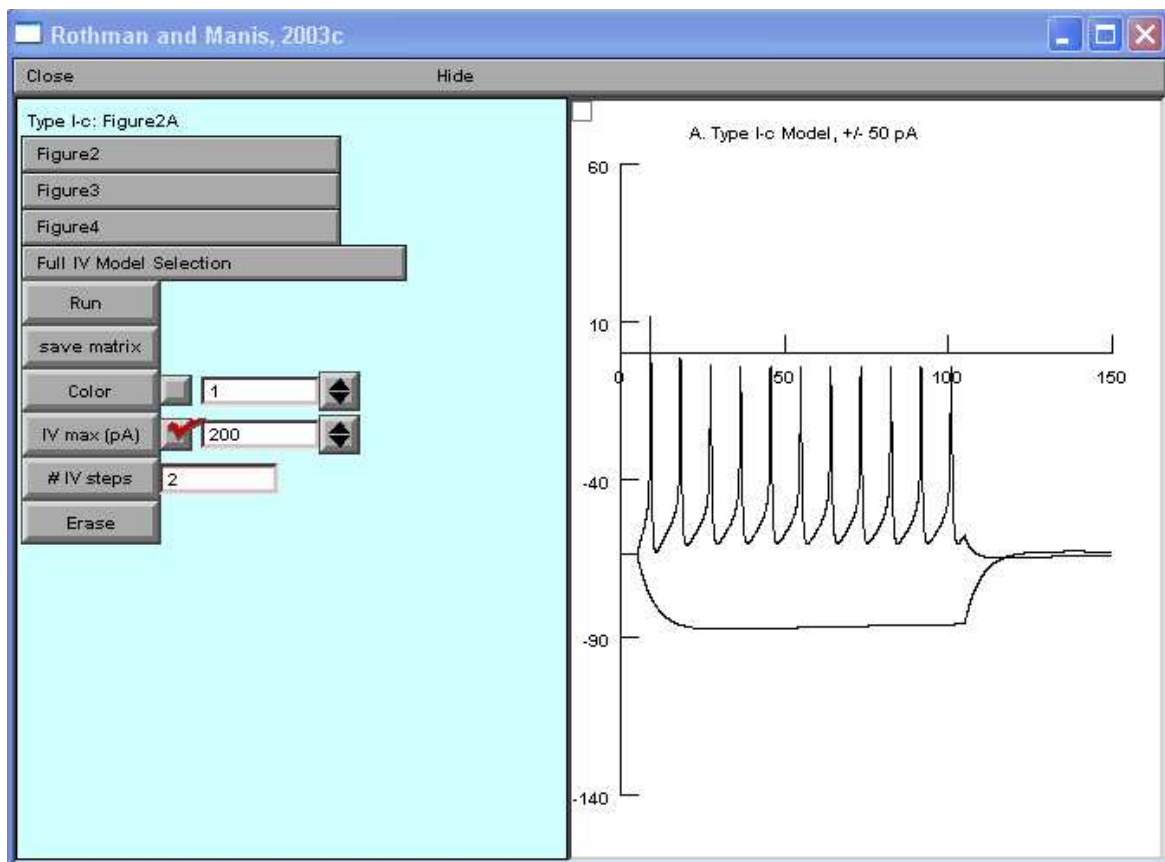


Figure 10.1: Single Rothman and Manis chopper model: NEURON graphical user interface

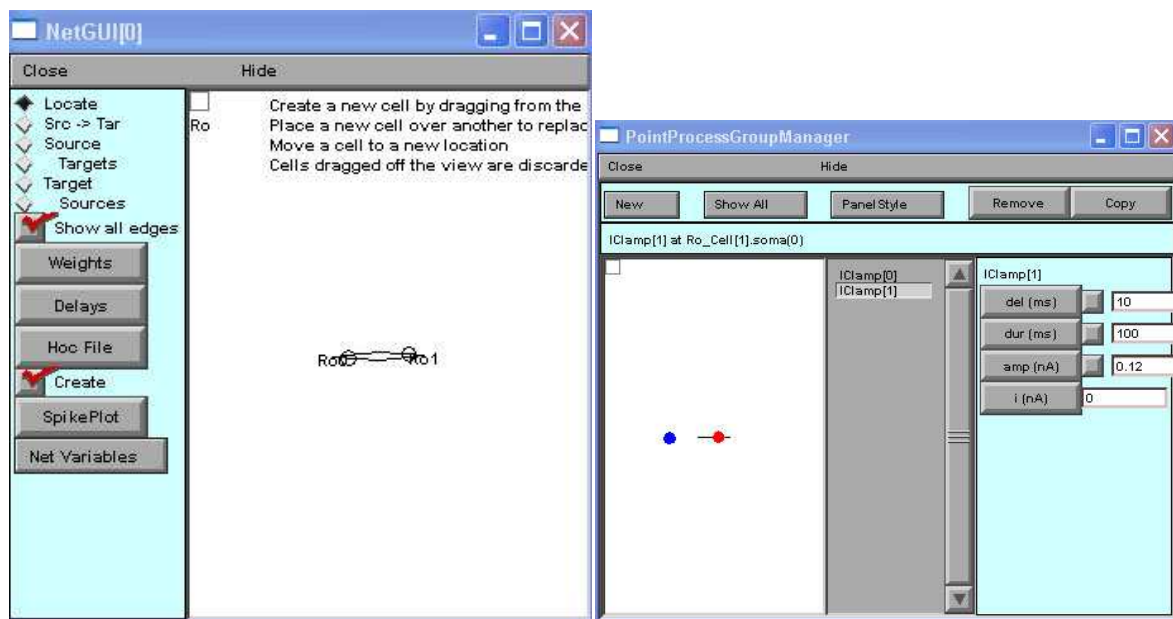


Figure 10.2: Network of two Rothman and Manis chopper models: NEURON graphical user interfaces I. *Left window*: Topology of the two chopper models. The two neurons are interconnected (first and second cell are circles with label ro0 and ro1). *Right window*: Patch clamp processes are attached to each neuron (blue and red). The displayed values are from the ro1 cell.

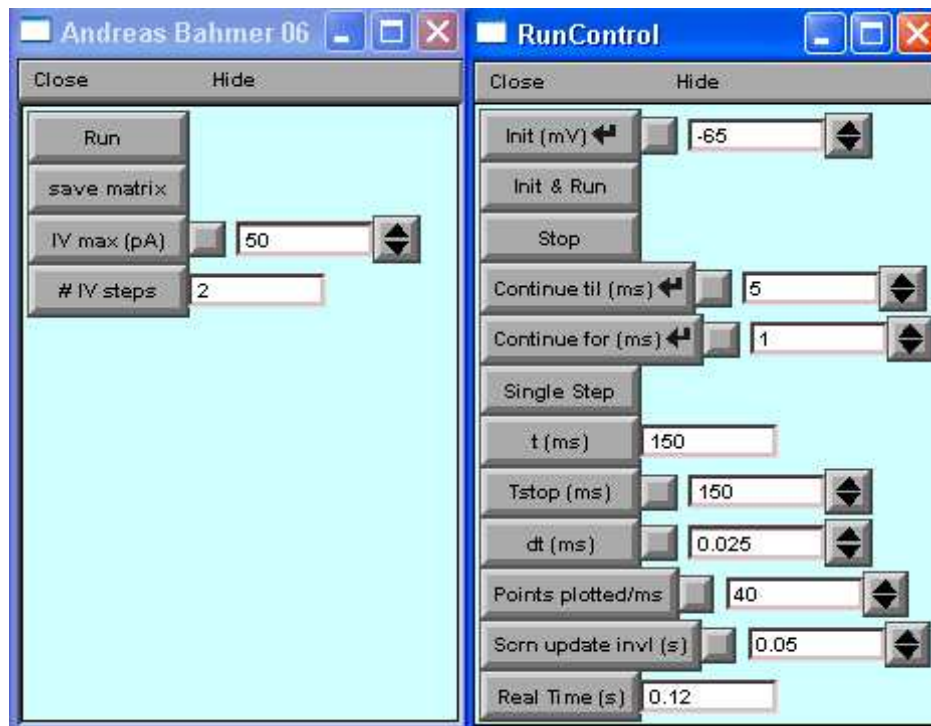


Figure 10.3: Network of two chopper models Rothman and Manis (2003c): NEURON graphical user interfaces II. *Left window:* The simulations are iterated with the help of a loop control and the results can be saved in a matrix, which is analyzed in Matlab. *Right window:* Parameters of the simulation run.

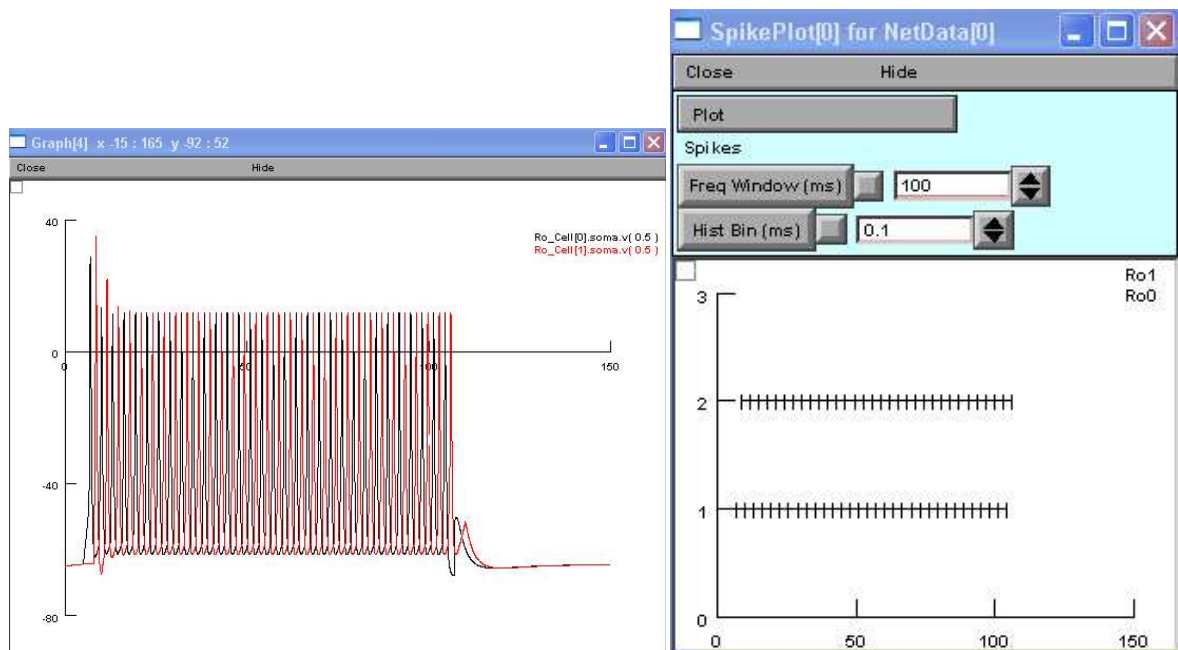


Figure 10.4: Network of two chopper models Rothman and Manis (2003c): NEURON graphical user interfaces III. *Left window*: Time progression of membrane voltage of both cells (black of the ro0 cell, blue of the ro1 cell). The curves show a phase delay of half of the period of each neuron. *Right window*: Spike plots of both cells.

10.5 Genetic Algorithm for the optimization of the membrane model of Rothman and Manis (2003c)

The genetic algorithms that was used for the optimization is implemented in the genetic algorithm toolbox from Matlab. The following outline summarizes how the genetic algorithm works:

1. The algorithm begins by creating a random initial population.
2. The algorithm then creates a sequence of new populations, or generations.
3. At each step, the algorithm uses the individuals in the current generation to create the next generation. To create the new generation, the algorithm performs the following steps:
 - a. Scores each member of the current population by computing its fitness value.
 - b. Scales the raw fitness scores to convert them into a more usable range of values.
 - c. Selects parents based on their fitness.
 - d. Produces children from the parents. Children are produced either by making random changes to a single parent – mutation – or by combining the vector entries of a pair of parents – crossover.
 - e. Replaces the current population with the children to form the next generation.
4. The algorithm stops when one of the stopping criteria is met.

10.5.1 Initial population

In the simulations the size of the initial population is set to 20 individuals, the initial range lies between $[0; 1]$ and $[0.9; 1, 1]$ for the time constants and conductances optimization, respectively.

10.5.2 Creating the Next Generation

At each step, the genetic algorithm uses the current population to create the offspring that make up the next generation. The algorithm selects a group of individuals in the current population, called parents, who contribute their genes – the entries of their vectors – to their children. The algorithm usually selects individuals that have better fitness values as parents. The function that the algorithm uses to select the parents is called the Selection function. The genetic algorithm creates three types of children for

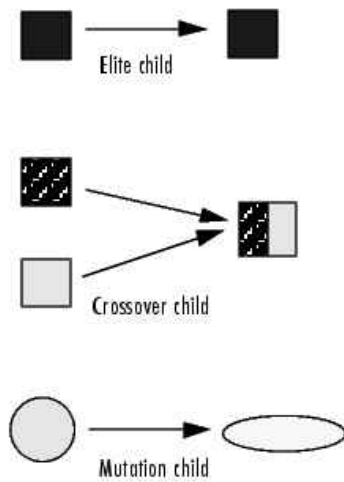


Figure 10.5: Genetic algorithm: Three types of children

the next generation: Elite children are the individuals in the current generation with the best fitness values. These individuals automatically survive to the next generation. Crossover children are created by combining the vectors of a pair of parents. Mutation children are created by introducing random changes, or mutations, to a single parent. The schematic diagram in Fig. 10.5 illustrates the three types of children.

Mutation and Crossover explains how to specify the number of children of each type that the algorithm generates and the functions it uses to perform crossover and mutation. The following sections explain how the algorithm creates crossover and mutation children.

Crossover Children: The algorithm creates crossover children by combining pairs of parents in the current population. At each coordinate of the child vector, the default crossover function randomly selects an entry, or gene, at the same coordinate from one of the two parents and assigns it to the child.

Mutation Children: The algorithm creates mutation children by randomly changing the genes of individual parents. The algorithm adds a random vector from a Gaussian distribution to the parent.

The type of children the algorithm creates can be chosen as follows:

Elite count, in Reproduction options, specifies the number of elite children.

Crossover fraction, in Reproduction options, specifies the fraction of the population,

other than elite children, that are crossover children.

For example, if the Population size is 20, the Elite count is 2, and the Crossover fraction is 0.8, the numbers of each type of children in the next generation is as follows: There are 2 elite children. There are 18 individuals other than elite children, so the algorithm rounds $0.8 \times 18 = 14.4$ to 14 to get the number of crossover children. The remaining 4 individuals, other than elite children, are mutation children.

10.5.3 Stopping Conditions for the Algorithm

The genetic algorithm uses the following five conditions to determine when to stop:

- Generations – The algorithm stops when the number of generations reaches the value of Generations.
- Time limit – The algorithm stops after running for an amount of time in seconds equal to Time limit.
- Fitness limit – The algorithm stops when the value of the fitness function for the best point in the current population is less than or equal to Fitness limit.
- Stall generations – The algorithm stops if there is no improvement in the objective function for a sequence of consecutive generations of length Stall generations.
- Stall time limit – The algorithm stops if there is no improvement in the objective function during an interval of time in seconds equal to Stall time limit.

The algorithm stops as soon as any one of these five conditions is met. It is possible to specify the values of these criteria in the Stopping criteria options in the Genetic Algorithm Toolbox. The default values are shown in the figure below. When the genetic algorithm is running, the Status panel displays the criterion that caused the algorithm to stop. The options Stall time limit and Time limit prevent the algorithm from running too long. If the algorithm stops due to one of these conditions, the results might be improved by increasing the values of Stall time limit and Time limit. The options Stall time limit and Time limit prevent the algorithm from running too long.

In the simulations, the vector of the individuals for the conductances optimization is $[\lambda_{Na}, \lambda_{HT}]$ and the vector for the time constant optimization is $[\kappa_m, \kappa_h, \kappa_n, \kappa_p]$. In the following HH-like equations the entries of each vector form factors:

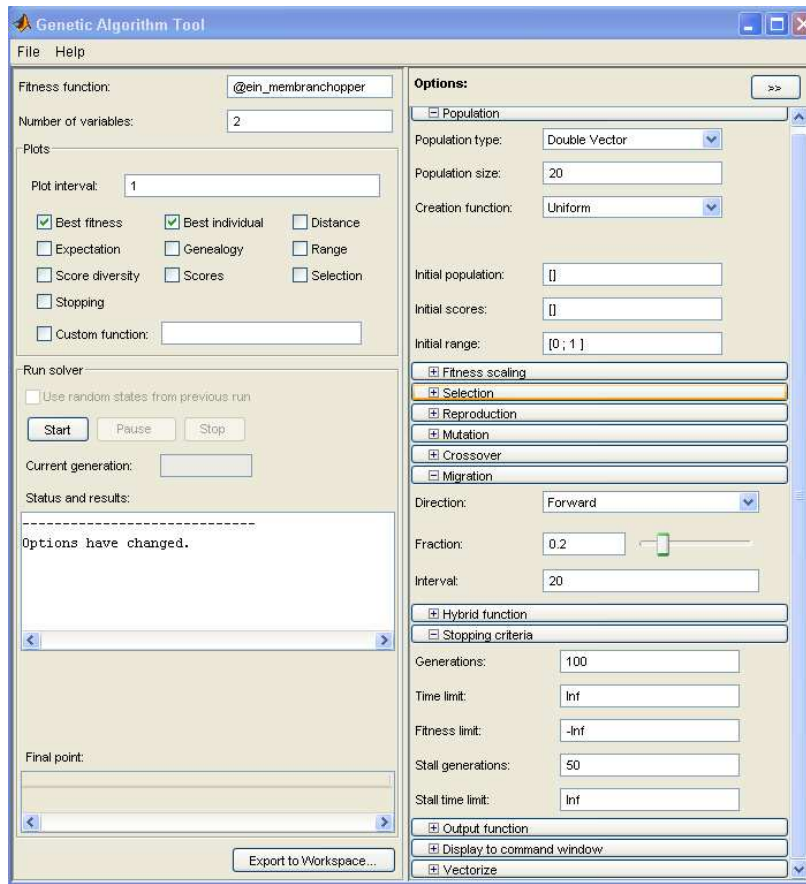


Figure 10.6: GA toolbox: GUI for conductances optimization.

Fast Na^+ current

$$I_{Na} = \lambda_{Na} \cdot \bar{g}_{Na} \cdot m^3 h \cdot (V - V_{Na})$$

$$\tau_m = \kappa_m \cdot 10 \cdot [5 \exp((V + 60)/18) + 36 \exp(-(V + 60)/25)]^{-1} + 0.04$$

$$\tau_h = \kappa_h \cdot 100 \cdot [7 \exp((V + 60)/11) + 10 \exp(-(V + 60)/25)]^{-1} + 0.6$$

High-threshold K^+ current

$$I_{HT} = \lambda_{HT} \cdot \bar{g}_{HT} \cdot [\varphi n^2 + (1 - \varphi)p] \cdot (V - V_K) \quad (\varphi = 0.85)$$

$$\tau_n = \kappa_n \cdot 100 \cdot [11 \exp((V + 60)/24) + 21 \exp(-(V + 60)/23)]^{-1} + 0.7$$

$$\tau_p = \kappa_p \cdot 100 \cdot [4 \exp((V + 60)/32) + 5 \exp(-(V + 60)/22)]^{-1} + 5$$

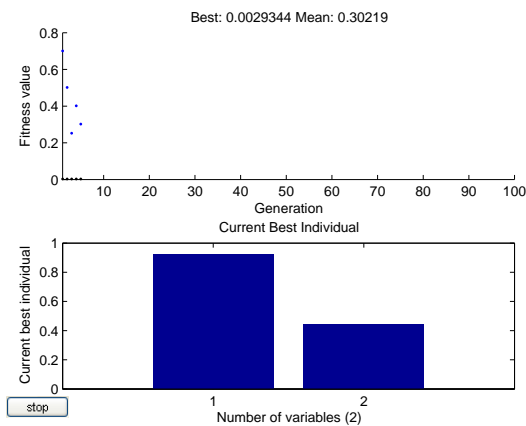


Figure 10.7: Optimization of conductances with GA toolbox: The upper plot displays the best and mean fitness values in each generation. The lower plot displays the coordinates of the point with the best fitness value in the current generation. Typically, the objective function values improve rapidly at the early iterations and then level off as they approach the optimal value.

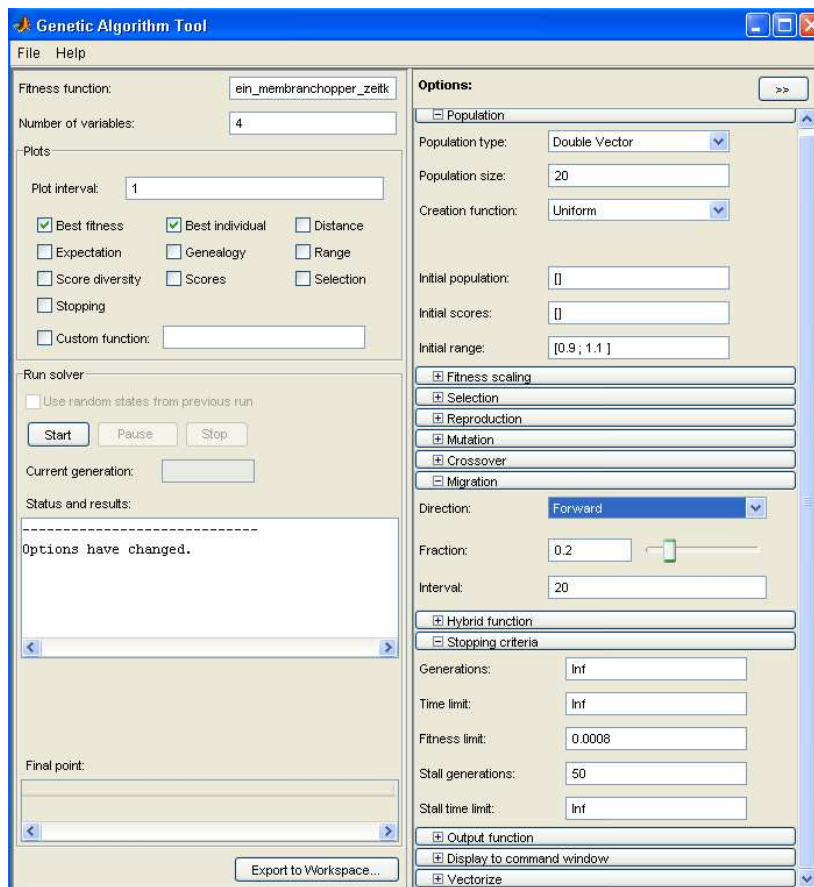


Figure 10.8: GA toolbox: GUI for time constants optimization

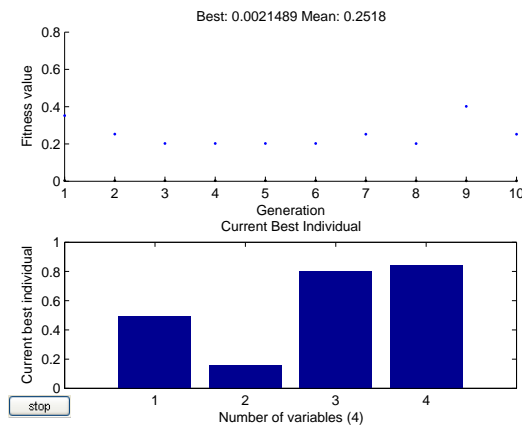


Figure 10.9: Optimization of time constants with GA toolbox: The upper plot displays the best and mean fitness values in each generation. The lower plot displays the coordinates of the point with the best fitness value in the current generation.

10.6 Iteration of Genetic Algorithm for the optimization of the membrane model of Rothman and Manis (2003c)

Each optimization for the conductances and the time constants was performed for decreasing capacity of the membrane because the capacity has to highest impact on the rapidness of the modelled neuron. The corresponding matlab script is as follows:

```
load gaproblem_cond
```

```
global za2
```

```
stor=[];
```

```
stor2=[];
```

```
stor3=[];
```

```
for za2=12:-1:4
```

```
[x, fval]= ga(gaproblem);
```

```
stor=[stor; x];
```

```
stor2=[stor2;fval]
```

```
stor3=za2;
```

```
end
```

Bibliography

- Adams JC (1983) Multipolar cells in the ventral cochlear nucleus project to the dorsal cochlear nucleus and the inferior colliculus. *Neurosci Lett* 37:205–208
- Andersen RA, Burdick JW, Musallam S, Pesaran B, Cham JG (2004) Cognitive neural prosthetics. *Trends Cog Sc* 8:486–493
- Anninos PA (1972) Cyclic modes in artificial neural nets. *Kybernetik* 11:5–14
- Arle JC, Kim DO (1991) Neural modeling of intrinsic and spike-discharge properties of cochlear nucleus neurons. *Biol Cybern* 64:273–283
- Arnesen AR, Osen KK (1978) The cochlear nerve in the cat: Topography, cochleotopy and fiber spectrum. *J Comp Neurol* 178:661–678
- Bahmer A, Langner G (2006a) Oscillating neurons in the cochlear nucleus: I. Experimental basis of a simulation paradigm. *Biol Cybern* 95:371–379
- Bahmer A, Langner G (2006b) Oscillating neurons in the cochlear nucleus: II. Simulation results. *Biol Cybern* 95:381–392
- Bahmer A, Langner G (2007) Simulation of oscillating neurons in the cochlear nucleus: A possible role for neural nets, onset cells, and synaptic delays. In: Kollmeier B, Klump G, Hohmann V, Langemann U, Mauermann M, Uppenkamp S, Verhey J (eds) *Hearing - from basis research to applications*, Springer, pp 126–132
- Bal R, Oertel D (2001) Potassium currents in octopus cells of the mammalian cochlear nucleus. *J Neurophysiol* 86:2299–2311
- Banks MI, Sachs M (1991) Regularity analysis in a compartment model of chopper units in the anteroventral cochlear nucleus. *J Neurophysiol* 65:606–629
- Banks MI, Pearce RA, Smith PH (1993) Hyperpolarization-activated cation current (I_h) in neurons of the medial nucleus of the trapezoid body: Voltage-clamp analysis and enhancement by norepinephrine and camp suggest a modulatory mechanism in the auditory brain stem. *J Neurophysiol* 70:1420–1432
- Basar E (1980) *EEG Brain Dynamics*. Elsevier, Amsterdam

- Basar-Eroglu C, Basa E, Demiralp T, Schueurmann M (1992) P300-response: Possible psychophysiological correlates in delta and theta frequency channels. a review. *Int J Psychophysiol* 13:161–179
- Batra R, Kuwada S, Standford TR (1989) Temporal coding of envelopes and their interaural delays in the inferior colliculus of the unanesthetized rabbit. *J Neurophysiol* 61:257–268
- Belluzzi O, Sacchi O, E, Wanke (1985) A fast transient outward current in the rat sympathetic neuron studied under voltage-clamp conditions. *J Physiol* 358:91–108
- Beutner D, Voets T, Neher E, Moser T (2001) Calcium dependence of exocytosis and endocytosis at the cochlear inner hair cell afferent synapse. *Neuron* 29:681–690
- Blackburn C, Sachs M (1989) Classification of unit types in the anteroventral cochlear nucleus: Pst histograms and regularity analysis. *J Neurophysiol* 62:1303–1329
- Bleek S (2000) Holistische Signalverarbeitung in einem Modell latenzverknuepfter Neuronen. PhD thesis, TU Darmstadt
- Bleek S (2007) A model of central cochlear nucleus units based on first order intervals. In: Kollmeier B, Klump G, Hohmann V, Langemann U, Mauermann M, Uppenkamp S, Verhey J (eds) *Hearing - from basis research to applications*, Springer, pp 25–31
- Borst M, Langner G, Palm G (2004) A biologically motivated neural network for phase extraction from complex sounds. *Biol Cybern* 90:98–104
- Bourk TR (1976) Electrical responses of neuronal units in the anteroventral cochlear nucleus of the cat. PhD thesis, MIT
- Bower JM, Beeman D (1994) *The Book of GENESIS*. Springer
- Buhusi CV, Meck WH (2005) What makes us tick? Functional and neural mechanisms of interval timing. *Nat Rev Neurosc* 6:755–765
- Cao XJ, Oertel D (2005) Temperature affects voltage-sensitive conductances differentially. *J Neurophysiol* 94:821–832
- Carney LH (1993) A model for the responses of low-frequency auditory-nerve fibers in cat. *J Acoust Soc Am* 93:401–417
- Caspary DM, Backoff PM, Finlayson PG, Palombi PS (1994) Inhibitory inputs modulate discharge rate within frequency receptive fields of anteroventral cochlear nucleus neurons. *J Neurophysiol* 72:2124–2133

- Cheveigné A (2000) The auditory system as a separation machine. In: Houtsma AJM, Kohlrausch A, Prijs VF, Schoonhoven R (eds) *Physiological and Psychophysical Bases of Auditory Function*, Shaker Publishing BV, Maastricht, The Netherlands, pp 453–460
- Costa PF (1996) The kinetic parameters of sodium currents in maturing acutely isolated rat hippocampal CA1 neurons. *Brain Res Dev Brain Res* 91:29–40
- Eckhorn R, Bauer R, Jordan W, Brosch M, Kruse W, Munk M, Reitboeck HJ (1988) Coherent oscillations: A mechanism of feature linking in the visual cortex? *biocyber* 60:121–130
- Ehret G, Merzenich MMJ (1988) Neuronal discharge rate is unsuitable for encoding sound intensity at the inferior colliculus level. *Hear Res* 35:1–7
- Ehret G, Romand R (1997) *The central auditory system*. Oxford University Press, Oxford
- Evans EF (1975) *Handbook of sensory physiology*, Springer, Berlin, Chapter: Cochlear nerve and cochlear nucleus, pp 1–108
- Ferragamo M, Golding N, Oertel D (1998a) Synaptic inputs to stellate cells in the ventral cochlear nucleus. *J Neurophysiol* 79:51–63
- Ferragamo MJ, Haresign T, Simmons JA (1998b) Frequency tuning, latencies, and responses to frequency-modulated sweeps in the inferior colliculus of the echolocating bat, *ptesicus fuscus*. *Journal of Comparative Physiology A: Sensory, Neural and Behavioral Physiology* 182:65–79
- Forsythe ZRI, Stanfield P (1996) Characterization of the hyperpolarization activated nonspecific cation current I_h of bushy neurons from the rat anteroventral cochlear nucleus studied in a thin brain slice preparation. *Neurobiology* 4:275–276
- Frisina RD, Smith RL, Chamberlain SC (1985) Differential encoding of rapid changes in sound amplitude by second order auditory neurons. *Exp Brain Res* 60:417–422
- Frisina RD, Smith RL, Chamberlain SC (1990a) Encoding of amplitude modulation in the gerbil cochlear nucleus: I. A hierarchy of enhancement. *Hear Res* 44:99–122
- Frisina RD, Smith RL, Chamberlain SC (1990b) Encoding of amplitude modulation in the gerbil cochlear nucleus: II. Possible neural mechanisms. *Hear Res* 44:123–142
- Frisina RD, Karcich KJ, Tracy TC, Sullivan DM, Walton JP (1996) Preservation of amplitude modulation coding in the presence of background noise by chinchilla auditory-nerve fibers. *J Acoust Soc Am* 99:475–490

- Fu XW, Brezden BL, Wu SH (1997) Hyperpolarization-activated inward current in neurons of the rats dorsal nucleus of the lateral lemniscus in vitro. *J Neurophysiol* 78:2235–2245
- Fylan F, Harding GFA, Edson AS, Webb RM (1999) Mechanisms of video-game epilepsy. *Epilepsia* 40:28–30
- Gabor D (1968a) Holographic model of temporal recall. *Nature* 217:584
- Gabor D (1968b) Improved holographic model of temporal recall. *Nature* 217:1288–1289
- Glass L (2001) Synchronization and rhythmic processes in physiology. *Nature* 410:277–284
- Godfrey DA, Kiang NYS, Norris BE (1975) Single unit activity in the dorsal cochlear nucleus of the cat. *J Comp Neurol* 162:269–284
- Golding NL, Ferragamo M, Oertel D (1999) Role of intrinsic conductances underlying responses to transients in octopus cells of the cochlear nucleus. *J Neurosci* 19:2897–2905
- Gray CM (1994) Synchronous oscillations in neuronal systems: Mechanisms and functions. *J Comput Neurosci* 1:11–38
- Gray CM, Singer W (1989) Stimulus-specific neuronal oscillations in orientation columns of cat visual cortex. *PNAS* 86:1698–1702
- Greenwood DD (1990) A cochlear frequency-position function for several species—29 years later. *J Acoust Soc Am* 87:2592–2605
- Grigg JJ, Brew HM, Tempel BL (2000) Differential expression of voltage-gated potassium channel genes in auditory nuclei of the mouse brain stem. *Hear Res* 140:77–90
- Hackett JT, Jackson H, Rubel EW (1982) Synaptic excitation of the second and third order auditory neurons in the avian brain stem. *Neuroscience* 7:1455–1469
- Heil P, Schulze H, Langner G (1995) Ontogenetic development of periodicity coding in the inferior colliculus of the mongolian gerbil. *Aud Neurosci* 1:363–383
- van Hemmen JL (2006) Editorial. *Biol Cybern* 94(1):1–1
- Hewitt MJ, Meddis R, Shakleton TM (1992) A computer model of a cochlear-nucleus stellate cell: Responses to amplitude-modulated and pure-tone stimuli. *J Acoust Soc Am* 91:2096–2109
- Hines M (1993) *Neural Systems: Analysis and Modeling*, Kluwer Academic Publishers, chap NEURON - a program for simulation of nerve equation, pp 127–136

- Hines ML, Carnevale NT (1997) The neuron simulation environment. *Neur Comp* 9:1179–1209
- Hines ML, Morse T, Migliore M, Carnevale NT, Shepherd GM (2004) ModelDB: A database to support computational neuroscience. *J Comp Neurosc* 17:7–11
- Hodgkin AL, Huxley AF (1952) A quantitative description of membrane current and its application to conduction and excitation in nerve. *J Physiol* 117:500–544
- Huguenard JR, McCormick DA (1992) Simulation of the currents involved in rhythmic oscillations in thalamic relay neurons. *J Neurophysiol* 68:1373–1383
- Josephson EM, Morest DK (1998) A quantitative profile of the synapses on the stellate cell body and axon in the cochlear nucleus of the chinchilla. *J Neurocyt* 27:841–864
- Kanemasa T, Gan L, Perney TM, Wang LY, Kaczmarek LK (1995) Electrophysiological and pharmacological characterization of a mammalian shaw channel expressed in NIH 3T3 fibroblasts. *J Neurophysiol* 74:207–217
- Langner G (1978) The periodicity matrix. A correlation model for central auditory frequency analysis. *Verh Dtsch Zool Ges* 71:194
- Langner G (1981) Neuronal mechanisms for pitch analysis in the time domain. *Exp Brain Res* 44:450–454
- Langner G (1983) Evidence for neuronal periodicity detection in the auditory system of the guinea fowl: Implications for pitch analysis in the time domain. *Exp Brain Res* 52:333–355
- Langner G (1988) Auditory pathway: Structure and function, Plenum Press, New York, Chapter: Physiological properties in the cochlear nucleus are adequate for a model of periodicity analysis in the auditory midbrain, pp 207–212
- Langner G (1992) Periodicity coding in the auditory system. *Hear Res* 60:115–142
- Langner G, Schreiner C (1988) Periodicity coding in the inferior colliculus of the cat: I. Neuronal mechanisms. *J Neurophysiol* 60:1799–1822
- Langner G, Schreiner CE (1996) Contributions of the auditory brainstem to periodicity pitch coding. *Adv in Speech, Hearing and Language Proc* 3:447–461
- Lashley KS (1963) Brain mechanisms and intelligence, a quantitative study of injuries to the brain. Dover, New York
- Lebedev MA, Nelson RJ (1995) Rhythmically firing (2050 hz) neurons in monkey primary somatosensory cortex: Activity patterns during initiation of vibratory-cued hand movements. *J Comp Neurosc* 2:313–334

-
- Lebedev MA, Wise SP (2004) Oscillations in the premotor cortex: Single-unit activity from awake, behaving monkeys. *Exp Brain Res* 130:195–215
- Li RYS, Guinan JJ (1971) Antidromic and orthodromic stimulation of neurons receiving calyces of held. *MIT Q Rpt* 100:227–234
- Longuet-Higgins HC (1968) Holographic model of temporal recall. *Nature* 217:104
- van der Malsburg C (1992) Sensory segmentation with coupled neural oscillators. *Biol Cybern* 67:233–242
- von der Malsburg C, Schneider W (1986) A neural cocktail-party processor. *Biol Cybern* 54:29–40
- Manis PB, Marx SO (1991) Outward currents in isolated ventral cochlear nucleus neurons. *J Neurosci* 11:2865–2880
- Migliore M, Morse TM, Davison AP, Marenco L, Shepherd GM, Hines ML (2003) ModelDB: Making models publicly accessible to support computational neuroscience. *Neuroinformatics* 1:135–139
- Moser T, Beutner D (2000) Kinetics of exocytosis and endocytosis at the cochlear inner hair cell afferent synapse of the mouse. *PNAS* 97:11,883–11,888
- Mountain DC, Cody AR (1999) Multiple modes of inner hair cell stimulation. *Hear Res* 132:1–14
- Mueller-Preuss P, Flachskamm C, Bieser A (1994) Neural encoding of amplitude modulation within the auditory midbrain of squirrel monkeys. *Hear Res* 80:197–208
- Murthy VN, Fetz EE (1992) Coherent 25- to 35-Hz oscillations in the sensorimotor cortex of awake behaving monkeys. *PNAS* 89:5670–5674
- Ochse M (2004) Neuronale kodierung von Tonhoehen und harmonischen Relationen im auditorischen Mittelhirn der Rennmaus (*Meriones unguiculatus*). PhD thesis, TU Darmstadt
- Oertel D (1983) Synaptic responses and electrical properties of cells in brain slices of the mouse anteroventral cochlear nucleus. *J Neurosci* 3:2043–2053
- Oertel D, Wu SH, Garb MW, Dizack C (1990) Morphology and physiology of cells in slice preparations of the posteroventral cochlear nucleus of mice. *J Comp Neurol* 295:136–154
- Oertel D, Bal R, Gardner SM, Smith PH, Joris PX (2000) Detection of synchrony in the activity of auditory nerve fibers by octopus cells of the mammalian cochlear nucleus. *PNAS* 97, 11773–11779

- Osen KK (1969) Cytoarchitecture of the cochlear nuclei in the cat. *J Comp Neurol* 136:453–484
- Ostapoff EM, Feng JJ, Morest DK (1994) A physiological and structural study of neuron types in the cochlear nucleus. II. Neuron types and their structural correlation with response properties. *J Comp Neurol* 346:19–42
- Palmer A, Jiang D, Marshall DH (1996) Responses of ventral cochlear nucleus onset and chopper units as a function of signal bandwidth. *J Neurophysiol* 75:780–794
- Perney TM, Kaczmarek LK (1997) Localization of a high threshold potassium channel in the rat cochlear nucleus. *J Comp Neurol* 386:178–202
- Pesaran B, Pezaris JS, Sahani M, Mitra PP, Andersen RA (2002) Temporal structure in neuronal activity during working memory in macaque parietal cortex. *Nat Neurosci* 5:805–811
- Pfeiffer RR (1966) Classification of response patterns of spike discharges for units in the cochlear nucleus: Tone-burst stimulation. *Exp Brain Res* 1:220–235
- Rall W (1967) Distinguishing theoretical synaptic potentials computed for different somadendritic distributions of synaptic inputs. *J Neurophysiol* 30:1138–1168
- Rees A, Langner G (2005) *The inferior colliculus*, Springer, Chapter: Temporal coding in the auditory midbrain, pp 346–376
- Rhode WS, Greenberg SR (1994) Encoding of amplitude modulation in the cochlear nucleus of the cat. *J Neurophysiol* 71:1797–1825
- Rhode WS, Smith PH (1986) Encoding timing and intensity in the ventral cochlear nucleus of the cat. *J Neurophysiol* 56:261–286
- Rothman JS, Manis PB (2003a) Differential expression of three distinct potassium currents in the ventral cochlear nucleus. *J Neurophysiol* 89:3070–3082
- Rothman JS, Manis PB (2003b) Kinetic analyses of three distinct potassium conductances in ventral cochlear nucleus neurons. *J Neurophysiol* 89:3083–3096
- Rothman JS, Manis PB (2003c) The roles potassium currents play in regulating the electrical activity of ventral cochlear nucleus neurons. *J Neurophysiol* 89:3097–3113
- Rothman JS, Young ED, Manis PB (1993) Convergence of auditory nerve fibers onto bushy cells in the ventral cochlear nucleus: Implications of a computational model. *J Neurophysiol* 70:2562–2583
- Ryugo DK, Parks TN (2003) Primary innervation of the avian and mammalian cochlear nucleus. *Brain Res Bull* 60:435–456

- Sanes JN, Donoghue JP (1993) Oscillations in local field potentials of the primate motor cortex during voluntary movement. *PNAS* 90:4470–4474
- Schneider P, Sluming V, Roberts N, Scherg M, Goebel R, Specht HJ, Dosch HG, Bleeck S, Stippich C, Rupp A (2005) Structural and functional asymmetry of lateral Heschl's Gyrus reflects pitch perception preference. *Nat Neurosci* 8(9):1241–1247
- Schouten JF (1970) The residue revisited. In: Plomp R, Smoorenburg GF (eds) Frequency analysis and periodicity detection in hearing, A W Sijthoff, Leiden, pp 41–53
- Semple MN, Kitzes LM (1985) Single-unit responses in the inferior colliculus - different consequences of contralateral and ipsilateral auditory-stimulation. *J Neurophysiol* 53:1467–1482
- Singer W (1998) Consciousness and the structure of neuronal representations. *Philos Trans R Soc Lond B Biol Sci* 353:1829–1840
- Stopfer M, Bhagavan S, Smith BH, Laurent G (1997) Impaired odour discrimination on desynchronization of odour-encoding neural assemblies. *Nature* 390:70–74
- Strube HW (1985) A computationally efficient basilar-membrane model. *Acustica* 58:207–214
- Taschenberger H, Gersdorff H (2000) Fine tuning an auditory synapse for speed and fidelity: Developmental changes in presynaptic waveform, EPSC kinetics, and synaptic plasticity. *J Neurosci* 20:9162–9173
- Traub RD, Wong RK (1982) Cellular mechanism of neuronal synchronization in epilepsy. *Science* 216:745–747
- Travagli RA, Gillis RA (1994) Hyperpolarization-activated currents, I_h and I_{KIR} , in rat dorsal motor nucleus of the vagus neurons in vitro. *J Neurophysiol* 71:1308–1317
- Voutsas K, Langner G, Adamy J, Ochse M (2005) A brain-like neural network for periodicity analysis. *IEEE Trans Syst Man Cybern B Cybern* 35:12–22
- Wang LY, Gan L, Forsythe ID, Kaczmarek LK (1998) Contribution of the KV3.1 potassium channel to high-frequency firing in mouse auditory neurons. *J Physiol* 509:183–194
- Wang X, Sachs MB (1995) Transformation of temporal discharge patterns in a ventral cochlear nucleus stellate cell model: Implications for physiological mechanisms. *J Neurophysiol* 73:1600–1616
- Wehr M, Laurent G (1996) Odour encoding by temporal sequences of firing in oscillating neural assemblies. *Nature* 384:162–166

- Westlake PR (1970) The possibilities of neural holographic processes within the brain. *Biol Cybern* 7:129–153
- Wiegrebe L, Meddis R (2004) The representation of periodic sounds in simulated sustained chopper units of the ventral cochlear nucleus. *J Acoust Soc Am* 115:1207–1218
- Wiegrebe L, Winter IM (2001) Temporal representation of iterated rippled noise as a function of delay and sound level in the ventral cochlear nucleus. *J Neurophysiol* 85:1206–1219
- Winter IM, Robertson D, Yates GK (1990) Diversity of characteristic frequency rate-intensity functions in guinea pig auditory nerve fibres. *Hear Res* 45:191–202
- Winter IM, Wiegrebe L, Patterson RD (2001) The temporal representation of the delay of iterated rippled noise in the ventral cochlear nucleus of the guinea-pig. *J Physiol* 537:553–566
- Winter IM, Palmer AR, Patterson LWRD (2003) Temporal coding of the pitch of complex sounds by presumed multipolar cells in the ventral cochlear nucleus. *Speech Communication* 41:135–149
- Woolley SMN, Casseday JH (2004) Response properties of single neurons in the zebra finch auditory midbrain: Response patterns, frequency coding, intensity coding, and spike latencies. *J Neurophysiol* 91:136–151
- Young ED, Robert JM, Shofner WP (1988) Regularity and latency of units in ventral cochlear nucleus: Implications for unit classification and generation of response properties. *J Neurophysiol* 60:1–29
- Zifkin BJ, Trenite DK (2000) Reflex epilepsy and reflex seizures of the visual system: A clinical review. *Epileptic Disorders* 2(3):129–136
- Zschau C (2006) Einfluss von Lautstärke und Modulationstiefe auf die Periodizitätsverarbeitung im Colliculus inferior der mongolischen Wüstenrennmaus (*Meriones unguiculatus*). Diplom work, TU Darmstadt
- Zwicker E (1986) A hardware cochlear nonlinear preprocessing model with active feedback. *J Acoust Soc Am* 80:146–153

Acknowledgements

Here, I want to express my gratitude to all those people who helped this work to become reality.

First of all I would like to thank Prof. Dr. G. Langner for the kind reception in his group and the possibility to prepare and finish my dissertation. His open and supportive supervision allowed me to induce my own ideas into my work and present them at several conferences. Especially I would like to acknowledge his encouragement of scientific discussions.

I would like to thank Prof. Dr. Galuske for the acceptance of the 'Korreferat' of my thesis.

Thanks to Prof. Dr. Adamy and Dipl. Ing. Kyriakos Voutsas of the department for electrical engineering of the TU Darmstadt, who encouraged the interdisciplinary work of the neuroscience and control theory, to Dr. Werner Hemmert and Dipl. Ing. Marcus Holmberg from Infineon Technologies for their technical support. Without their help it would not have been possible to finish the thesis within this time.

My very special goes to Dr. Elisabeth Wallhäuser-Franke, who supported me in the beginning of my Ph.D. and helped me to get insight in the academic world. Unfortunately, she is no longer a member of the Neuroacoustics group in Darmstadt.

For the friendly reception in the group I would also like to thank Gaby Wenz and Manuel Camargo; especially Gaby for the constant support with carbohydrates and Manuel for the endless discussion about Matlab.

A best thank goes to my colleague Peter Baumhoff for the fruitful discussions both in science and in social aspects of our work, thanks also to Christine Zschau, part of her work is discussed in this thesis.

Last but not least I want to thank my family and my friends for their lasting and unreserved support during my studies and my graduation. Without their help this work surely would not have been possible.

Curriculum Vitae

Personal Data

Name: Andreas Bahmer

Date of birth: 14.08.1975

Place of birth: Aschaffenburg

School Education

1981-1984 Grundschule in Aschaffenburg

1985-1994 Friedrich-Dessauer-Gymnasium in Aschaffenburg
Abitur in July 1994

Studies

1994-2003 Studies of Physics and Medicine at the
Christian-Albrechts University Kiel,
Rheinische-Friedrich-Wilhelms University Bonn,
Johann-Wolfgang-Goethe University Frankfurt am Main,
and Darmstadt University of Technology.

1999 Intermediate diploma in medicine (Physikum)

2001 Intermediate diploma in physics (Vordiplom)

2003 Diploma thesis under supervision of Prof. Dr. T. Tschudi
at the Institute of Applied Physics,
Title: *Diffraktive optische Elemente (DOEs)*
in der Lasermaterialbearbeitung

Graduation (Ph.D. thesis)

from August 2004 Ph.D. thesis under supervision of Prof. Dr. G. Langner
at the Institute for Zoology,
Darmstadt University of Technology

Ich erkläre hiermit an Eides statt, dass ich die vorliegende Dissertation selbständig und nur mit den angegebenen Hilfsmitteln angefertigt habe.

Aschaffenburg, den 28. Februar 2007

Authors list of Publications

Publications in referred journals and books

Oscillating neurons in the cochlear nucleus: I. Experimental basis of a simulation paradigm,

A. Bahmer and G. Langner, Biological Cybernetics, 95:371-379, 2006

Oscillating neurons in the cochlear nucleus: II. Simulation results,

A. Bahmer and G. Langner, Biological Cybernetics, 95:381-392, 2006

Simulation of oscillating neurons in the cochlear nucleus: a possible role for neural nets, onset cells, and synaptic delays,

A. Bahmer and G. Langner, Hearing - from basic research to applications, Springer, Heidelberg, 2007

Spectral integration in a simulation of onset and chopper neurons in the cochlear nucleus,

A. Bahmer and G. Langner, submitted to Hearing Research.

Networks of Hodgkin-Huxley-like neuron models for the simulation of oscillating neurons in the cochlear nucleus,

A. Bahmer and G. Langner, in preparation.

Oscillating neurons in the cochlear nucleus: Experimental evidences for a new simulation topology, simulation results, and consequences for pitch perception,

A. Bahmer and G. Langner, Proceedings 31st Göttingen Neurobiology Conference, German Neuroscience Society, in preparation.

Modeling intrinsic oscillations in the auditory system: a neuronal mechanism for quantal pitch shifts and absolute pitch?,

A. Bahmer and G. Langner, Annals New York Academy of Sciences, Vol. 1060, 2005.

Oral Presentations

Simulation of oscillating neurons in the cochlear nucleus: a possible role for neural nets, onset cells, and synaptic delays A. Bahmer and G. Langner, 14. International Symposium on Hearing, Cloppenburg, Germany, 18.-23.8.2006

“Spike synchronization and firing rate in a population of motor cortical neurons in relation to movement direction and reaction time, A. Bahmer, according to the paper from F. Grammont and A. Riehle (2003) Biol Cybern 88, 360-373, Course on Computational Neuroscience at Max-Planck-Institut für Strömungsforschung and Center for Computational Neuroscience Göttingen, Germany, 22.-26.9.2004.

Poster Presentations

*Modeling intrinsic oscillations in the auditory system: a neuronal mechanism for quantal pitch shifts and absolute pitch? A. Bahmer and G. Langner, Conference: The neurosciences and Music II: from Perception to Performance, Leipzig, Germany, 5.-8.5.2005
Poster price of the Mariani Foundation.*

Computer simulation of intrinsic oscillations in the auditory system, A. Bahmer and G. Langner, Symposium on Dynamics and adaptivity of neuronal systems: Integrative approaches to analyse cognitive functions, Hamburg, Germany, 27.-29.10.2005.

Evidence for an auditory time constant supported by simulation of chopper neurons , BSA Short papers meeting on experimental studies of hearing and deafness, Cambridge, UK, 14.-15.9.2006.

Oscillating neurons in the cochlear nucleus: Experimental evidences for a new simulation topology, simulation results, and consequences for pitch perception, 31st Göttingen Neurobiology Conference, German Neuroscience Society Göttingen, Germany, 29.3.-1.4.2007.